Contribution to prognostics of proton exchange membrane fuel cells : approaches based on degradation information at multiple levels

Dacheng Zhang

Communauté
UNIVERSITÉ Grenoble Alpes

THÈSE

pour obtenir le grade de
Docteur de la Communauté Université Grenoble Alpes

Spécialité : **Automatique - Productique**

Arrêté ministériel : 25 mai 2016

Présentée par
Dacheng ZHANG

Thèse dirigée par **Catherine CADET** et
codirigée par **Christophe BÉRENGUER**

préparée au sein du **Laboratoire Grenoble Images Parole Signal Automatique (GIPSA-lab)**
dans **l'école doctorale Electronique, Electrotechnique, Automatique, Traitement du Signal (EEATS)**

Contribution to prognostics of PEM fuel cells: approaches based on degradation information at multiple levels

Thèse soutenue publiquement le **18 Janvier 2018**,
devant le jury composé de:

Monsieur Daniel HISSEL, Président
Professeur des Universités, Université de Franche-Comté
Madame Mitra FOULADIRAD, Rapporteur
Professeur des Universités, Université de Technologie de Troyes
Monsieur Rachid OUTBIB, Rapporteur
Professeur des Universités, Aix-Marseille Université
Monsieur Piero BARALDI, Examinateur
Professore Associato, Politecnico di Milano
Madame Catherine CADET, Directeur de thèse
Maître de Conférences HDR, Université Grenoble Alpes
Monsieur Christophe BÉRENGUER, Co-directeur de thèse
Professeur des Universités, Grenoble INP
Madame Nadia YOUSFI-STEINER, Co-encadrent de thèse
Maître de Conférences, Université de Franche-Comté

Remerciements

Tout d'abord, je voudrais remercier Catherine et Christophe, mes directeurs de thèse, de m'avoir proposé un sujet super intéressant et passionnant, et de m'avoir dirigé tout au long de ces années de thèse. Je voudrais remercier Nadia, mon encadrante de thèse, pour son précieux conseil et son aide durant toute la période du travail. Je remercie chaleureusement pour leurs qualités scientifiques, leurs patiences et leurs sympathies. Ils sont toujours été présents pour m'écouter et me proposer leurs conseils avisés. Leurs nombreuses relectures et corrections de cette thèse ont été très appréciables. J'ai beaucoup appris à leurs côtés et je leur adresse ma gratitude pour tout cela. J'ai pris un grand plaisir de travailler avec eux.

Je remercie Pr. Mitia Fouladirad et Pr. Rachid Outbib d'avoir accepté de rapporter cette thèse. Merci à tous les membres du jury d'avoir accepté d'examiner mon travail.

Merci à toutes les personnes du Département Auto du Gipsa pour leurs sympathies, leurs amitiés. J'ai beacoup de plaisir de travailler avec eux. Merci à tous mes amis rencontrés à Grenoble, à Belfort et à Milano. Leur amitié sera un des plus beaux souvenirs dans ma vie.

Un grand merci à mes parents. Ils m'ont toujours soutenu et encouragé dans mes choix au cours de ma vie. Enfin, je remerci à Jingyi, qui m'a supporté, encouragé et accompagné jusqu'à la fin de cette thèse.

Merci à toute personne qui m'a aidé de près ou de loin tout au long de ces années.

Dacheng

Résumé

Dans le contexte de la transition énergétique, la pile à combustible devient l'une des sources d'énergie alternatives les plus prometteuses. Récemment, la recherche a mis l'accent sur les piles à combustible, et plus particulièrement sur celles à membrane échange de protons (Proton Exchange Membrane Fuel Cell ou Polymer Electrolyte Membrane Fuel Cell ou PEMFC) qui est l'une des meilleures candidates pour les applications stationnaires et transport. Même si cette technologie évolue constamment, elle n'est pas encore prête pour un déploiement industriel à grande échelle en raison de sa durabilité et de sa fiabilité limitées. Le "Prognostics and Health Management" (PHM) est une approche récente pour gérer et prolonger la durée de vie des systèmes. Les techniques de pronostic sont capables de fournir une estimation de l'état de santé (State of Health ou SOH) des piles à combustible et une prédiction de leur durée de vie résiduelle (Remaining Useful Life ou RUL) afin d'aider les fabricants à améliorer les performances et à gérer leur durée de vie de ces systèmes. Ce travail a pour objectif de développer de nouvelles méthodes d'estimation de la durée de vie adaptée à la complexité des systèmes PEMFC. En effet, ces systèmes sont multi-échelle et multi-physique, et présentent divers défis sont à relever :

1. La définition de SOH pour construire un indicateur de dégradation.
2. La coexistence de phénomènes de dégradation à la fois réversibles et irréversibles.
3. Prise en compte des différentes causes de détérioration et des effets des conditions opératoires.

Dans la première partie, nous effectuons une analyse bibliographique de l'utilisation du PHM pour les PEMFCs, dans le but de proposer une définition de SOH et de construire un indicateur de dégradation. Etant donné que les mesures PEMFC sont peu nombreuses, nous avons également exploré l'état de l'art sur les batteries au lithium, qui sont d'autres cellules électrochimiques. Dans la deuxième partie, nous développons un algorithme de pronostic basé sur le filtrage particulaire utilisant la mesure de puissance de la PEMFC. Les premiers résultats montrent que l'algorithme de pronostic est perturbé par la dégradation réversible existante. L'ambiguïté peut être levée en estimant la dégradation irréversible grâce à des tests de caractérisation, tels la spectroscopie d'impédance électrochimique (Electrochemical Impedance Spectroscopy ou EIS), appliquée de temps en temps. Nous proposons donc un algorithme de pronostic étendu et adapté, prenant en compte deux indicateurs : la dégradation de la puissance et le SOH estimé à partir de la caractérisation EIS. La performance de l'algorithme proposé est évaluée par différentes indicateurs de performance, et les résultats montrent l'intérêt de cette approche. Dans la troisième partie, les problèmes sont abordés d'un point de vue plus théorique. En effet, l'évolution de la dégradation d'un système est souvent corrélée à des covariables internes et externes qui sont généralement difficiles d'accès en raison des coûts de mesure élevés. Par conséquent, nous avons d'abord développé une approche comprenant des inspections en ligne de la covariable de dégradation à un autre niveau, puis nous

avons proposé une approche d'estimation de la RUL basée sur un ensemble de modèles en utilisant différentes sources à différents niveaux. Les RULs prédites par les deux modèles sont agrégées dynamiquement sur la base des performances évaluées sur les données historiques. Par conséquent, la précision de la prédiction est améliorée car les inconvénients des deux modèles ont été surmontés en tirant parti de leurs avantages. Dans la dernière partie, le problème est étendu au pronostic multi-niveaux qui ouvre de nouveaux aspects pour la recherche future sur le pronostic et la gestion de la PEMFC.

Mots clés : PEMFC, PHM, pronostics, état de santé, filtrage des particules, pronostic à plusieurs niveaux

Abstract

In the context of the energy transition, fuel cell becomes one of the promising alternative energy sources. Recently the spotlight is on fuel cell systems research, and more particularly on Proton Exchange Membrane Fuel Cell (PEMFCs) which is one of the best candidates for both stationary and transportation applications. Even if this technology is close to being competitive, it is not yet ready to be considered for a large scale industrial deployment because of its limited durability and reliability. Prognostics and Health Management (PHM) is a recent approach to manage and possibly extend life duration of technological systems. Prognostic techniques can provide an estimation of fuel cell State Of Health (SOH) and a prediction for their Remaining Useful Life (RUL) to help the manufacturers improving fuel cell performance and managing its lifespan. The objective of this work is to develop prognostic methodologies for the RUL prognosis adapted to the complexity of PEMFCs. Indeed, the PEMFC is a multi-scale and multi-physics system, and various challenges are faced:

1. The definition of SOH to build a degradation indicator.
2. The coexistence of both reversible and irreversible degradation phenomena.
3. Taking into account different deterioration causes and effects of operating conditions.

In the first part of our work, we conduct a state of the art analysis on PHM for PEMFCs, with the aim of proposing a SOH definition and building a degradation indicator for PEMFC prognosis purposes. Moreover, since PEMFC measurements are scarce, state of the art on Lithium batteries, other electrochemical cells, is also explored. In the second part, we develop a particle filtering based prognostic algorithm for PEMFC, based on output power measurements. The first results show that the prognosis algorithm is disturbed by the existing reversible degradation. However, the irreversible degradation can be estimated thanks to characterization tests, such as Electrochemical Impedance Spectroscopy (EIS), which is applied from time to time. We propose thus an adapted & extended prognostic algorithm to take into account both health indicators: the output power degradation and the SOH degradation estimated from EIS characterization. The performance of the proposed algorithm is evaluated by different prognostic performance metrics, and the results show the interest of this approach. In the third part, the problem is addressed from a more theoretical point of view. Indeed, a system's degradation behavior is often correlated with internal and external covariates which are usually difficult to access owing to expensive measurement cost. Therefore, we first developed a prognostic approach with online inspections on the degradation covariate at a different level, and then we propose an approach for RUL prognosis based on an ensemble of models using different sources at different levels. The RUL predictions of both models are dynamically aggregated on the basis of prognostic performance evaluated on a set of historical data. Consequently, the prediction accuracy is improved by overcoming both models' drawbacks and leveraging their strengths. In the last part, we extend the problem to multi-level prognostics and explore new possibilities, which open new aspects for future research on PEMFC lifetime prognosis and management.

Keywords: PEMFC, PHM, Prognostics, State of Health, Particle Filtering, Multi-level Prognostics

Contents

List of Figures

List of Tables

General Introduction

For the past three decades, the increase in global energy demand, combined with the scarcity of fossil fuels and their increasing prices, as well as the growth of polluting emissions and the Greenhouse effects, are contributing to the development of alternative energy sources. Recently, a "climate plan" [1] has been presented by the Minister of Ecological Transition in July 2017, to draw French environmental strategy. The Climate Plan presents the vision and ambition of the French Government to lay the foundations for a new model of prosperity, more energy, and natural resources, and seize the opportunities offered in terms of innovation, investment and creation jobs. It proposes a profound change for the main sectors emitting greenhouse gases: buildings, transport, energy, agriculture and forestry, industry and waste, *e.g.* the government wants to put an end to the marketing of cars running on gasoline or diesel in France by 2040, where a target for 2030 has been set in India and Germany as well. Towards research, the Horizon 2020 [2] program was launched in Paris in December 2013 by the Minister of Higher Education and Research, in the presence of European personalities. The challenge is to mark the entry into force, on January 1^{st} 2014, of the new European research and innovation funding program. A total of 16 countries have already organized their launch event. The Horizon 2020 program brings together European Union funding for research and innovation and focuses on three main priorities: scientific excellence, industrial primacy, and societal challenges. Since the energy transition becomes a priority in environmental, economic and political, fuel cell becomes one of those promising alternative energy sources and recently the spotlight is on the research of fuel cell systems among energy conversion devices.

Fuel cells have been developed for decades but still not commercialized in large-scale markets. Although some long-term operations of the fuel cell have been proven and some countries put substantial investments in this technology such as US, Germany, Japan and South Korea, its commercialization in industrial applications and our daily life are still facing challenges. For instance, the maximum current life span of a Fuel Cell Electric Vehicle (FCEV) is around 2500 hours where 5000 hours are required, and the maximum current life duration of a Fuel Cell Electric Bus (FCEB) is around 10000 hours where 25000 hours are required [3]. We consider here only the ones of the type Proton Exchange Membrane, abbreviated as PEMFC, which represent the current majority of fuel cell technologies.

As a result, many improvements are still required to extend the lifespan and enhance the reliability of fuel cell systems. Prognostics and health management (PHM) is a recent dynamic approach to extend and manage the life duration of industrial systems. This technique has been relatively studied for batteries, and it is pioneering in fuel cells technologies. The prognostic results can be helpful in making decisions such as maintenance scheduling and control strategy: early notification of degradation can be detected, and early failures can be avoided. Meanwhile, the repairing cost can be reduced. Prognostic techniques can provide

[1] http://www.gouvernement.fr/action/plan-climat
[2] http://www.horizon2020.gouv.fr/
[3] https://energy.gov/eere/fuelcells/doe-technical-targets-fuel-cell-transit-buses

an estimation of fuel cell State Of Health (SOH) and a prediction for their Remaining Useful Life (RUL) in order to help the manufacturers extending its lifespan and improving fuel cell performance.

The objective of this work is to develop prognostic methodologies for the RUL prognosis adapted to the complexity of PEMFCs. Indeed, the PEMFC is a multi-scale and multi-physics system, and various challenges are faced:

1. The definition of SOH to build a degradation indicator.
2. The coexistence of both reversible and irreversible degradation phenomena.
3. Taking into account different deterioration causes and effects of operating conditions.

Degradation measurements data are required as aging indicators to determine the RUL. For PEMFC, the output power degradation is mostly used as an aging indicator. However, the power degradation is a symptom of the combined impacts of different degradation factors and temporary effect of poor operating conditions, which lead to the coexistence of reversible and irreversible phenomena. This work aims to improve the accuracy and precision of the RUL prognosis by using additional information. To that ends, we have been studying different ways to reach this goal. For PEMFC, the SOH characterization measurements, such as the Electrochemical Impedance Spectroscopy (EIS) and polarization curves, are giving rich information but they are intermittent and costly. Thus, a practical approach and two more theoretical approaches have been developed based on the use of degradation information at multiple levels.

This work has been done with several collaborations. GIPSA-lab [4] and FCLAB [5] work in collaboration to develop new methods of prognostics for fuel cells. The work also benefits from the support of InnoEnergy PhD School [6], which enables the collaboration with LASAR [7] at University Politecnico Milano. The manuscript is organized into three main parts:

1. In the first part, the background of fuel cell technologies (Chapter 1) and PHM techniques (Chapter 2) are introduced. The operation of PEMFC and its degradation issues are addressed in Chapter 1. The definition of degradation indicators is explored by investigating the knowledge of Li-ion batteries. Chapter 2 presents the PHM approach. Then the conception and limitations of PHM for PEMFC are explored by reviewing current works. Finally, a description of the issues that need to be addressed is explained in the problem statement part.
2. In the second part, a methodology of RUL prognosis for PEMFC is developed. In Chapter 3, the particle filtering-based approach is presented with a simple example. In

[4] Gipsa-lab is internationally recognized for the research achieved in Automatic Control, Signal and Images processing, Speech and Cognition. http://www.gipsa-lab.fr/

[5] The Federation for Fuel Cell Research FCLAB gathers all research groups of Franche-Comté Region in the field of fuel cell systems and hydrogen-energy. http://www.fclab.fr/

[6] InnoEnergy http://www.innoenergy.com/education/phd-school/

[7] The Laboratory of signal and risk analysis focus its research activity on the most modern computational techniques. http://www.lasar.polimi.it/

Chapter 4, we implement this approach on real data. Two PEMFC stacks are operated throughout its lifespan under constant current (stationary regime) and solicited current (dynamic regime), respectively. In the first part, we apply the RUL prognosis on the measurement data of stack output power. This method is improved in the second part, by additionally taking into account the information of SOH characterization in degradation trends prediction. The idea of using degradation information from different sources is developed further.

3. In the third part, the problem statement is addressed from a more theoretical point of view. Indeed, a system's degradation behavior is often correlated with internal and external covariates which are usually difficult to access owing to expensive measurement cost. In Chapter 5, we develop an approach to online inspection on the degradation covariates at different levels and use this knowledge to update the precision of degradation tracking. The approach developed in Chapter 6 is based on an ensemble of models using different sources at different levels: internal SOH (estimated from characterization measurements) and external stack voltage direct measurements. The RUL predictions of both models are dynamically aggregated on the basis of prognostic performance evaluated on a set of historical data.

This manuscript ends with a general conclusion summarizing the highlights in this thesis and providing the ideas for the future investigation.

Chapter 1

Proton Exchange Membrane Fuel Cells

In this chapter, we first introduce the generalities of fuel cells and the challenges regarding their durability and reliability. We focus on a specific type of fuel cells: the Proton Exchange Membrane Fuel Cell (PEMFC) and its performance characteristics. After Fuel Cell background description and SOH characterization, a first attempt is realized to define appropriate degradation indicators for PEMFCs by comparing the mechanisms from a similar electrochemical device: Li-ion battery. As electrochemical power sources technologies, namely Li-ion batteries and fuel cells, have been considered as one of the most promising technologies for both stationary and transportation applications. However, the fuel cell has not been as thoroughly studied as Li-ion battery, which is by far the most popular in the worldwide in electric mobility applications [1], [2]. Thus, studying the degradation behavior of fuel cell systems and Li-ion batteries could lead to a better understanding of these technologies, in order to extend systems lifespan and to enhance their performance. Thus, the work reported in the last part has been published in the international journal "Fuel Cells" [3].

Contents

1.1 Fuel Cells Background

The fuel cell was invented in 1838 by the German scientist Christian Friedrich Schönbein and firstly demonstrated by Sir William Robert Grove in the following year. The first success in commercial use came after being a source of energy in NASA's Apollo missions. Since then, fuel cells have been used in many other applications. Figure 1.1 shows the timeline of the deployments of fuel cells.

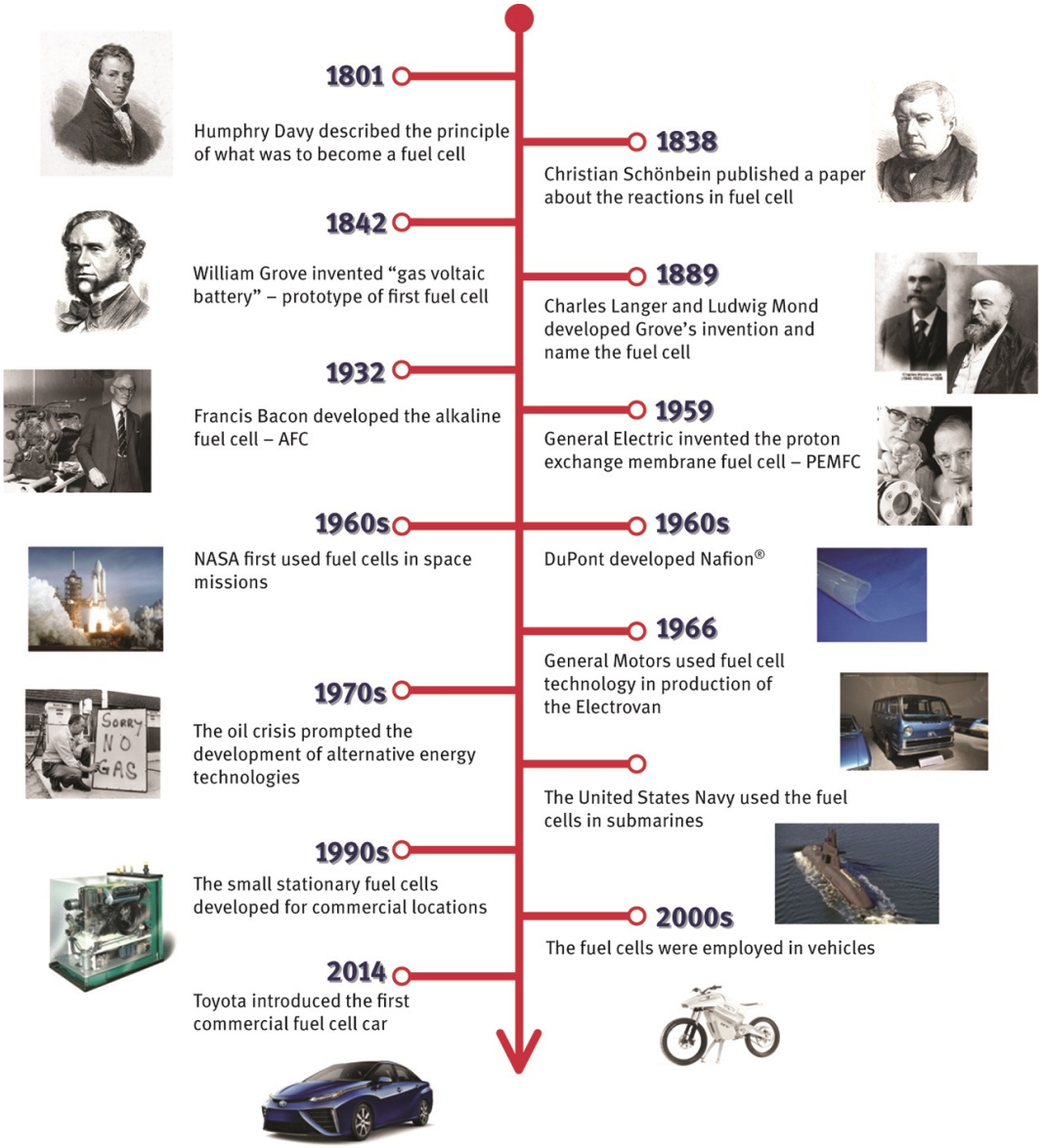

Figure 1.1: Fuel Cell history [4].

1.1.1 Principles and Types

Fuel cells are generators of electricity that convert the energy of a chemical reaction into electrical power continuously. There are many advantages of fuel cells. Compared to rechargeable batteries, the fuel cells have been strengthened in recent years as an attractive alternative. The principle, known for ages, is almost too good to be true. Hydrogen, combined with oxygen from the ambient air, produces current capable of powering the engine of a vehicle. Instead of exhaust gases from internal combustion engines, the by-products are water and some heat. A fuel cell stack is an assembly of several cells in series and produces electricity through an electrochemical reaction. The simultaneous two electrochemical half-cell and overall reactions for a fuel cell are:

$$\begin{aligned} Anode: &\quad H_2 \rightarrow 2H^+ + 2e^- \\ Cathode: &\quad \frac{1}{2}O_2 + 2H^+ + 2e^- \rightarrow H_2O \\ Overall: &\quad \frac{1}{2}O_2 + H_2 \rightarrow H_2O \end{aligned} \tag{1.1}$$

There are various types of fuel cells for different applications. A brief summary of this classification is proposed in Table 1.1. One also distinguishes the fuel cell operating at a low temperature of those operating at high temperature. The fields of application are thus different. We consider here only the ones of the type Proton Exchange Membrane Fuel Cell, abbreviated as PEMFC, which represent the current majority of fuel cell technologies.

The areas of application of PEMFCs are increasingly varied [6]. By far it can be identified in mobile applications including transportation (cars, buses, bikes, aircraft, boats or submarines), aerospace and electronics. Many prototypes of buses and cars are already in circulation and more and more hydrogen fueling stations [7] are emerging. Stationary applications such as micro-Combined Heat and Power (μ-CHP), consists of simultaneously producing two energies: electricity and heat. In this way, a μ-CHP unit allows the power supply for a building without external energy input. In many cases, the Fuel Cell stack is coupled with other energy systems, such as batteries, supercapacitors and solar powers, *etc.* The MYRTE platform [8], located in Corsica France, implements the coupling of solar energy with a hydrogen chain as an energy vector for the storage of renewable energies. It aims to study the deployment of a storage of photovoltaic energy via hydrogen to guarantee the power of renewable energies. Japan's ENE-FARM Program [9] started in 2009 is now the most successful fuel cell commercialization program in the world. It has supported the deployment of well over $120,000$ residential fuel cell units and is providing proof that long-term public-private partnerships can push new technology into the marketplace. The H2ME Project [10] started in 2015 and will run through to 2020. This 5-year project will increase the number of FCEV operating on Europe's roads and will lead to the creation of a pan-European hydrogen fueling station network. In 2016, Toyota presented the world's first commercialized vehicle powered by hydrogen fuel cells [11].

Table 1.1: Comparison of fuel cell technologies [5]

Fuel Cell Type	Operating Temperature	Typical Stack Size	Electrical Efficiency	Applications	Advantages	Challenges
Proton Exchange Membrane (PEM)	$< 120^oC$	$< 1kW - 100kW$	60%	Backup power Portable power Distributed generation Transportation Specialty vehicles	Solid electrolyte reduces corrosion & electrolyte management problems Low temperature Quick start-up and load following	Expensive catalysts Sensitive to fuel impurities Durability Reliability
Alkaline (AFC)	$< 100^oC$	$1 - 100kW$	60%	Military Space Backup power Transportation	Wider range of stable materials allows lower cost components Low temperature Quick start-up	Sensitive to CO2 in fuel and air Electrolyte management Electrolyte conductivity
Phosphoric Acid (PAFC)	$150 - 200^oC$	$5kW - 400kW$, 100 kW module	40%	Distributed generation	Suitable for CHP Increased tolerance to fuel impurities	Expensive catalysts Long start-up time Sulfur sensitivity
Molten Carbonate (MCFC)	$600 - 700^oC$	$300kW - 3MW$, 300 kW module	50%	Electric utility Distributed generation	High efficiency Fuel flexibility Suitable for CHP Hybrid/gas turbine cycle	High temperature corrosion and breakdown of cell components Long start-up time Low power density
Solid Oxide (SOFC)	$500 - 1000^oC$	$1kW - 2MW$	60%	Auxiliary power Electric utility Distributed generation	High efficiency Fuel flexibility Solid electrolyte Suitable for CHP Hybrid/gas turbine cycle	High temperature corrosion and breakdown of cell components Long start-up time Limited number of shutdowns

1.1.2 Balance of Plant

A typical PEM fuel cell system contains three major subsystems: 1) the reactant conditioning system; 2) the thermal management system; 3) the electronic control system. These subsystems are commonly referred to as the fuel cell Balance of Plant (BoP) as shown in Figure.1.2.

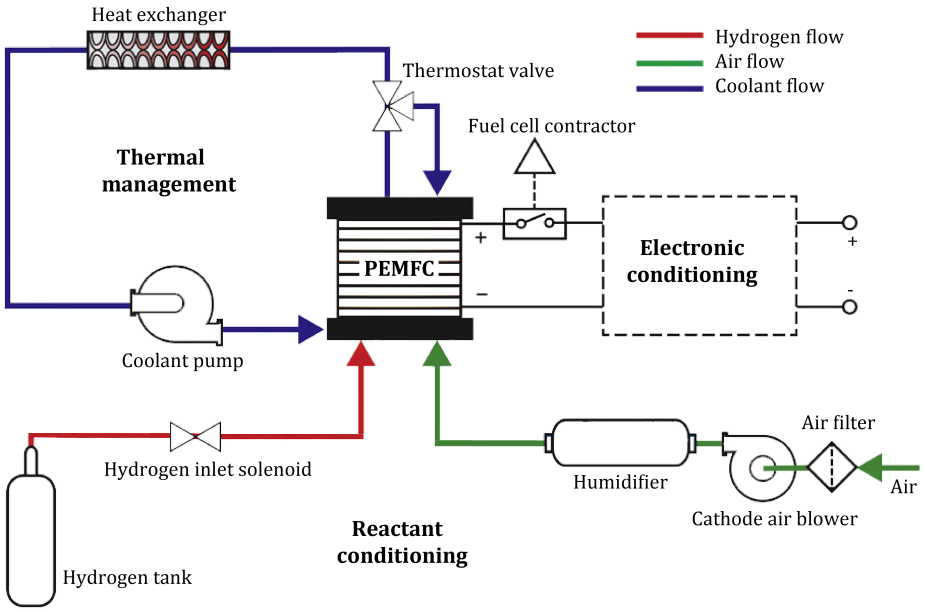

Figure 1.2: Schematic diagram of the PEMFC system [12].

The operating principle is:

- The reactant conditioning system is subjected to transform reactants into a suitable form for the stack fuel consumption. It usually contains the supply tank, the pump, the control valves, the purification parts (*e.g.* filters), and the humidifier.
- The thermal management system is subjected to manage the thermal characteristics of the fuel cell stack. The fuel cell will produce thermal energy while it produces electricity. This amount of heat needs to be dissipated out of the stack to prevent overheating. A fuel cell thermal management system typically contains pumps, control valves, an accumulator, and a heat exchanger to conduct heat to the environment.
- The control electronics system is subjected to regulate and control subsystem operation and stack electrical output. A control electronics subsystem manages the operation of the reactant conditioning and thermal management subsystems as a function of electrical output requirements. This subsystem also incorporates load regulation, *i.e.* via a DC/DC converter, and output buffering capabilities, *i.e.* via a rechargeable battery, to manage system electrical output.

Available measurements on a PEMFC stack test bench are listed in Table 1.2. The measurements are obtained from a test bench which is designed in [13] to continuously control and

measure the operating condition such as stack temperature, gas flows, air hydrogen hygrometry rates, as well as stack voltage and current. During the aging test, two characterization tests including Electrochemical Impedance Spectroscopy (EIS) test and polarization curves are conducted intermittently to understand dynamic and static behaviors of the PEMFC, respectively.

Table 1.2: Measured data from the aging test of a PEMFC [13]

Continuously measured data	**Intermittently measured data**
Single cells and stack voltage	EIS before polarization
Fuel Cell current	Polarization curve
Temperature of cooling Water	EIS after polarization
Cooling flowrate	
Gas temperature	
Gas humidification	
Gas pressure	
H2 flowrate	
Air flowrate	

1.1.3 Stack and Cell

A single cell (type PEM) consists of two primary components [14]. It is depicted in Figure 1.3: 1) the bipolar plates (cathode and anode), and 2) the Membrane Electrode Assembly (MEA). A typical MEA is composed of two gas diffusion layers (GDLs), two active layers (ALs) and a proton exchange membrane (PEM). The GDL is a porous material composed of a dense array of carbon fibers, which provides an electrically conductive pathway for current collection. It performs the following essential functions: the pathway for reactant transport until the AL, medium that optimizes liquid water removal by using polytetrafluoroethylene (PTFE), mechanical support to the MEA and protection of the catalyst layer from corrosion or erosion caused by flows. The AL is a porous structure composed of a network of catalyst nanoparticles of platinum and ionomer fragments. It is the layer where the electrochemical reactions take place. The reaction activity is quantified as the active surface. PEMFC electrodes' materials are similar. Both of the positive (anode) and negative (cathode) electrode are formed by an AL and a GDL. The electrochemically active surface area cannot be measured directly but estimated in specific operating conditions. The PEM is a thin layer of polymer with high ionic conductivity, which conducts protons from the anode to the cathode while preventing electron transport and the crossover of hydrogen fuel and oxygen reactant.

A single cell of the fuel cell stack is structured by stacking two bipolar plates on top of an MEA. Figure 1.4 shows the layout of a typical PEMFC stack with the depictions of operation.

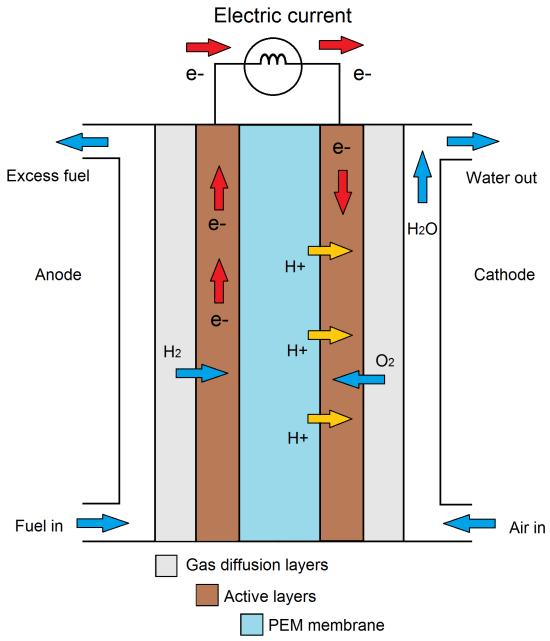

Figure 1.3: PEMFC single cell.

1.1.4 Durability, Reliability and Stability

PEMFC has been developed the past 50 years but still not commercialized in large-scale markets. Although some long-term operations of the PEMFC have been proven [16], and some countries put substantial investments in this technology such as US, Germany, Japan and South Korea, the technology in most parts of the world is still relatively lagging behind. This delay can be firstly caused by the safety issues of hydrogen (highly combustible) and its high prices of production and acquisition.

Another technical barrier for the acceptance of fuel cells as a practical power source is the operation in a wide range of conditions, which may negatively affect durability. For different applications, the requirements for fuel cell lifetime vary significantly, ranging from 5000 h for cars to 20,000 h for buses and 40,000 h of continuous operation for stationary applications [17]. Although the lifespan targets for automobiles are much shorter than those for stationary applications, the operating conditions of dynamic load cycling and startup/shutdown make this goal very challenging for current fuel cell technologies. Unfortunately, at present, most PEMFC stacks provided by manufacturers and research institutes cannot meet the durability requirements listed above.

Moreover, the performance of PEMFCs can and will be affected by several internal and external factors, such as fuel cell design and assembly, deterioration of materials, operating conditions, and contaminants *etc.* Sometimes the performance decay due to the short-term impacts can be recovered. To understand the concepts of PEMFC durability and performance decay discussed in this section, we first clarify the relevant terms [18]:

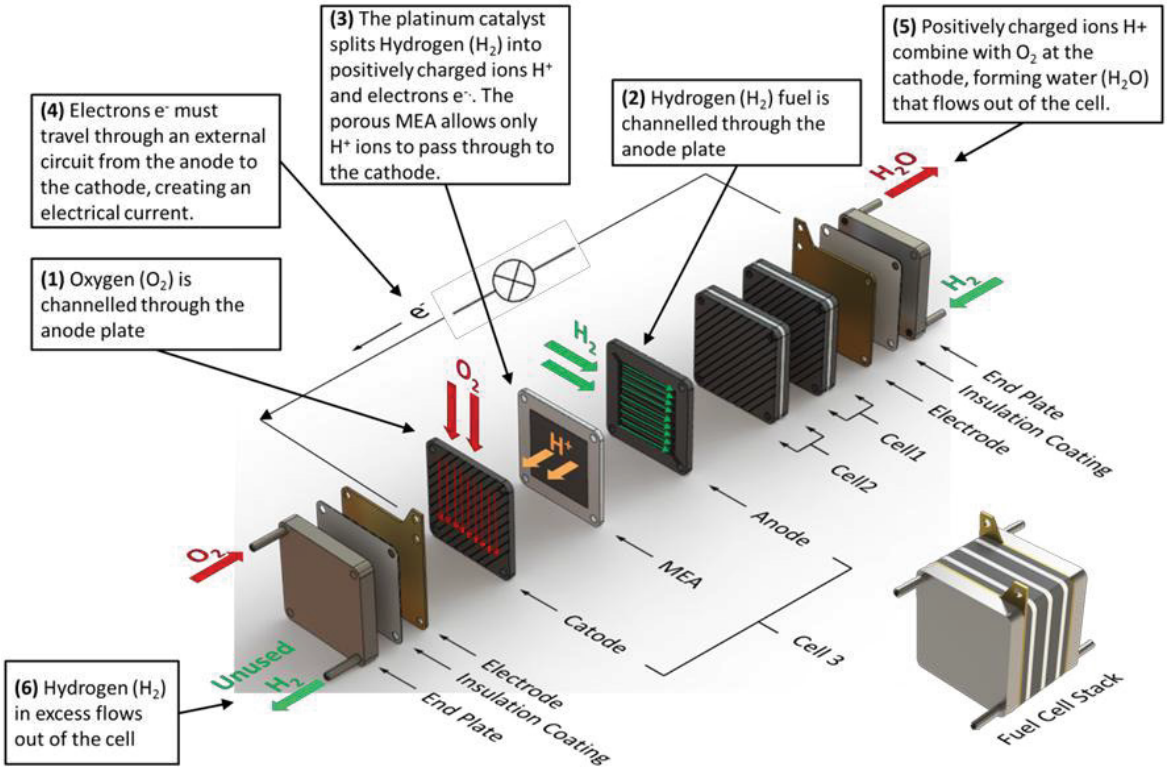

Figure 1.4: Layout and operation of a typical PEMFC stack [15].

- Durability is the ability of a PEMFC to resist permanent change in performance over time. Durability decay does not lead to catastrophic failure but simply to a decrease in performance that is not recoverable or reversible (i.e., due to loss of electrochemical surface area, carbon corrosion, etc.). This issue is referred as aging or irreversible degradation.
- Reliability is the ability of a PEMFC to perform the required function under stated conditions for a period such as the combination of degradation and failure modes that lead to catastrophic failure.
- Stability is the ability to recover power lost during continuous operation. In durability studies, it must always be remembered that part of the decay may be reversible such as the recoverable function of efficiency, voltage or current density decay. The decay is always owing to operating conditions, such as water management, and reversible material changes. This issue is referred as defaults or reversible degradation.

A difficulty is to distinguish the reversible and irreversible. To tackle the issues, understandings of the aging and defaults phenomena are firstly required, which is referred as the degradation mechanisms.

1.1.5 Degradation Mechanisms

Performance degradation is unavoidable but can be minimized through a comprehensive understanding of degradation mechanisms: aging and defaults. PEMFC aging modes are: calendar aging under constant optimal conditions; start and stop cycles and inadequate operating conditions such as temperature, pressure and poor water management. In a fuel cell, the aging process modifies both the performance and components materials. The degradation factors (or "stress factors") are determined by the manner in which the fuel cell is used, and are partly identified by diagnostics studies [19]. However, fuel cell stacks degradation phenomena are still far from being well understood. Consequently, material degradation can be seen on each cell component [20]:

- Gas diffusion layers: changes in GDL properties such as decrease of conductivity and loss of hydrophobicity.
- Active layers: the pure Pt catalyst may be contaminated by supply reactants [21]. The catalyst may lose activity due to migration of Pt particles on the carbon support, or detachment/dissolution of Pt into the electrolyte. It may also lose activity due to the corrosion of carbon support and thus the active surface decreases.
- Membrane: the mechanical, thermal, chemical and electrochemical mechanisms may cause pinhole formation, conductivity loss as well as fuel crossover.

A specific issue with fuel cells is that reversible damages can occur, which may be confused with aging. For instance, incidents due to poor operating conditions that lead to flooding of the channels or the membrane, or drying out of the membrane are reversible when corrected rapidly, and the fuel cell recovers its entire performance after correction. Figure 1.5 shows the performance degradation of a fuel cell stack performance where the recovery phenomena are visible. Sudden drops take place due to the incidents mentioned before, and the jumps represent the recovery. However, if these problems persist, they can lead to material degradation and aging of the fuel cell.

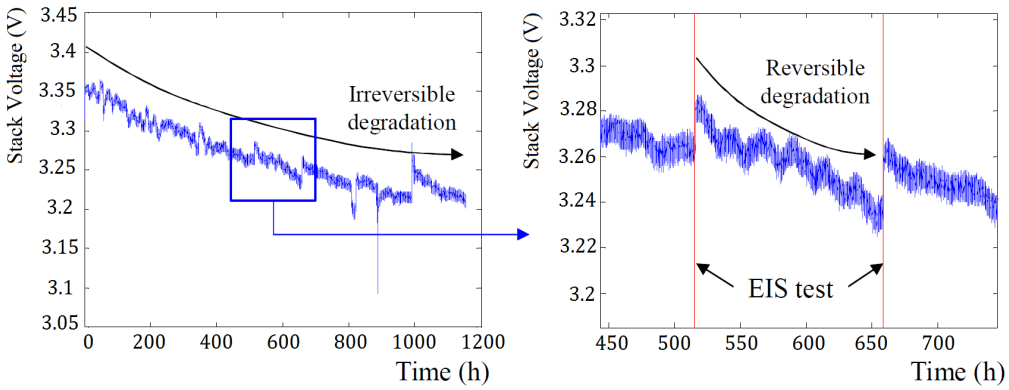

Figure 1.5: Performance degradation of a PEMFC stack with revocery phenomena [22].

The performance decay (*e.g.* decreasing power delivery) is the consequence of all internal and external impacts. To interpret the degradation, the characterization of the electrochemical

device is commonly used.

1.2 PEMFC Characterization

The characterization of PEMFC allows the access to the State Of Health (SOH) of the stack.

1.2.1 State Of Health

The SOH (e:g: from its Begin Of Life (BOL) status of 100% performance to its End Of Life (EOL) status of 0%) provides an indication (not an absolute measurement) of the performance which can be expected from the PEMFC in its current condition and of the amount of lifetime already spent by the component.

During the lifetime of a PEMFC, its performance or "health" tends to deteriorate gradually owing to irreversible physical and chemical changes, which take place with usage and with aging, until the moment the stack is no longer usable.

Any parameter that changes significantly with age, such as cell impedance or conductance, can be used as the basis for indicating the SOH of the cell. These changes of parameters can be identified thanks to the characterization measurements.

1.2.2 Polarization Curve

As any electrochemical cell, fuel cells obey to thermodynamic and kinetic laws. To express the static thermodynamic voltage of an electrochemical cell, E_n, the Nernst Equation can be written as:

$$E_n = E_0 + \frac{RT}{nF} ln(\frac{A_P}{A_R}) \tag{1.2}$$

where E_0 is the electromotive force (emf) in standard conditions, R is the gas constant, A_P and A_R are the activity product of the products and reactants, respectively. For an ideal cell, E_n corresponds to the open circuit voltage (OCV). When a current is drawn from the cell, three kinds of "overvoltage" appear: activation polarization η_{act} (charge transfer at the interface electrode/electrolyte that slows down kinetics), ohmic losses η_Ω (due to the electrical resistance of individual components and their contact), and concentration polarization η_{mass} (due to mass transport limitation at the electrode/electrolyte interface).

For electrochemical cells [23], the voltage behavior is impacted by these polarizations when a current is drawn and the voltage E can be expressed as:

$$E = OCV - \eta_\Omega - \eta_{act} - \eta_{mass} \tag{1.3}$$

A typical polarization curve of PEMFC is shown in Figure 1.6. The polarization curves are related to the stack SOH, thus identifying the parameters of models (such as the one de-

scribed in Equation (1.3)) allows assessing different influences on the parameter, such as aging, changes in temperature, changes in membrane resistance. To obtain dynamical information the Electrochemical Impedance Spectroscopy (EIS) characterization is performed.

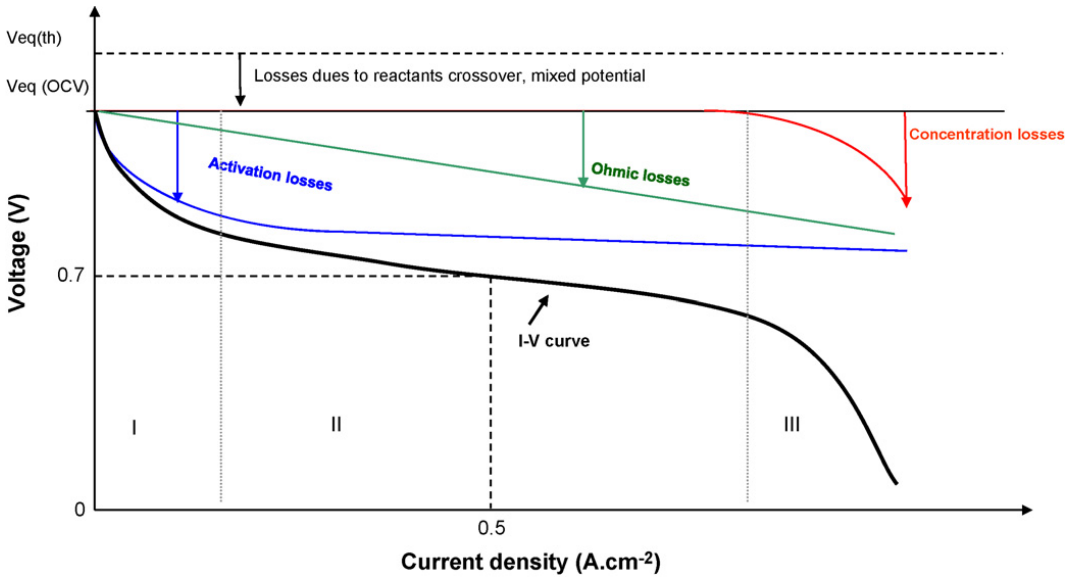

Figure 1.6: Typical polarization curve of PEMFC [24].

1.2.3 Electrochemical Impedance Spectroscopy

Electrochemical impedance spectroscopy (EIS) is a fruitful tool used to characterize dynamics of different phenomena and component materials of electrochemical generators. The principle of the EIS is the following: a sinusoidal low-amplitude current I_{dyn} is applied to the device, which response regarding voltage is U_{dyn}. The impedance of the electrochemical device is thus:

$$Z = \frac{U_{dyn}}{I_{dyn}} \tag{1.4}$$

For fuel cells, the sinusoidal current is added to a static current I_{stat}, and the corresponding part of the voltage is U_{stat}. For a given frequency range, calculation of the impedance Z allows constructing an EIS, which is a Nyquist plot. Figure 1.7 represents the Nyquist diagram for a PEMFC. It can be divided into four parts:

- An inductive part at the highest frequencies (above the kHz), due to connection cables' inductance;
- A purely resistive part, high-frequency resistance Re: around 1 kHz. Mainly due to the ionic resistance of the membrane.
- For intermediate frequencies (usually between 1Hz and 1 kHz), a capacitive loop (C_{dl}) which is due to the accumulation of charges at the electrode-electrolyte interface and the resistance of transfer of the electrons; i.e., charge transfer. The electrochemical reaction with the fastest kinetics is usually preponderant;

- A diffusional part at lowest frequencies (<1Hz) due to diffusion of species (reactants and products), *i.e.*, the mass transfer (Z_W). This part is dominated by the electrochemical reaction with the slowest kinetics.

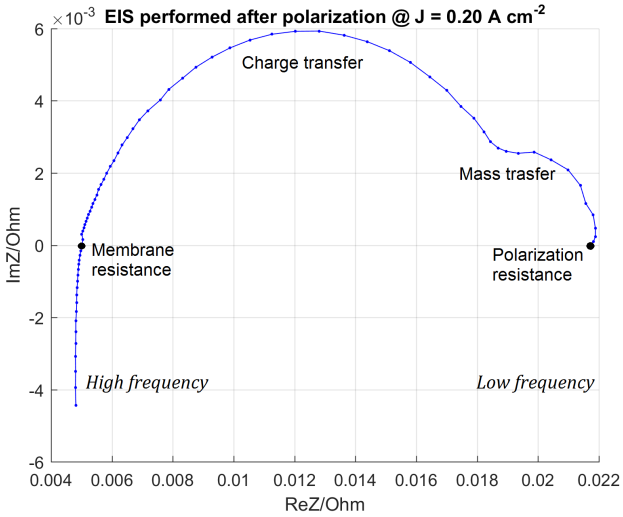

Figure 1.7: Typical EIS curve of PEMFC [25].

The Equivalent Circuit Model (ECM) is commonly used to represent the aging phenomena or default of operation [26] of electrochemical cells (batteries and fuel cells). A general ECM for electrochemical cells is shown in Figure.1.8. The parameters are Re, the ohmic resistance for high frequency; R_{ct}, the charge transfer (polarization) resistance, C_{dl}, the double layer capacitor and Z_W, the non-linear Warburg impedance. The resistance of membrane is modeled as ohmic resistance Re. Thus, the pinhole formation or the conductivity loss at PEM due to aging could reflect on the variation of Re. To describe the effects of the electrodes polarization, the electrode impedance is considered taking into account both the activation and the diffusion losses. It is a combination of a resistance R_{ct} for the charge transfer resistance and a non-linear Warburg impedance Z_W adopted to reproduce the effects of the mass transfer *i.e.*, water and gas diffusion. This value will reflect issues linked to water and gas management, such as flooding, oxygen and hydrogen starvation, etc. Any variation of R_{ct} and Z_W indicates a variation of the activation loss and diffusion loss due to, *i.e.*, PTFE/carbon composition at GDL and Pt catalyst dissolution at AL. The double layer capacitor C_{dl} explains the porous electrodes effect, *i.e.*, inhomogeneous electrode surface or relaxation processes [25]. The ECM parameters can be identified [22] by fitting the Nyquist curves (Figure 1.7) to the ECM depicted in Figure 1.8.

To define a SOH indicator, those parameters could be used as they change with the cell degradation and aging.

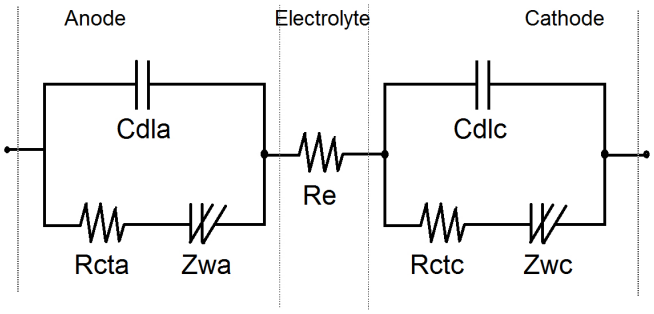

Figure 1.8: A general equivalent circuit model for electrochemical cells.

1.3 Degradation Indicator for PEMFC

In this section, we investigate how to determine a relevant degradation indicator for PEMFC. Unlike for PEMFC, the Li-ion battery's prognosis has been studied for many years, and the experiments are less expensive and much easier to achieve. Batteries and fuel cells are both electrochemical devices with structural similarities, and thus some knowledge on batteries can be transferred to fuel cells.

1.3.1 Li-ion Battery Generality

A Li-ion battery consists of several cells that are electrically connected in series (increasing the maximum voltage) or in parallel (increasing the maximum current). An electrochemical cell, presented in Figure 1.9, comprises a negative electrode where an oxidation reaction occurs and releases electrons as the cell discharges, and a positive electrode where reduction occurs. A stable electrolyte with required high ionic conductivity enables ion transfer between the two electrodes. This process reverses when the cell is at charging: the positive electrode takes the role of oxidation, and the negative takes the role of reduction. The electrodes consist of composite and porous materials: a mixture of a conductive carbonaceous with a polymer ensuring a good mechanical property. The two electrodes are separated by a porous polymer membrane (separator). There is an interface between negative electrode and electrolyte, known as Solid Electrolyte Interphase (SEI). The SEI is naturally generated in the first cycle allowing only the passage of Li-ions to protect the negative electrode from possible corrosion and to protect the electrolyte from reduction. The degradation of the SEI layer is considered as the main factor that influences batteries aging. The external reasons that could cause material degradation and thus accelerate aging (calendar or cycling) may be the improper management of operating conditions (*e.g.*, environmental temperature).

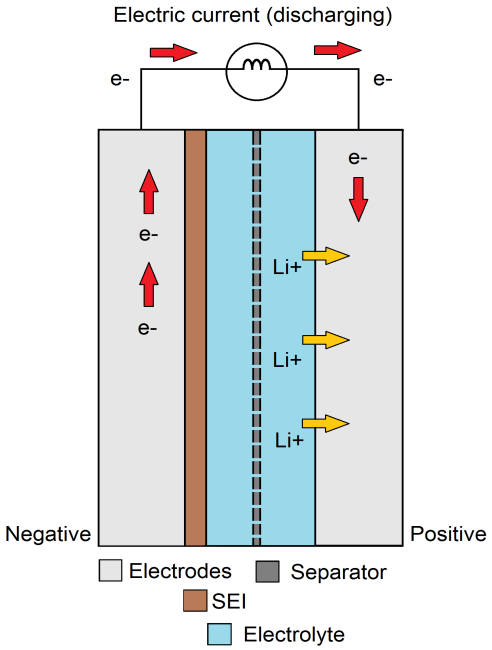

Figure 1.9: Schematics of a Li-ion battery

1.3.1.1 Li-ion battery characterization

For batteries, Figure 1.10 gives the shape of the Nyquist plot obtained in [27], which can be seen similar to the Nyquist plot in Figure 1.7. EIS curves for PEMFC and Li-on batteries show similar shapes of the ideal electrochemical cell. Nevertheless, specific shapes appear for the low frequencies: the battery has a 45^o slope (Warburg line) whereas the PEMFC shows the second semi-circle. Depending on the usage history of the cell, additional semi-circles can be observed. For batteries, for instance, these semicircles originate from the solid electrolyte interface (SEI) layer and the electronic properties of the materials.

The ECM depicted in Figure 1.8 can also be used for Li-ion batteries. For batteries, the double layer capacitor C_{dl} represents the result of the variation of electric potential at the electrode/electrolyte interface, characterizes the charge accumulation phenomena in the double layer. The non-linear Warburg impedance Z_W represents the diffusion phenomena. Li-ion batteries and PEMFC have similar structures with a stack consisting of several elementary cells, each one composed of an assembly of electrode/electrolyte/electrode. Also, the electrochemical principles of battery discharging and PEMFC are nearly the same.

1.3.1.2 Li-ion Battery SOC and SOH

The State Of Charge (SOC) and State Of Health (SOH) are the indicators that are commonly used for batteries. The residual life of batteries is usually the remaining time or the number

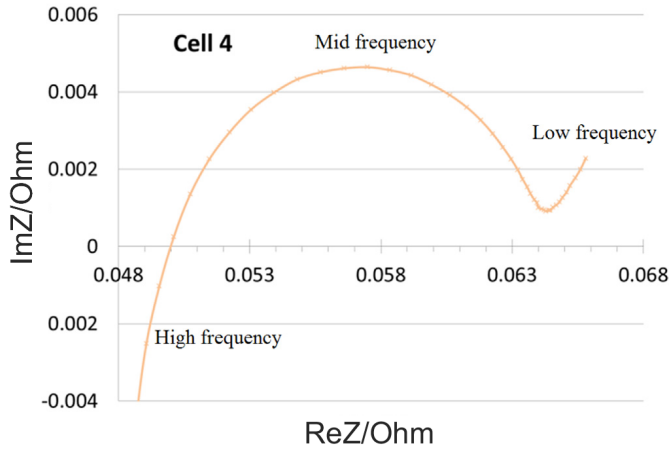

Figure 1.10: Typical EIS curve of lithium battery [27].

of load cycles until the battery reaches its End Of Life (EOL) [2]. The battery SOC can be employed in the figurative sense as a replacement for a fuel gauge used in conventional vehicles. The SOC is the relationship between the residual battery capacity in its present state ($Q_{available}$) and total capacity Q after completely charging the battery, expressed in a percentage (0% = empty; 100% = full):

$$SOC(t) = \frac{Q_{available}(t)}{Q(t)} \tag{1.5}$$

The definition of SOH described in Section 1.2.1 is also suitable for Li-ion batteries. Different methods are proposed to define these indicators. One way of defining SOC and SOH is given visually in Figure 1.11. Compared to battery SOC variation, battery SOH typically changes much slower.

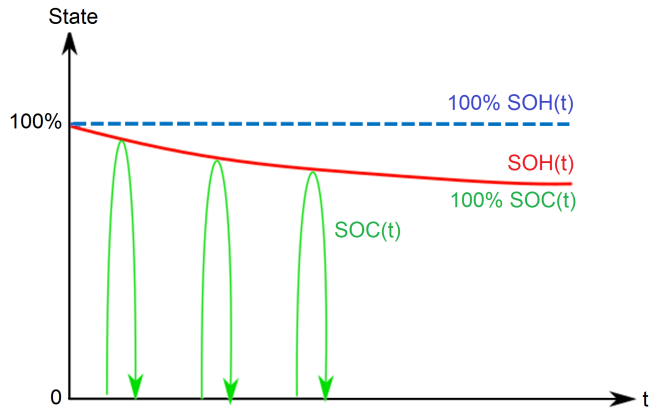

Figure 1.11: SOC and SOH definition based on battery capacity.

1.3.2 Degradation Indicators: from Li-ion Battery to PEMFC

In 2001, Piller et al. [28] proposed an overview of the methods for SOC determination and linked their ability also to determine SOH. Some methods are presently more usual than others, and the most common methods for SOC estimation are open circuit voltage (OCV) and capacity fading. Moreover, EIS is usually considered the best way to determine the SOH. Contrary to batteries, SOC does not exist for fuel cells. Since PEMFCs are continuously fed by external gaseous, it is considered being always fully charged. Subsequently, its 'capacity state' exists neither, or at least it does not have the same meaning. It might be equivalent to the external fuel (hydrogen) storage. However, this 'capacity' does not represent the PEMFC aging. Nevertheless, considering the gases and water management inside the cell could be interesting to introduce the State of Supply (SoS). The health issues of SoS thus can be owing to gas starvation. As for Li-ion battery, SOH has no unique definition since it does not correspond to a particular physical quality. The broader experience in batteries will be used as a basis to discuss the fuel cell SOH determination, and therefore OCV, capacity fading, and EIS will be considered in the sequel.

1.3.2.1 Open Circuit Voltage

The battery Open Circuit Voltage (OCV) gives information about its capacity at current charge status and is therefore widely used for both SOC and SOH estimations [29]–[31]. In [31], a reading of the battery OCV is converted to SOC by using an ECM. A look-up table of OCV-SOC is usually built by an experimental approach. OCV is a common measurement for batteries but for PEMFCs, the OCV measurement can cause severe damage to the fuel cell stack if it takes too long time. Chemical degradation caused by reactant (hydrogen or oxygen) crossover is most severe under OCV conditions. The crossover may lead to the formation of peroxide species, which will accelerate the degradation of the electrolyte membrane and lead to failure of the MEA by compromising the integrity of the electrolyte membrane [31]. For these reasons, this method is not recommended. However, in normal operation, some accidental transient crossing of OCV can still be exploited.

The OCV can be seen on polarization curves. Figure 1.12 depicts the OCV (current density very close to zero) on a time series polarization curves of a PEMFC.

1.3.2.2 Capacity

Capacity is rated in Ampere-hours (Ah) quantifying the available energy stored in a battery. The loss of capacity results in increased impedance and reduced performance. The rate of capacity loss is highly dependent on the operating conditions, such as maximum charge voltage, depth of discharge, the magnitude of current, load profiles and temperature. The traditional charge/discharge/charge cycle still offers a dependable way to measure battery capacity [2], [32], [33]. However, the process is time-consuming, and the battery needs to be removed from service for the duration of the test. Thus, on-board capacity estimation meth-

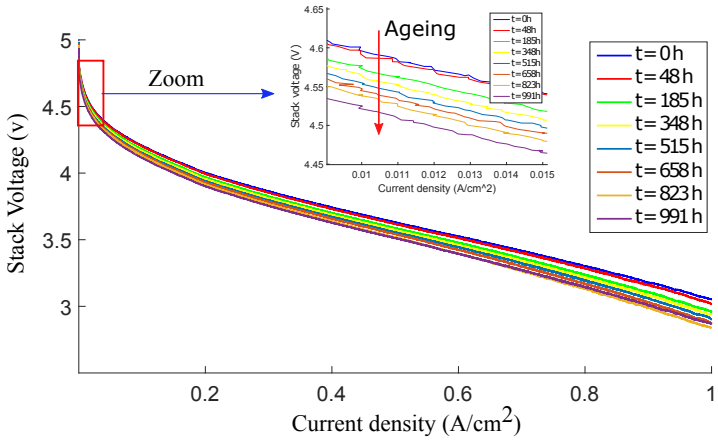

Figure 1.12: Polarization curves with stack aging [13].

ods are searched [2]. When the battery is being charged or discharged, its voltage increases or decreases, respectively. The discharging or charging of a certain amount of Ampere-hours creates a higher voltage change for a battery with a lower capacity than that of a battery of the same type but with a higher capacity. Therefore, the battery capacity can be considered as a parameter defining the relationship between the Ampere-hours charged or discharged from the battery and voltage difference before and after the respective charging or discharging. The determination of this relationship is, therefore, the basic principle of almost all methods for on-board capacity estimation [2]. Those studies on battery capacity fading are based on measurements such as OCV curves.

The performance of Li-ion battery can also be expressed regarding Watt-hours which is the unit of energy measurement indicating how much energy can be drawn from the battery for a certain number of hours [34]. Thus, power fade becomes a more meaningful indicator of battery performance in applications such as hybrid electric vehicles. As a result, power fade modeling and prediction can utilize the same functional forms as used for the capacity fade models. In respect of storage, the PEMFC is not working as an energy pool as Li-ion battery but as an online power converter, and the capacity has thus no meaning. PEMFCs indicator is usually the stack power, which, according to the above section, leads to the same information as the capacity.

1.3.2.3 Electrochemical Impedance Spectroscopy

Figure 1.13 shows the typical trend of the impedance spectroscopy of a lithium battery when it is fully charged [35]. It highlights the aging spectroscopy comparison between experimental impedance spectroscopy and the equivalent circuit model results at different cycle aging. Except for the first cycle of activation, the entire module of the impedance enhances with the aging. In [35], the parameters of the model (Figure 1.14) are reported versus the SOC and at a different number of cycles. Among the different parameters, the ohmic resistance of the battery increases during the aging, but it remains mostly constant during the discharge

cycle. Excluding the aging effects related to the temperature, the enhancement of the ohmic resistance with the aging is probably due to a growth of the SEI on the anode side of the battery, and it is one of the principal reasons for the lithium battery failure.

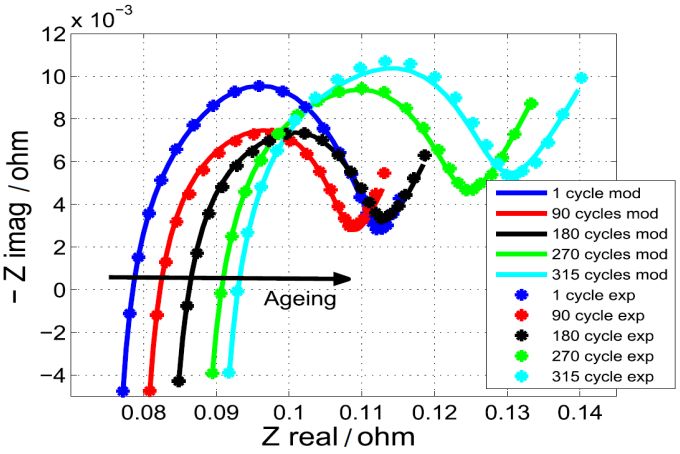

Figure 1.13: Battery EIS acquired at different number of cycles [35].

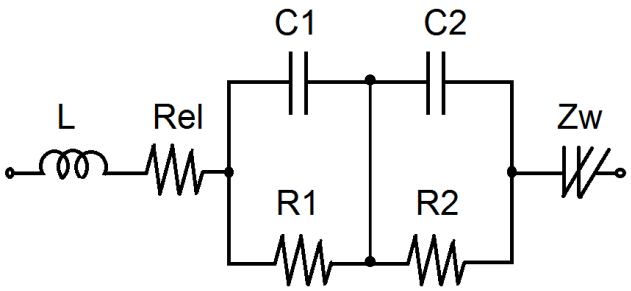

Figure 1.14: A general equivalent circuit model for Li-ion battery [35].

The evolution of the PEMFC EIS diagram at different time stages is shown in Figure 1.15 with data taken in [13]. Similar to Li-ion batteries, the EIS of PEMFC also can be modeled by the ECM which is depicted in Figure 1.16. The two semi-circles are represented by a parallel connection of a resistance and a constant phase element (CPE), which is serially connected to resistance for ohmic resistance. Two inductances are introduced in parallel and in serial, respectively, to describe the inductive behaviors at the high and low frequency. In [22], it is reported that the low-frequency inductance is usually influenced by water transport at the anode and possible carbon monoxide poisoning, while other researchers invoked relaxation of adsorbed intermediates species associated with cathodic reactions. The high-frequency inductive part, on the other hand, is usually associated with connecting element and wires.

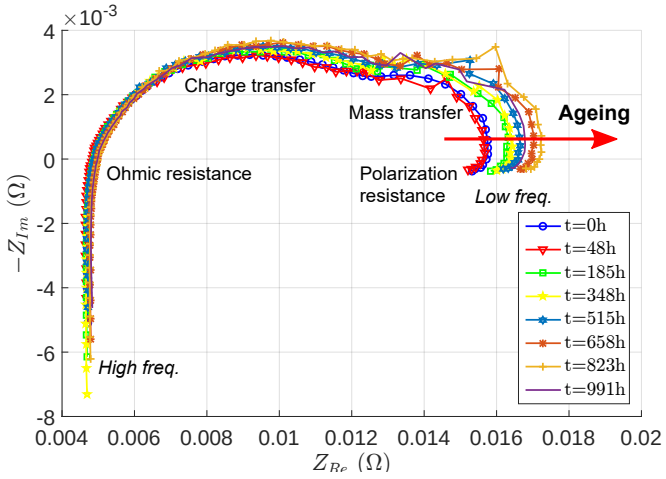

Figure 1.15: PEMFC EIS at different aging stages [13].

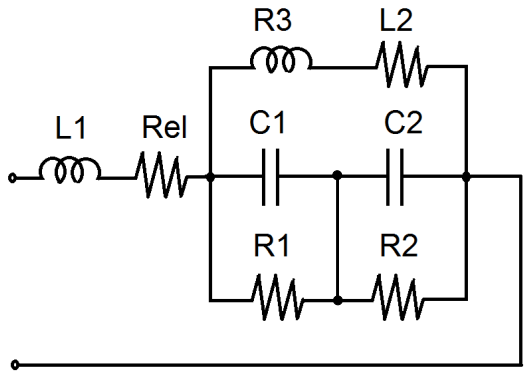

Figure 1.16: A general equivalent circuit model for PEMFC [22].

The ECM model, represented in Figure 1.16, has the following parameters: the resistances R_{el}, R_1, R_2, and R_3 ; the changing phase capacitances C_1, C_2 and the inductances L_1, L_2. According to Kim et al. [22], some parameters remain unchanged with aging (capacitances and inductances) while others (resistances) seem to be sensitive to aging. Thus, R_{el}, R_1, R_2, and R_3 are considered as primary parameters linked to aging. Besides the different resistances, Onanéna et al. [36] selected other parameters to describe the evolution of the EIS diagrams with aging: the minimum value of the imaginary part in the impedance spectrum, its corresponding real part values and its occurring frequency (3 parameters in total). Above all, the aging effects can be seen in EIS either for Li-ion battery or PEMFC, and there are possible models to extract these aging features to interpret their SOH. The EIS is an applicable SOH indicator.

1.3.3 Degradation Indicators for PEMFC

Due to the multi-physic nature of the PEMFC, its SOH is influenced by several interacting parameters. Jouin et al. [37] stated that studying the SOH and aging of the PEMFC require the availability of at least one good indicator that represents the evolution of the system. Several candidates have been reported by the authors, like the catalyst area degradation or the rate of hydrogen that crosses over the membrane. However, these parameters cannot be easily measured, and their monitoring strongly disturbs the PEMFC operation, exacerbates the degradation and accelerates the aging. On the other hand, aging and the majority of degradation mechanisms have a direct impact on the output voltage/power, which is a non-invasive and easy-to-monitor parameter in a PEMFC system. Consequently, voltage is a good candidate to understand and predict the aging of the PEMFC. The observation of an operating PEMFC voltage signal shows the presence of both irreversible and reversible degradations. The irreversible process is due to permanent degradation (aging), and the reversible part is due to incidents or characterization actions. Discriminate between causes is currently an unsolved problem for fuel cells, and is limited by the measurement possibilities and the difficulties of establishing a physical model. Some solutions have been explored to overcome this obstacle for diagnosis purpose, and either using conventional measures [19], the combination of EIS and physical model [26] or using innovative ones [38] are still open ways. Until new approaches are available, EIS is a very interesting characterization tool, either for diagnosis or prognostics. As described before, in addition to the voltage or power signal, extracted parameters from EIS, such as resistances, are good degradation indicators for fuel cells [22], [36]. Since these measures give different information on the fuel cell SOH, it would be interesting to combine them in a hybrid approach.

1.4 Conclusion

In this chapter, we presented the function of the PEMFC. In our view, the interpretation of its lifespan could be expressed regarding both durability and stability. The PEMFC is a very complex system, and the measurement is scarce. Consequently, we investigated what could be transposed from the experience of batteries aging indicators, to the PEM fuel cells. However, a strong limitation of the transplantation is due to the much more complex operation of fuel cell because of the fluidic part. This comparison also reveals that the hybrid approaches, which are developed for batteries, seem to be more suitable to characterize aging and build aging indicators and should be investigated for PEMFC too. SOH is a degradation indicator that has to be defined more precisely in the next chapters. This indicator will be used in the PHM approach. In the next chapters, the PHM approaches will be introduced and ready to be employed for PEMFC.

Chapter 2

Prognostics and Health Management

This chapter introduces first the general concept of Prognostic and Health Management (PHM) and its essential contents of our interests, the Prognostics. Then different techniques are described by reviewing recent literature in this domain and the interests of PHM for PEMFC are explained. Finally, the contributions of this thesis are presented.

Contents

2.1 Prognostics and Health Management

The Prognostics and Health Management (PHM) is a recent dynamic approach to master the lifespan of industrial systems. The objective of PHM is to maximize equipment return on investment by 1) increasing availability and reducing operating costs to optimize maintenance, 2) improving the safety of the system and 3) improving the decision-making process to increase the lifespan of the equipment. It combines scheduled maintenance, condition-based maintenance, and predictive maintenance to enable effective cost versus performance.

Practically, the PHM can be described using several layers (Figure 2.1) which can be grouped into three stages. The system is monitored and data are collected in the observation stage. In the analysis stage, the current state of the system is analyzed and the future state can be investigated. Finally, the action stage allows decisions and transmit the information.

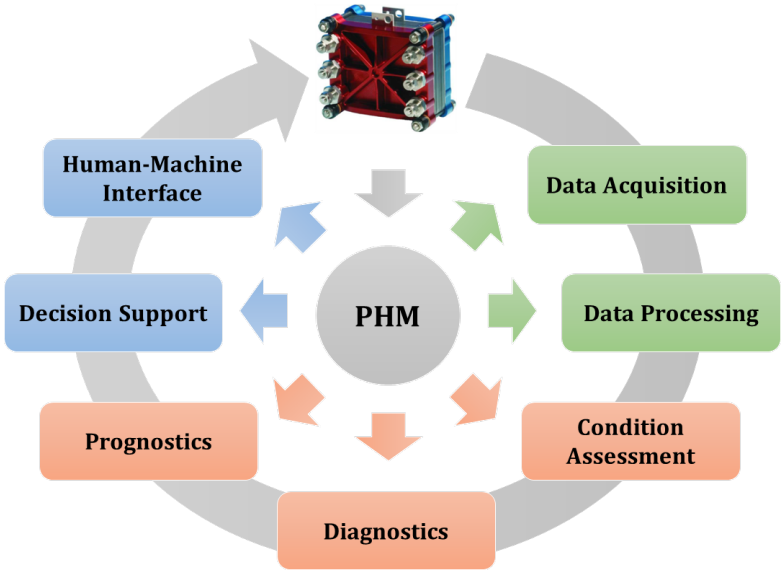

Figure 2.1: PHM framework.

1. *Data Acquisition* In the first step of the process, raw information of the system is obtained by measuring sensors. For a PEMFC, these measurements can be temperature, pressure, humidity, current density, *etc.*
2. *Data processing* The raw data can usually not be used directly. It is necessary to transform them by eliminating noise and extracting useful information which allows the analysis process to take place.
3. *Condition Assessment* The objective in this step is to determine the system state by detecting faults. The data acquired online are compared with the expected values of the system parameters. Alerts must be generated when certain parameters reach critical thresholds.
4. *Diagnostics* This layer suggests the probable causes of the defects. Diagnostics is applied by determining whether the system state has deteriorated. It enables the fault detection, isolation, and identification.
5. *Prognostics* Based on the extracted features and/or the diagnostics information, the prognostics could be implemented. The main objective of this stage is to estimate the remaining useful life (RUL) of the monitored system. As the prediction is always uncertain, uncertainties should be characterized in this layer, *i.e.* with the help of confidence intervals. The future state of the observed component or system is thus predicted from the information obtained in the previous 4 layers.
6. *Decision Support* In this layer, the maintenance decision, i.e. repair, overhaul, etc., can be made on the basis of both diagnostics and the RUL prediction result. This will help to avoid catastrophic failures as well as unnecessary interventions, in other words, to minimize the maintenance cost and improve the availability of systems.
7. *Human-Machine Interface* The different information obtained by the analysis and action layers are transmitted to the user of the property for information and action.

However, the number of layers may vary in literature and this decomposition is not the subject of a standardized definition. According to [39], PHM is a field of research and application which aims at making use of past, present and future information on the environmental, operational and usage conditions of an equipment in order to detect its degradation, diagnose its faults, predict and proactively manage its failures. The main divergence lies in the the nature of the decisions to be taken: the PHM is intended to be more general and adapted to any type of activity. Our research focus on the prediction of PEMFCs' RUL, which leads us to concentrate on the fifth layer: prognostics.

2.2 Prognostics and RUL

2.2.1 Generalities

The key point of PHM approach, as its denomination suggests, is the prognosis [37], [40], the prediction to carry out the maintenance actions at the proper time thanks to the *Prognostics* layer. The definition of prognostics is: analysis of the symptoms of faults to predict future condition and residual life within design parameters [41]. Compared to diagnostics, the literature of prognostics is much scantier mainly due to its new emerging. Diagnostics deals with fault detection, isolation and identification when it occurs. Fault detection is a task to indicate whether something is going wrong in the monitored system; fault isolation is a task to locate the component that is faulty; and fault identification is a task to determine the nature of the fault when it is detected. Prognostics deals with fault prediction before it occurs. Fault prediction is a task to determine whether a fault is impending and estimate how soon and how likely a fault will occur. In general, as illustrated in Figure 2.2, diagnostics is posterior event analysis and prognostics is prior event analysis. In theory, prognostics is likely to be more efficient than diagnostics to achieve zero-downtime performance.

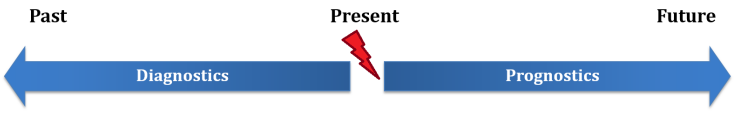

Figure 2.2: Diagnostics vs Prognostics.

The main action in prognostics is the estimation of operating time before failure and risk of existence or subsequent occurrence of one or more failure modes. This allows us to define the Remaining Useful Life (RUL). The RUL is the estimation of the time elapsed between the current moment and the moment when the machine monitored is deemed to be down.

Figure 2.3 shows a typical degradation path estimation. The degradation measurements are used to train the prognostic tool during the learning phase until the prediction time

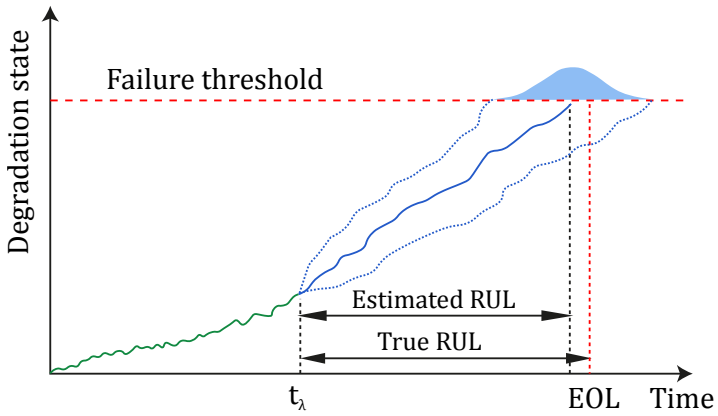

Figure 2.3: Degradation state estimation.

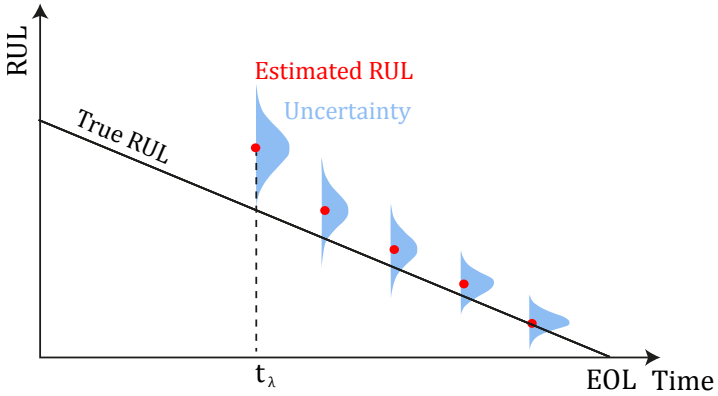

Figure 2.4: RUL predictions at different time.

step t_λ. Then the learned behavior of this degradation path is used to predict the future evolution. The End of Life (EOL) is the time when the degradation path reaches the failure threshold. Then, the RUL can be computed when the predicted degradation path reaches a failure threshold. As shown in Figure 2.4, RUL predictions can be made at different prediction time steps with their uncertainties. Those prediction results can to be used to evaluate the prognostic performance, *e.g.* by comparing with the true RUL.

2.2.2 Prognostic Performance Evaluation

Prognostic performance evaluation is important for a successful PHM system deployment. The early methods borrowed from statistics for prognostic performance evaluation lack of standards due to the varied end-user requirements for different applications, timescales, available information, domain dynamics, etc [42]. However, a missing aspect is the capability of tracking prognostic performance with time. Thus dynamically evaluating the performance is important because prognostics is a dynamic procedure where predictions get updated as more observation become available. Similarly, the performance of life prediction changes with time must be tracked and quantified. As a system approaches a failure threshold, the time window

(or prognostic horizon) to take a corrective action becomes shorter, and consequently, the accuracy of predictions becomes more critical for decision making. Hence, several prognostic performance metrics have evolved with consideration of these issues:

- Prognostic Horizon (PH) quantifies how much in advance an algorithm can predict with a desired accuracy before a failure occurs. A longer PH is preferred as more time is then available for a preventive or corrective action.
- α-λ accuracy further tightens the desired accuracy levels using a shrinking cone of desired accuracy as EOL approaches. In order to comply with desired α-λ specifications at all times an algorithm must improve with time to stay within the zone.
- Relative accuracy index quantifies the accuracy relative to the actual time remaining before failure.
- Coverage index is a binary index which considers whether the true RUL lies within the RUL prediction interval at time index.
- Precision index computes the relative width of the prediction interval.
- Steadiness index quantifies the variance of the predicted RUL distribution.
- Risk index indicates the probability of in-time notifications.

They can be mainly categorized into two types: one is the evaluations based on the estimation errors while the other one is on the basis of the uncertainty assessments. The synthesis of those metrics and the corresponding literature references are listed in Table 2.1.

Table 2.1: Evaluation metrics

Type	Metric	References
Estimation Error-based	Accuracy	[42], [43], [44], [45], [46], [47]
	Steadiness	[46], [48]
Uncertainty-based	α-λ Accuracy	[42], [43], [46]
	Precision	[45], [48]
	Risk	[45], [46], [48], [49]
	Coverage	[48]

A visual representation of these metrics are usually used to depict prognostic performance over a long time horizon. The prognostic performance metrics will be explained in details later on in the following chapter.

2.2.3 Prognostic Approaches

Different approaches to implement the prognostic process can be distinguished in literature, but the definitions are not homogeneous. In earlier works such as [50], the approaches are categorized into four kinds: 1) Knowledge-based models such as expert systems and fuzzy systems; 2) Life expectancy models including conditional probability methods and trend extrapolation;

3) Artificial Neural Networks and 4) Physical models. In most of recent works [51]–[53], the prognostic approaches are commonly categorized into three major types: 1) Model-based methods; 2) Data driven methods and 3) Hybrid methods.

Data-driven Approaches This type of approach does not request system models and is often considered as a "black box" because they can learn the behavior of the system directly from the data collected in the observation layers (*e.g.* by Neural networks [54]). Data driven strategies to prognostics have been applied in various engineering applications [44], [47], [54]–[57]. It is usually simple to implement, and it does not link the internal phenomena with the external observation or predicted states. This approach is therefore flexible to different problems but imposes a high cost of data collection [58], [59]. One of the limitations of data-driven approaches lies in the requirement of training data. Data-driven approaches highly depend on historical data to determine correlations, establish patterns, and evaluate data trends leading to failure. In many cases, there will be insufficient historical or operational data to obtain health estimates and determine trend thresholds for failure prognostics.

Model-based Approaches This type of approach uses mathematical equations to describe the degradation phenomena and predict the physics governing failures. It usually requires knowledge such as the failure mechanisms, material properties, and the external loading *etc* [32], [60]–[63]. This approach is therefore dedicated to the specific applications that were developed and rely on the assumption that the behavior of the system can be described analytically while remaining accurate. However, the necessary knowledge is not always available or mature. Thus it is often deployed in an application where the precision dominates. However, their major disadvantage lies in the fact that, for a real system, it is difficult (sometimes even impossible) to obtain the dynamic model in analytic form to integrate the degradation phenomenon. Hence, the model built for one application cannot be transferred to another application.

Hybrid Approaches The hybrid approaches are the combination of the two previous types. This type of approach is based on physical equations while the parameters change over time are estimated by learning [64]–[66]. The aim is to improve the prognostic accuracy and capability by leveraging their strengths. However, the drawbacks of both approaches are also accumulated. It is necessary to have both types of knowledge, a precise physical model description and a sufficient database. Thus the costs of implementation are getting heavier.

These three categories are debatable. Indeed, model-based approach usually requires a minimum amount of data or measurements for the validation. Therefore, the type of approach should be chosen by considering specifically the characteristics of data and knowledge. Thus appropriate approaches are to be chosen according to the available degradation indicators of the PEMFC.

2.3 Prognostics for PEMFC

2.3.1 State of the Art

The PEMFC has been studied for decades with different research objectives. Indeed, this technology is not completely understood even today. The operation principles are well studied, but certain phenomena produced within the stack are always the hardcore to conquer. Recently, the consideration of prognostics for this system becomes more and more attractive. Numbers of publications are now paying attention to it. The PHM approach is found taking on the responsibility in the face of mastering the PEMFC lifetime.

Diagnostics and Fault Tolerant Control for PEMFC Many works about the PEMFC stack diagnostics exist [67], being linked to diagnostics layer of the PHM framework. A diagnosis of the faults on water management is realized by correlating the support vector machine and a fluidic model in [68]. In [69], a new methodology for determining the complex impedance parameters for PEMFC is proposed to have a general model for embedded diagnosis. The tolerant control strategies applied on PEMFC are reviewed in [70]. The aim of these strategies is to maintain the system performance at the expected level, by detecting and identifying the faults, and finding the optimal operating point to recover/mitigate the faults. In [71], the PEMFC control sub-systems namely the reaction, thermal, water management and power electronic subsystems are reviewed critically, with special attention on control strategies to avoid fuel starvation. The aim of those works is to provide comprehensive basis for optimizing PEMFC lifespan and/or utilization.

PHM Data Challenge Unlike the diagnostics, the prognostics of PEMFC is a more recent problem. The link between PEMFC and PHM have been realized in recent years and a management of multi-stacks fuel cell systems has already been proposed in [72] to extend systems useful life in a PHM framework. The (possibly) first systematic work on prognostics and RUL estimation for PEMFC is presented in 2012 [73]. They investigate a physics-based model for prognostics based on an electrochemical surface area (active area) under different operating conditions. The prognostics of PEMFC was promoted thanks to the PHM challenge in 2014 which was carried out as part of the IEEE PHM 2014 conference in France [13]. This challenge focuses on the RUL prediction of the stack using the data provided by the Federation of Research FCLAB. This challenge proposes two ways of PEMFC prognostics:

1. The RUL estimation from stack output voltage/power.
2. The SOH prediction thanks to the EIS future estimation.

For the RUL estimation challenge, the winner [74] proposes a prognostic approach on the basis of an adaptive particle filtering algorithm. Moreover, five state degradation models (exponential, logarithmic, log-linear, linear and polynomial) are tested and compared. The polynomial degradation model is stated the best. The novelty of this method lies in the introduction of a self-healing factor (reversible degradation) after each characterization and

the adaption of the degradation model parameters to fit the changing degradation trend. The method is depicted in Figure 2.5.

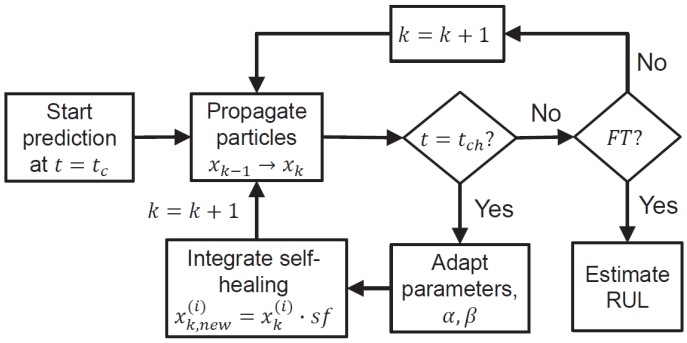

Figure 2.5: Work-flow of parameter adaption and integration of self-healing factors [74]. t_c is the current time, t_{ch} is the characterization time, $x_k^{(i)}$ is the system state for particle i.

The results show that their method is effective in estimating the RUL of PEMFC. However, when the characterization time is reached, they use only the voltage trend changes to adapt the degradation trend model. The information of the characterization itself, such as EIS measurement, has not been used.

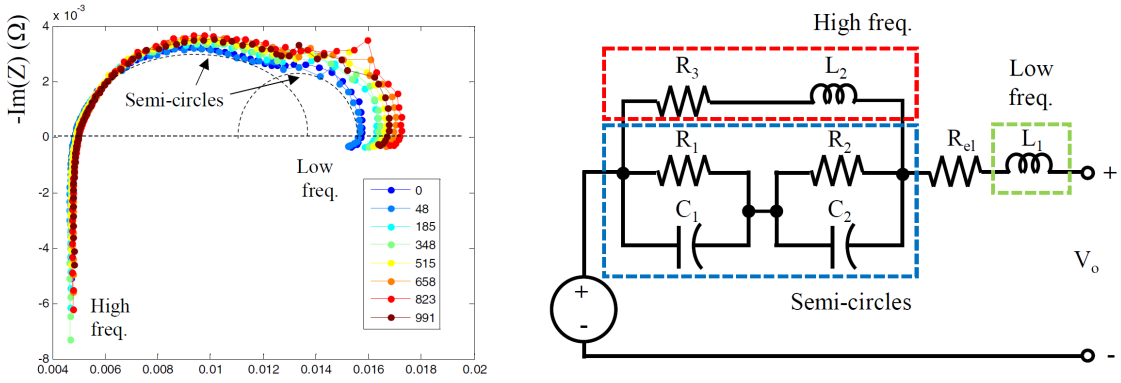

Figure 2.6: EIS curves (lest) and ECM (right) of the PEMFC stack [22].

For the SOH estimation challenge, the winner [22] estimates the impedance values of the PEMFC stack (which represents its SOH) by fitting the EIS spectroscopy curves in Figure 2.6 to an Equivalent Circuit Model (ECM) which is expressed in Equation 2.1.

$$Z_{eq} = \frac{\left(\frac{R_1}{R_1C_1(j\omega)^{n_1}+1} + \frac{R_2}{R_2C_2(j\omega)^{n_2}+1}\right)\cdot R_3 + j\omega L_2}{\frac{R_1}{R_1C_1(j\omega)^{n_1}+1} + \frac{R_2}{R_2C_2(j\omega)^{n_2}+1} + R_3 + j\omega L_2} + R_{el} + j\omega L_1 \tag{2.1}$$

where R_{el}, R_1, R_2, and R_3 are the resistances, C_1, C_2 are the capacitances, L_1, L_2 are the inductance and n_1, n_2 are the Constant Phase Element (CPE) exponents changing the

curvature of the semi-circles (Figure 2.6). The parameters are then identified by fitting the curve to the ECM. The resistances are verified having a linear relationship with the voltage values. Then the voltage values are predicted by a linear regression with the consideration of reversible degradation. Consequently, the corresponding resistance values representing the SOH are obtained.

The former work focuses on RUL prediction and the latter focuses on SOH estimation. Both winners have taken the reversible degradation into account when estimating the voltage degradation. These two works suggest that:

- The output voltage/power is a necessary degradation indicator for RUL prognosis.
- Characterization measurements such as EIS and polarization curves are related to the irreversible degradation and SOH. The parameters of ECM could be used as degradation indicator.

Degradation Trend-based Prognosis A sequence of works has been conducted in this field [17], [37], [74]–[76]. First, a State-of-the-art and remaining challenges of PHM for PEMFC have been reviewed in [37], which identifies the crucial requirements of a great quantity of data to develop complete models for behavior, aging and degradation. Moreover, data for different application and different operating conditions should be gathered to ensure the generality and the transferability of the models. A Particle Filtering-based approach for PEMFC RUL prognosis is proposed in [75] and then the reversible degradation is taken into account in RUL prediction by a joint particle filtering-based prognostic approach in [17]. The PEMFC RUL prognosis are carried out by predicting the stack output power with Particle Filtering-based approaches. These works provide a promising basis of PEMFC RUL prognosis.

Model-based Prognosis Physical model-based approaches for the degradation phenomena have also been developed. A PEMFC model for prognostics purpose is proposed in [77], [78]. The model is composed of a static part and a dynamic parts that are independent. The static part is developed thanks to equations describing the physical phenomena and is based on the Butler-Volmer law that takes into account the activation loss at the cathode and at the anode:

$$V_{DC} = n \cdot \left(E_n - r \cdot j - \frac{1}{A} \cdot asinh(\frac{j}{2 \cdot j_{0a}}) - \frac{1}{B} \cdot asinh(\frac{j}{2 \cdot j_{0c} \cdot (1 - \frac{j}{j_L})} \right) \tag{2.2}$$

where j is the loading current density, E_n is the Nernst potential described in Equation (1.2), r is the internal resistance, A, B are the Tafel parameters; j_{0a}, j_{0c} are the exchange current density, of the anode and the cathode, respectively. j_L is the limit current density at the cathode only. The parameters in the static model described in Equation (2.2) can be identified by fitting it to the polarization curves that represents the stack's static behavior. The dynamic part V_{AC} is an electrical equivalency of physical phenomenon related to the ECM impedance and its model parameters can be identified by fitting it to the EIS spectrum that represents the stack's dynamic behavior. The static model developed from Equation (1.3) can be developed

in different forms. In [79], the PEMFC RUL prediction subjected to a μ-CHP profile is carried out by using an Extended Kalman Filter (EKF) through out a physics-based voltage model:

$$V_{st} = n \cdot \left(E_0 - A \cdot T \cdot ln(\frac{j}{j_0}) - r \cdot j - B \cdot T \cdot ln(1 - \frac{j}{j_L}) \right) \tag{2.3}$$

where n the number of cells in a stack, E_0 is the OCV, V_{st} is the stack voltage, n is the number of cells of the stack, j is the load current density, j_0 is the exchange current density, j_L is the limiting current density, T is the temperature, r is the internal resistance, A is the Tafel constant, and B is the concentration constant. Our interests in these works are that with the physic-based model (voltage model), the information of polarization curve can be extracted.

Moreover, a new definition of SOH is proposed in [79]. It is defined as the degradation rate of the voltage model parameters which can be estimated from polarization curves. This definition allows the investigation on the SOH degradation of the stack, rather than interpreting its output voltage. Moreover, the degradation under different temperature can be investigated with taking into account the temperature T in the voltage model.

Hybrid Prognosis Recently, hybrid approaches are gradually developed and therefore received more attention. The advantage of combining data-driven approach (such as degradation trend regression and Artificial Neural Networks) and physical model-based approach is that, the data limitation or the lack of knowledge can be compromised. In [80], the RUL predictions are carried out by involving statistical degradation model obtained using real degradation tests with Bond-graph. Prognostics problem is formulated as the joint state-parameter estimation problem in PF framework where estimations of state of health (SOH) is obtained in probabilistic domain. In [64], an innovative robust prediction algorithm for performance degradation of PEMFC is proposed based on the combination of a degradation trend model and a Nonlinear Auto Regressive Neural Network (ANRNN) model.

A recent review on PHM for PEMFC is presented in [52] this year with the aiming at identifying research and development opportunities. Through the review of those works, it was found that, although several important research works have already been reported on PHM and RUL prognosis of PEMFC systems, this field is still at the early stage and needs further development. One of the main obstacles identified is the lack of available test and failure data. Another problem is that the aging and failure mechanisms of the PEMFC is not yet entirely clear due to different operating conditions. Moreover, tests for lifetime prediction and durability enhancement studies are usually long-term experimentation (over thousands hours). The possibility of time reduction is proven in [81] by two μ-CHP durability tests, based on the same load demand. The first test is realized in 1000 hours while the second one is reduced to 500 hours resulting in a compressed profile, and the observed voltage degradation rates are similar. An idea is therefore proposed to support accelerated tests protocol development. With the data available now, it can be foreseen that the number of contributions in this domain will significantly increase in the future.

2.3.2 Problem Statement

The prognostics and RUL prediction process for a PEMFC consists of two main steps, each of them leads to specific technical difficulties:

1. Assessing the current degradation level of the PEMFC (stack) by investigating the possible SOH indicators gathered online (output voltage/power, polarization curves and EIS, *etc.*) and developing a degradation model. This model should describe the temporal evolution of the stack performance degradation and support the prediction of future evolution.
2. Developing the RUL prediction on the basis of the degradation model for the stack, integrating available online information on its internal state and/or the external operating conditions.

As being discussed in previous sections, applying prognostics to PEMFC stacks is a good solution in respect of extending their lifespan. However, since PEMFC is a multi-scale and multi-physics system, the development and implementation of an efficient prognostics procedure face various challenges:

1. Although various measurements of the PEMFC are available, the definition of a proper health indicator of a PEMFC stack for prognostic purpose is rare. Not every information from measurements is a good candidate.

   Our starting point -and first research subject- is to identify the PHM-oriented features (degradation indicators) of the PEMFC.
2. The reversible/irreversible degradation behaviors significantly impact the lifespan of the PEMFC. The reversible degradation (often refer to 'defaults') can be recovered sometimes, but it may result in the performance decay and contribute to the degradation at the stacks level.

   On this issue, our aim is to take into account different degradation behaviors, irreversible and reversible degradation, in the degradation path estimation and thus give more accurate and precise RUL predictions.
3. It becomes more difficult when applying prognostics to the PEMFC under different operating conditions, together with multiple causes that lead to degradation (degradation covariates). The intertwined effects lead to complexity and difficulty in building an appropriate degradation model and to apply prognostics to PEMFC. With only information from only one level would not be enough to handling the complicated degradation mechanisms. Our objective is to investigate and explore different ways of using the degradation covariates from the intermittently measurements at different levels, such as EIS and polarization curves, such that different sources at different levels of the PEMFC can be merged and contribute to the RUL prognosis.

2.4 Contributions of the Thesis

The main work of this thesis concentrates on the development of prognostic approaches for PEMFCs' RUL with the consideration of dynamic operating conditions and degradation covariates at multiple levels. In this thesis, a complete review of the existing deterioration models and the corresponding RUL estimation methods have been conducted first in Chapter 2. This review is essential to develop extended degradation models for PEMFC and methods for RUL prediction in Chapter 3. Indeed, it helps to have a comprehensive overview of the models and methods that have been used in the literature as well as to analyze their advantages and limitations.

The analysis of the literature on PEMFC prognostics, and even on prognostics in general, shows that no work (or only few works as far as prognostics in general is concerned) has addressed the issue of using heterogeneous deterioration gathered at different levels in a system to perform a RUL estimation. In a deteriorating system, there are often degradation covariates or deterioration indicators that cannot be directly observed but that can be interesting and useful to use to improve the prognostics performance. Thus, we have paid a special attention on the possible use of these degradation covariates and we have focused our work on proposing solutions to perform RUL predictions using the information at different levels in Chapter 4 (to tackle the problem raised by the existence of reversible deterioration vs. irreversible deterioration) and Chapter 5.

In addition, many works found in literature providing prognostic methods based on large quantity of historical run-to-fail data. Those methods rarely appear in PEMFC applications because of the high costs of long-term run-to-fail tests on PEMFC stacks. However, we consider them another possible future solution to PEMFC RUL assessments as the growth of researches on prognostics for PEMFC continues. Therefore, we propose also an ensemble approach which uses the historical knowledge and the monitoring information at different levels to improve the RUL prediction accuracy in Chapter 6.

Based on the literature review analysis and motivated by some issues found still open, the main contributions of this thesis can be summarized as follows:

1. Adaptation of the state-of-the-art of stochastic deterioration models and associated RUL estimation methods to the PEMFC application (Chapter 3).
2. Extension beyond the state-of-the-art to take into account in different ways the different deterioration information available at different levels of the system ; on this problem our contribution is threefold:
    - Development of a RUL prognosis approach taking into account the reversible degradation by using multiple degradation indicators (Chapter 4).
    - Proposition of a deterioration covariate inspection scheme to gather additional deterioration information when necessary in order to reach an optimal tradeoff between performance (accuracy and precision) and cost (monitoring cost due to inspections) for the deterioration estimation and RUL prediction (Chapter 5).

- Development of a model ensemble approach that combines the RUL predictions from different sources at different levels, to improve the prognostic accuracy and precision. The RUL uncertainties from different sources are also merged by the ensemble to provide more precise and complete predictions (Chapter 6).

These contributions are presented in details in the following chapters.

List of Publications

During the thesis, several papers have been published to present these contributions:

- D. Zhang, P. Baraldi, C. Cadet, N. Yousfi-Steiner, C. Bérenguer and E. Zio (2018) An ensemble of models for integrating dependent sources of information for the prognosis of the remaining useful life of Proton Exchange Membrane Fuel Cells. *Mechanical Systems and Signal Processing*, under review.
- D. Zhang, C. Cadet, N. Yousfi-Steiner and C. Bérenguer (2018) PEMFC RUL Prognostics Considering Degradation Recovery Phenomena. *Proceedings of the Institution of Mechanical Engineers, Part O: Journal of Risk and Reliability*, accepted.
- D. Zhang, C. Cadet, N. Yousfi-Steiner, F. Druart and C. Bérenguer (2017) PHM-oriented Degradation Indicators for Batteries and Fuel Cells. *Fuel Cells*, 17(2), pp.268-276. DOI: 10.1002/fuce.201600075.
- D. Zhang, C. Cadet, N. Yousfi-Steiner and C. Bérenguer (2017) A Study of Online Inspection for Multi-level Prognostics. In: *IFAC-PapersOnLine*, 50(1), pp.13716-13721. DOI: 10.1016/j.ifacol.2017.08.2549.
- D. Zhang, P. Baraldi, C. Cadet, N. Yousfi-Steiner, C. Bérenguer and E. Zio (2017) A Study of Local Aggregation of An Ensemble of Models for RUL Prediction. In: *The 10th International Conference on Mathematical Methods in Reliability (MMR 2017)*, July 3-6, 2017, Grenoble, France.
- D. Zhang, C. Cadet, N. Yousfi-Steiner and C. Bérenguer (2016) Some Improvements of Particle Filtering Based Prognosis for PEM Fuel Cells. In: *IFAC-PapersOnLine*, volume 49. pp.162-167. DOI: 0.1016/j.ifacol.2016.11.028.
- D. Zhang, C. Cadet, N. Yousfi-Steiner and C. Bérenguer (2015) PHM-oriented degradation indicators for PEM fuel cells:What can be learnt from battery State of Charge estimation . In: *Proc. 6th International Conference on Fundamentals & Development of Fuel Cells*, Paper 190. Feb 2015, Toulouse, France.

Chapter 3

Particle Filtering-based Prognostics

This chapter presents the methodology in the context of prognostics. We review the degradation models and present a Particle Filtering-base approach for the RUL prediction purpose. The procedure will be described in detail by implementing a numerical example. The way of interpreting the results is introduced and discussed.

Contents

3.1 Degradation Models

Information on system state and performance can often be collected over its operating time. This information is converted to system durability and reliability information with appropriate models and data analysis techniques. It can be used to provide assessments of short-term and long-term durability and reliability, and for planning maintenance actions such as repairs and replacements. Information on system state and performance collected over time is referred as degradation data. Depending on the application, various types of system state information can be used as a degradation indicator, such as the delivered performance, size of a fatigue crack, the temperature of a system, or the resistance or conductivity of individual components.

3.1.1 General regression models

The approximate data analysis approach is simple and commonly used [82] to construct a degradation path model by the following steps:

1. Find a transformation for the observed degradation path such that the transformed degradation paths are approximate functions of time.
2. Fit simple regression lines to the observed degradation path for the system.
3. Use the fitted lines to predict the time at which the system will reach the specified failure-definition level.

Furthermore, random coefficient regression methods are used to depict the degradation path and then infer the RUL distribution [58]. A general nonlinear regression model to characterize the degradation path of a population of units is described in [83]:

$$Y(t) = D(t, \phi, \theta) + \nu(t) \tag{3.1}$$

where $Y(t)$ is the observed measurement at time t, $D(t, \phi, \theta)$ is the actual degradation state at time t , ϕ is the fixed regression coefficients for all units, θ is the random effect for individual unit, and $\nu(t)$ is the measurement noise. This Equation (3.1) can be transferred on single operating unit whereas θ becomes the random time varying effect for the single unit. With this model, the RUL can be defined as:

$$RUL_t = \{r_t : D(t + r_t; \phi, \theta) \geq FT | D(t; \phi, \theta) < FT\} \tag{3.2}$$

where FT is a predefined Failure Threshold, r_t is the RUL given the current state at time t.

For simple problems, the degradation paths can be approximated with the regression models, which is attractive because the computations are relatively simple. However, when the degradation paths cannot be approximated, the stochastic models are employed for more practical cases.

3.1.2 Stochastic models

Stochastic models are used for modeling the processes that have some randomness. They represent the situation where uncertainties are present. Probabilities are assigned to the events within the model. These probabilities can be used to make predictions or provide other relevant information about the process. Stochastic models that specify the degradation paths are useful in degradation analysis. It is used to account for example time-varying or unit-to-unit variability in the degradation paths. This variability might be caused, *e.g.* by initial conditions, material properties, operating and environmental conditions, *etc.* The stochastic models, such as Gamma process model and Wiener process model, are more general approaches for analyzing degradation data [84].

Gamma process model Sometimes, degradation processes are monotonic and evolving only in one direction, as in wear processes or fatigue crack propagation for examples. In such cases, a Gamma process is a natural model for the degradation processes in which the deterioration is supposed to take place gradually over time in a sequence of tiny positive increments. The increment $\Delta Y = Y(t_k) - Y(t_{k-1})$ for a given time interval $\Delta t = t_k - t_{k-1}$ has a Gamma distribution:

$$Y(t) = \Gamma(\alpha(t_k) - \alpha(t_{k-1}), \beta) \tag{3.3}$$

with shape function $\alpha(t) > 0$ and scale parameter $\beta > 0$. Over a time interval of length t, the average degradation speed-rate for a Gamma process is $\alpha(t) \cdot \beta$ and its variance $\alpha(t) \cdot \beta^2$. The choice of α and β allows modeling various degradation behaviors from almost-deterministic to chaotic. Given the degradation data, these parameters can be estimated using classical statistical methods such as maximum likelihood method, moment method, Bayesian statistics method, etc [85]. The definition of the RUL at time t can be represented by the First Hitting Time (FHT) of $Y(t), t \geq 0$ crossing the FT:

$$RUL_t = inf\{r_t : Y(t + r_t) \geq FT | Y(t) < FT\} \tag{3.4}$$

The advantage of the Gamma process for RUL estimation is that the required mathematical calculations are relatively straightforward and the physical meaning is easy to understand, and Gamma process-based degradation models can take the temporal variability into account [58]. However, we should note that the Gamma process seems to be only appropriate to represent degradation by the strictly monotonic process. This property is usually held for the direct health indicators.

Such models can model a wide range of degradation processes. However, they suffer from the limitation that is those models do not take into account the dynamic operating conditions. In practical, changes of environmental factors, such as changes in temperatures, humidity, pressure, *etc.*, could significantly affect the deterioration processes.

3.1.3 Bayesian approaches

When the interest is in dynamic operating condition, Bayesian updating models are often used. A Bayesian updating method is developed in [86]. It uses real-time condition monitoring information to update the stochastic parameters of degradation models, where θ in Equation (3.1) becomes the time-varying parameter for the degradation model. Many variants have been developed along this line through taking time-varying environments and absence of prior knowledge into account [87], [88].

Consider a system under operation subject to degradation from new till its EOL. The system and the observation that describes the evolution of the degradation are assumed to be governed by discrete-time state transition models. They are composed of the evolution equation, $f(\cdot)$, describing the system's dynamics, and the observation equation, $g(\cdot)$, which links the measurements with the true (hidden) system's state. The following discrete-time state space description represents a very general dynamic system:

$$x_k = f_k(x_{k-1}, \omega_{k-1}, \Theta_{k-1}) \tag{3.5a}$$

$$z_k = g_k(x_k, \nu_k) \tag{3.5b}$$

where k is the time index, x is the system state, z is the observation, Θ is the vector of the model parameters ($\Theta = [\theta_1, \theta_2, ...]$), ω and ν are the process noise and measurement noise, respectively. In the Bayesian theory, everything unknown is considered as a stochastic variable. This leads to a description, where the initial or prior distribution is assumed to be known. Using the observations, the estimate can be revised by computing the posterior density. The following regression models are usually deployed to approximate the PEMFC output voltage/power degradation path:

- Linear model:
$$x_k = \beta_k \cdot (t_k - t_{k-1}) + x_{k-1} \tag{3.6}$$
- Polynomial model:
$$x_k = \alpha_k \cdot (t_k - t_{k-1})^2 + \beta_k \cdot (t_k - t_{k-1}) + x_{k-1} \tag{3.7}$$
- Exponential model:
$$x_k = exp\,(\beta_k \cdot (t_k - t_{k-1})) \cdot x_{k-1} \tag{3.8}$$
- Logarithmic model:
$$x_k = \alpha_k \cdot ln(\frac{t_k}{t_{k-1}}) + x_{k-1} \tag{3.9}$$

where α_k and β_k are the degradation model parameters. The Bayesian estimation techniques provide a framework which can estimate the parameters or the state of a nonlinear stochastic system using noisy measurements as observations. The Bayesian estimation techniques provide a framework which can deal with high uncertainties in degradation processes. Various recent developments in the area of nonlinear state estimators from a Bayesian perspective are reviewed in [89]. Bayesian estimation with the particle filtering (PF) is not limited by either linearity or Gaussian noise assumption. PF-based approaches are more and more employed for prognostics purposes, the development of this tool in the prognostics' field is thoroughly reviewed and discussed in [90].

3.2 Particle Filtering

In estimation problems, the task is to estimate unknown quantities from noisy observations, often with the prior knowledge available. Thus, it is natural to use a Bayesian approach. Particle Filtering (PF) is an accurate recursive state estimation techniques for nonlinear and non-Gaussian problems. It provides general solutions to many problems, where linearizations and Gaussian approximations are intractable or would yield too low performance [91]. Therefore, non-Gaussian noise assumptions and incorporation of constraints on the state variables can also be performed naturally.

3.2.1 Particle Filtering Algorithm

In a PF framework [92], the estimation of the degradation state is based on its prior Probability Density Function (PDF) and the degradation model parameters. The Bayesian update is processed sequentially by propagating particles carrying probabilistic information on the unknown states and model parameters, as illustrated in Figure 3.1.

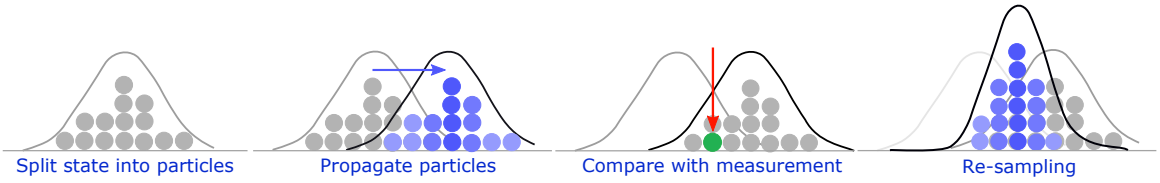

Figure 3.1: Illustration of Particle Filtering

The PF algorithm is summarized in Algorithm 1. The approximation of the probability distribution of the system state is based on sampled particles and associated weights. Bayesian updating is processed sequentially by propagating particles carrying probabilistic information on the unknown states and model parameters. The probabilistic model for the particles propagation relies on the state transition model (5.1) and the probability distribution of the process noise ω_k:

1. Split the initial state into $i = 1, \ldots, n$ particles representing the system state probability density function (PDF).
2. Propagate $i = 1, \ldots, n$ particles representing the system state probability density function (PDF) from x_{k-1} to x_k by the state transition model described in Equation (5.1) (*Algorithm 1, line 5*).
3. For each particle, estimate the associated weight by calculating its likelihood given an online measurement z_k (*Algorithm 1, line 6*). This gives the corresponding weight of each particle (assuming the measurement noise $\nu_k \sim \mathcal{N}(0, \sigma_{\nu_k}^2)$ is normally distributed):

$$\mathcal{L}(z_k | x_k^i, \sigma_{\nu_k}^i) = \frac{1}{\sqrt{2\pi}\sigma_{\nu_k}^i} exp[-\frac{1}{2}(\frac{z_k - x_k^i}{\sigma_{\nu_k}^i})^2] \tag{3.10}$$

4. Perform resampling [93] to remove the particles with small weights relative to a given weight limit and replicated those with large weights (*Algorithm 1, line 10 to 17*).
5. The posterior PDF built using resampling in step (4) is used as the prior for the following iteration.

The process is performed until no measurement is available (prediction time $t_\lambda = k_p \cdot \Delta t$ reached). For the RUL prediction, the posterior PDFs of the state and model parameters, given the observation sequence up to time t_λ, are used to estimate the future evolution of the particles. The RUL PDF can be obtained when the particles representing the system state reach the preset failure threshold. The prognostic procedure is summarized in Algorithm 2.

Algorithm 1 Particle Filtering

Initialize $x_0^i, \sigma_{\omega 0}^i, \sigma_{\nu 0}^i$ and Θ_0^i // Drawn from initial uniform distribution
Time step $k = 1$
while $x_k^i > FT$ and $k \leq k_p$
  for $i = 1, \ldots, n$
  // Importance sampling:
    Draw particles $x_k^i \sim p(x_k^i | x_{k-1}^i, \sigma_{\omega k-1}^i, \Theta_{k-1}^i)$
    Assign weight $w_k^i = \mathcal{L}(z_k | x_k^i, \sigma_{\nu k}^i)$ using Equation (3.10)
  end for
  Normalize weight $w_k^i = w_k^i / \sum_{i=1}^{n} w_k^i$
  Calculate the cumulative sum of normalized weights:
  $\{Q_k^i\}_{i=1}^n = Cumsum\left(\{w_k^i\}_{i=1}^n\right)$
  for $i = 1, \ldots, n$
  // Re-sampling (Multinomial):
    $j = 1$
    Draw a random value $u^i \sim \mathcal{U}(0, 1]$
    while $Q_k^j < u^i$
      $j = j + 1$
    end while
    Update state $x_k^i = x_k^j$
    Update noises $\sigma_{\omega k}^i = \sigma_{\omega k}^j, \sigma_{\nu k}^i = \sigma_{\nu k}^j$
    Update parameters $\Theta_k^i = \Theta_k^j$
  end for
  $k = k + 1$
end while

Algorithm 2 RUL prediction

$k = k_p$ // Start from the prediction time
for $i = 1, \ldots, n$
  Use model parameters estimated at time t_p (from Algorithm 1) : $\Theta_k^i, \sigma_{\omega k}^i$
  while $x_k^i > FT$
    Propagate particles $x_k^i = f(x_{k-1}^i, \sigma_{\omega k-1}^i, \Theta_{k-1}^i)$
    $k = k + 1$
  end while
  Estimate $\widehat{RUL}_k^i = (k - k_p) \cdot \Delta t$
end for

3.3 Numerical Example

3.3.1 Data Generation

We generate a set of data to simulate a degradation process, of which the true model parameters are known whereas the process noise, and the measurement noise can be manipulated. A simple linear model is chosen to generate the degradation state:

$$f(x_{k-1}, t_{k-1}, t_k) = \beta_k \cdot (t_k - t_{k-1}) + x_{k-1} + \omega_k, \quad \omega_k \sim \mathcal{N}(0, \sigma_\omega^2) \tag{3.11}$$

where ω_k is a Gaussian zero-mean process noise (variance σ_ω^2). The observation is simulated as a Gaussian distribution around the true value of the state x with a known standard deviation σ_ν for measurement noise:

$$z_k = x_k + \nu_k, \quad \nu_k \sim \mathcal{N}(0, \sigma_\nu^2) \tag{3.12}$$

The values of initial degradation state and all the model parameters are listed in Table 3.1

Table 3.1: Parameters values used for degradation simulation

Parameter	x_0	β_k	σ_ν	σ_ω
Values	235	0.04	0.1	1

Measurements data are generated (Figure 3.2) to have similar phenomena to the PEMFC. The failure threshold is fixed to 87.5% of its initial value, so the true End of Life (EOL) is found at 970 steps.

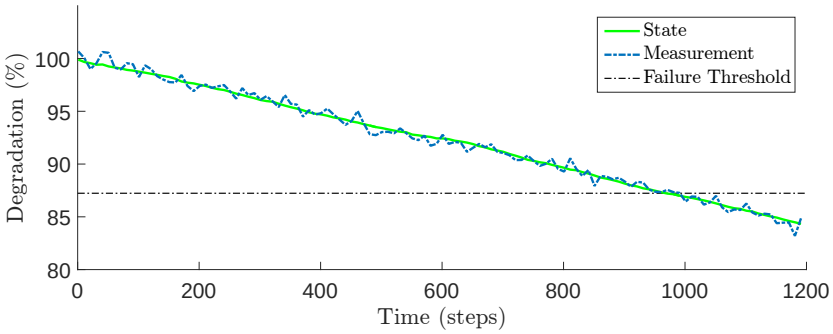

Figure 3.2: Observation generated from the model.

3.3.2 Degradation Model

The same degradation model used in data generation is chosen such that the tuning of the parameters can be easily notices:

$$f(x_{k-1}, t_{k-1}, t_k) = \beta_k \cdot (t_k - t_{k-1}) + x_{k-1} \tag{3.13}$$

Considering the randomness in process and the measurement noise in observation, the state transition equation and the measurement equation can be thus written:

$$\begin{aligned} x_k &= \beta_k \cdot (t_k - t_{k-1}) + x_{k-1} + \omega_k \\ z_k &= x_k + \nu_k \end{aligned} \tag{3.14}$$

where ω_k is a Gaussian zero-mean process noise (variance σ_ω^2), ν_k is a Gaussian zero-mean measurement noise (variance σ_ν^2) and z_k is the observation.

3.3.3 Particle Filter Settings

3.3.3.1 Number of particles

To avoid the degeneracy problem, a large number of particles is preferred. For the choice of the number of particles, there is no specific algorithm. The most common way is to think about the trade-off between computational cost and the variance of the resulting estimations. As we increase the number of particles or sample size the former increase, while the latter decreases. We create a grid of potential numbers of particles (*i.e.* $1000, 2000, \cdots, 2.10^4$) and run the filtering several times using each sample size. We plot the sample variance of the quantity where we are interested in (*i.e.* the variance of the estimation error) on the Y axis, with the number of particles on the X-axis. The curves in Figure 3.3 becomes flat as the number of particles increases after around $N = 2000$. We can choose the number of particles that seems reasonable in the sense that increasing the number of particles further would not reduce the variance by much. However, this is a practical approach since there are not significantly rigorous ways of dealing it. In most literature [37], [74], [94], [95], the number of particles are set to from 250 to 2000, the maximum number of particle used is 5000 in [96]. Thus we set $N = 5000$ with the respect of calculation time.

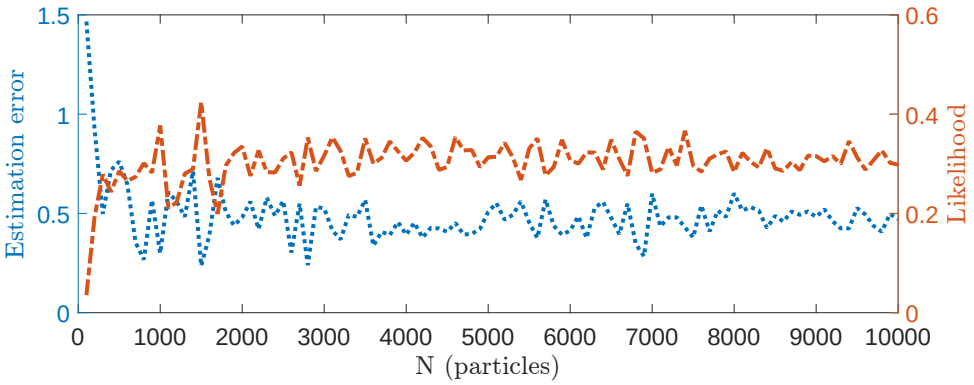

Figure 3.3: Influence of N with respect to PF-based tracking performance.

3.3.3.2 System state initial distribution

The initial distribution of the unknown system state must be constructed according to the known state. Very often, the initial state is determined by some level of uncertainty. However, it is always possible that the degradation of the system cannot be indicated by the measurements. Therefore, we propose a uniform initial distribution whose mean value is the assumed state of the system. Figure 3.4 shows the evolution of estimated states of different initial distribution variances (blue: $var = 50\%$; red: $var = 20\%$; green: $var = 10\%$). The three different cases all show a quick convergence of estimated states (around 20 steps). Therefore, the initial state value does not contribute significant impact to the estimation. Thus we set the variance to 10% of the first available measurement.

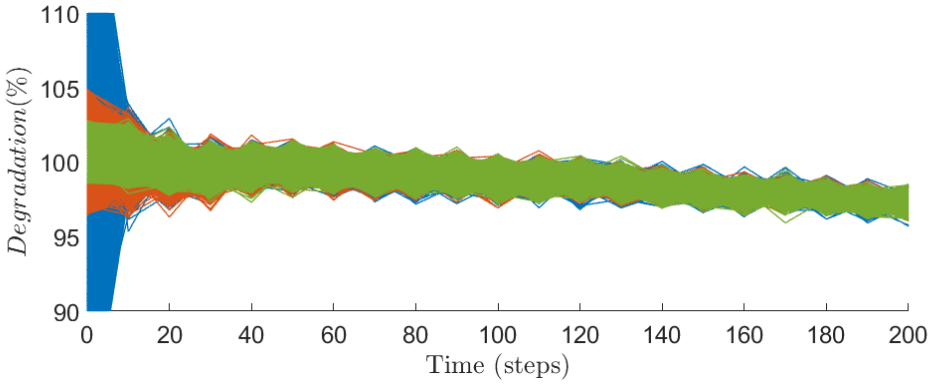

Figure 3.4: Influence of different initial distributions on the estimated degradation state x

3.3.3.3 Model unknown parameters initial distribution

A practical way of implementation is incorporating the model parameters in the state vector and updating them as well. Therefore, an adequate initialization is required. There is no standard method for this initialization, several techniques have been reviewed in [90], the initialization is possible when empirical knowledge is available. In that case, the initial parameters can be obtained by applying techniques such as Least Squares Regression (LSR) or fitting toolbox on the historical degradation path. We can thus apply the PF with broad initial distribution boundaries. After PF process, the boundary width will be narrowed down by the regression as being shown in Figure 3.5, and the posterior estimation will be used as the prior estimation to start over again. The red lines indicate the true values of degradation model parameters: trend parameter β=0.04, process noise std. σ_ω=0.1, and measurement noise std. σ_ν=1.

Figure 3.6 shows an example of measurement noises evolution. Initial distributions of σ_ν=50 (blue), σ_ν=20 (red) and σ_ν=10 (green) all converge into a smaller range.

For all parameters, the effects of initialization decrease with time. The optimal distribution boundary can be obtained by repeating sequentially this process until no significant change

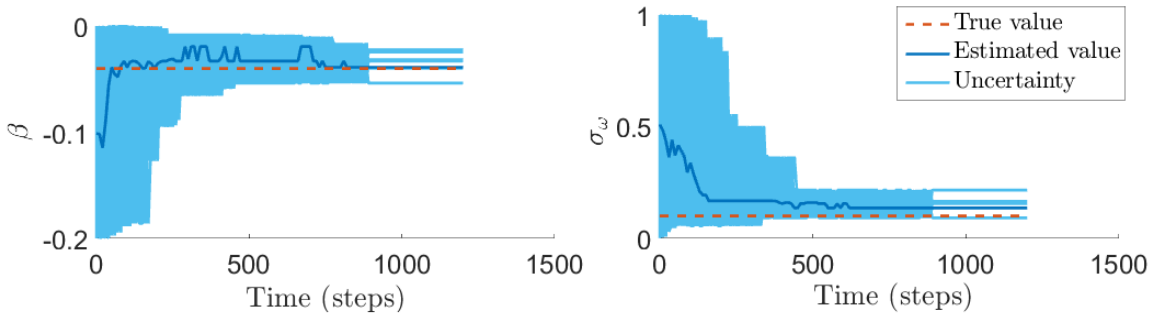

Figure 3.5: Influence of parameter initial distribution on the estimated model parameter.

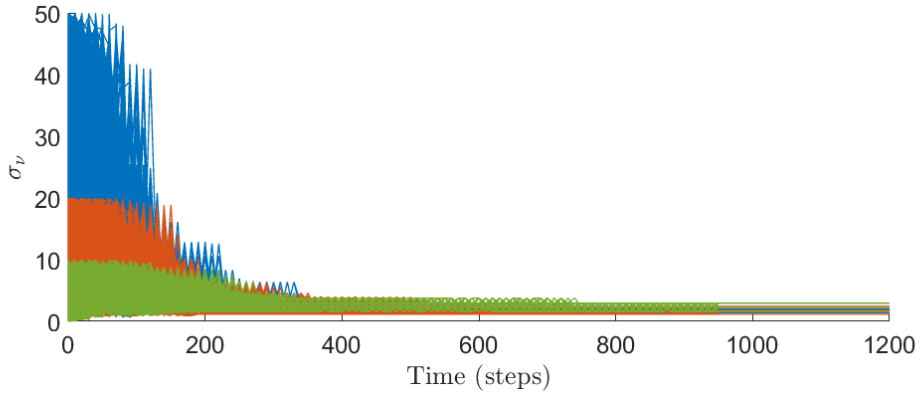

Figure 3.6: Influence of different initial distributions on the estimated measurement noise.

in parameters' boundary width even if the prior parameters are unknown.

3.3.4 RUL Prediction

We applied PF-based prognostics on the generated data example. Figure 3.7 shows the degradation estimation from observation, and the degradation prediction at $t_\lambda = 600$ steps. The estimation uncertainty is represented by a Confidence Interval (CI) and the median value is commonly chosen to represent the estimated point values in PHM. The RULs are calculated when the predicted degradation paths reach the failure threshold. The predicted RUL is shown in Figure 3.8. The Probability Density Function of RUL represents the uncertainties of the prediction. The median value of the RUL PDF is commonly chosen to represent the predicted RUL value in PHM.

In this numerical example, the predicted RUL at $t = 600$ steps is 350 steps with confidence interval $CI = [300, 420]$, where the true RUL is 380 steps. The model parameters are estimated at the same time, which is listed in Table 3.2. One can see that the true value lies within the

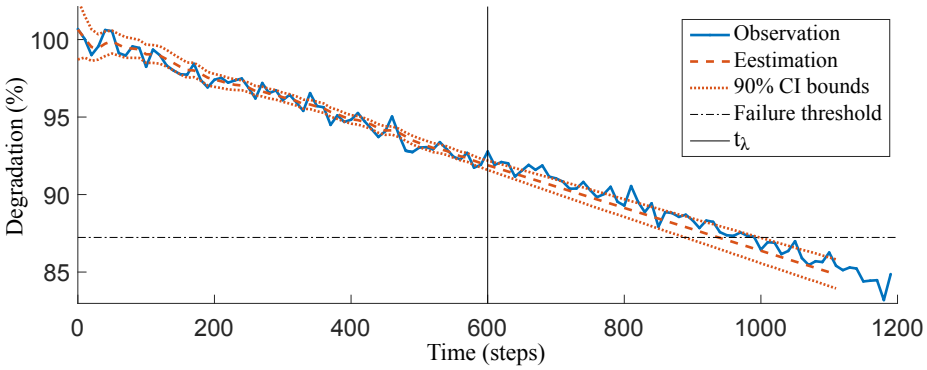

Figure 3.7: Estimation of system state degradation and its prediction at $t_\lambda = 600$ steps.

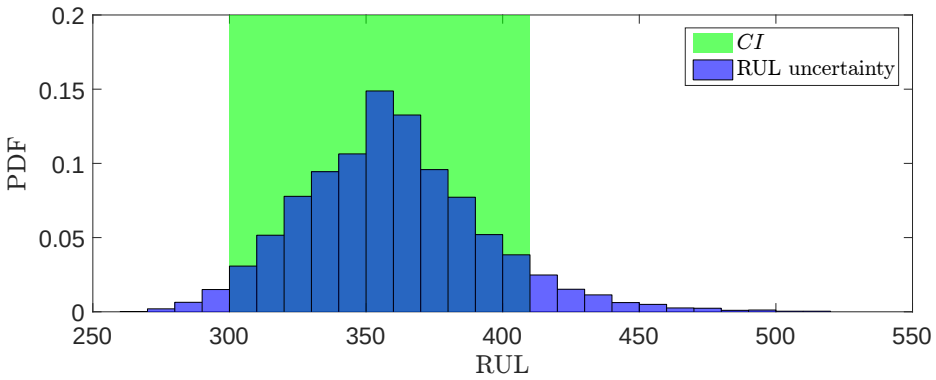

Figure 3.8: Histogram of predicted RUL at prediction time $t_\lambda = 600$ steps.

prediction CI.

Table 3.2: Estimated parameter values

Parameter	RUL (steps)	α (10^{-4})	β (10^{-2})	σ_ω	σ_ν
True values	380	10	4	0.1	1
Estimated values	350	9.61	4.12	0.15	1.33

3.4 Prognostic Performance Assessment

In order to evaluate the average performance of RUL predictions, the common way is to apply several RUL predictions at different time steps to obtain a sequence of predicted RULs [42]–[44]. Figure 3.9 illustrates the RUL predictions with uncertainties at different prediction time steps t_λ. The uncertainties are represented by the Probability Density Function (PDF). The accuracy bounds of a width of 2α shrinks with the prediction time index t_λ, which creates the α - λ accuracy zone covering the true residual life RUL^*. The upper bounds of the accuracy

zone $\alpha^+ = RUL^*_\lambda \cdot (1+\alpha)$ and lower bound $\alpha^- = RUL^*_\lambda \cdot (1-\alpha)$. $\widehat{RUL}^+$ and $\widehat{RUL}^-$ are the upper and lower bounds of the predicted RUL uncertainties, whereas CI^+ and CI^- are the bounds of the confidence interval.

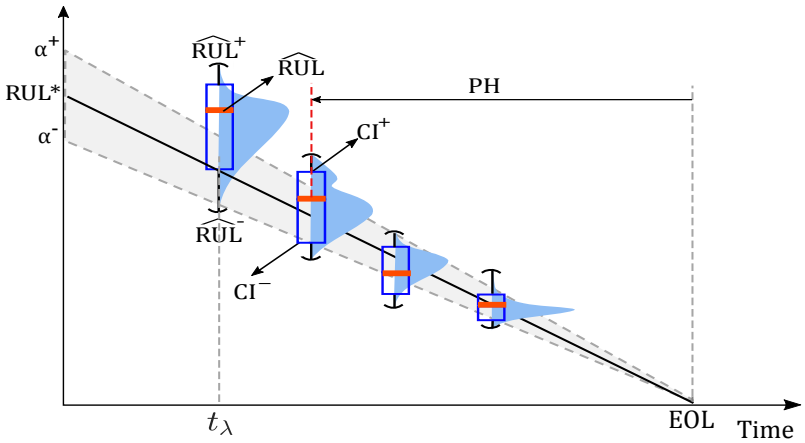

Figure 3.9: α-λ with the accuracy zone shrinking with time on RUL vs. time plot.

The notations will be further explained with the results of the numerical example. In our example, we applied the PF-based RUL predictions at different time steps ranging from 300 steps to 960 steps, with an interval of 20 steps (34 predictions). The values of CI and α are chosen according to the requirement of the application. Here we choose the values used in most literature which can meet the requirement of most industry systems, $CI = 80\%$ and $\alpha = 0.2$. Figure.3.10 shows the predicted RULs and their uncertainties for the previous example.

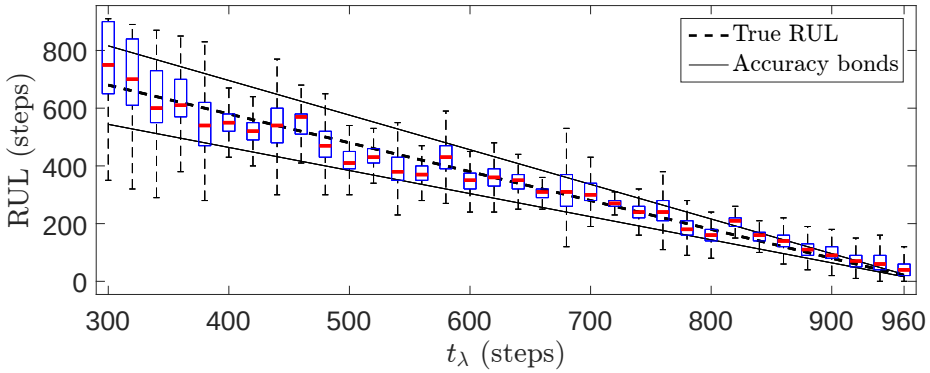

Figure 3.10: RUL predictions with accuracy bounds.

The results will be evaluated in the following section.

3.4.1 Metrics for Offline Evaluation

To evaluate the quality of prognostic outcomes, the prognostic metrics mentioned in Chapter 2 are commonly used.

Prognostic Horizon The Prognostic Horizon (PH) is the horizon between the end of life (EOL) and the first time index i when predictions satisfy $\pm\alpha$ bounds.

$$\begin{aligned} PH &= EOL - i \\ i &= min\{t_\lambda | \alpha_\lambda^- \leq \widehat{RUL}_\lambda \leq \alpha_\lambda^+\} \end{aligned} \tag{3.15}$$

In our example, the first prediction already laid in the α-λ accuracy zone. Thus the prognostic horizon $PH = 980 - 300 = 680$ steps.

Accuracy The Accuracy index Acc_λ is computed from the RUL prediction absolute errors relative to the true RUL. It directly reflects the distances between the true RUL and predicted RUL.

$$Acc_\lambda = 1 - \frac{|RUL_\lambda^* - \widehat{RUL}_\lambda|}{RUL_\lambda^*} \tag{3.16}$$

where RUL_λ^* the ground true RUL and $\widehat{RUL}_\lambda$ the median value of predicted RULs at prediction time t_λ. A Larger value of Acc_λ indicates better accuracy. In this numerical example, the predicted RUL at each prediction time step t_λ are listed in Table 3.3 and the local accuracy are calculated. We can see that the relative accuracy calculated near EOL is very low. It is because that, according to Equation (3.16), the tolerances of prediction error becomes smaller when the RUL is smaller. Thus the accuracy performance results Acc is calculated as the average value of all local relative accuracy Acc_λ values.

Table 3.3: Relative accuracy results

t_λ	300	320	340	$\cdots$	600	$\cdots$	920	940	960	Average
RUL_λ^*	680	660	640	$\cdots$	380	$\cdots$	60	40	20	-
$\widehat{RUL}_\lambda$	750	700	600	$\cdots$	350	$\cdots$	70	60	40	-
Acc_λ	0.90	0.94	0.94	$\cdots$	0.92	$\cdots$	0.83	0.50	0.00	**0.87**

Steadiness The Steadiness index (Std) measures the variance of the expected value of the End of Life (EOL) when new measurements become available. It is defined as:

$$Std_\lambda = \sqrt{var(\widehat{EOL}_{(\lambda-L):\lambda})} \tag{3.17}$$

Where L is the length of a sliding time window filtering the variances of the predicted EOL. The aim is to remove short-term fluctuations and gives us stable values for analysis. The steadiness index Std_λ with different window size L are shown in Figure 3.11. It suggests that:

- The steadiness index becomes smaller with time in general. It implies that RUL predictions become more stable with more incoming measurements, which meets the expectation of the prognostic approach.

- If the steadiness performance is evaluated with smaller window size (*i.e.* $L = 50$ steps), the results show larger variances; On the other hand, larger L leads to smaller variance. However, larger window size reduces sample size. Therefore, we choose $L = 100$ time steps (around 1/10 of the lifespan) to compromise between variation and sample size.

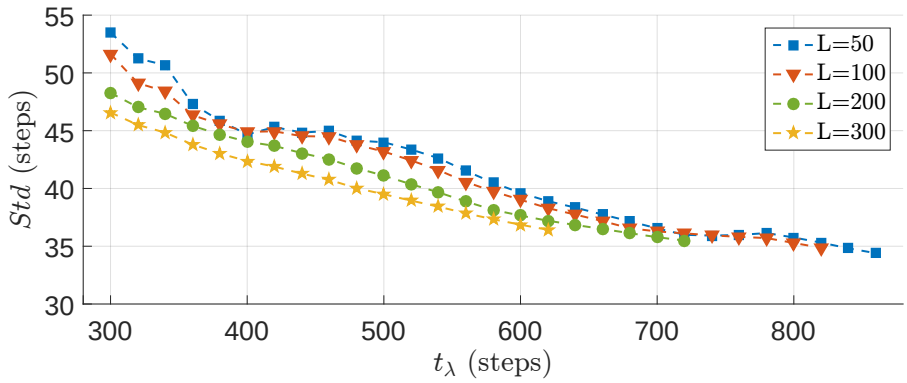

Figure 3.11: Steadiness with different window sizes.

Table 3.4: Steadiness results

t_λ	300	320	340	$\cdots$	600	$\cdots$	920	940	960	Average
$\widehat{RUL}_\lambda$	750	700	600	$\cdots$	350	$\cdots$	70	60	40	-
$\widehat{EOL}_\lambda$	1050	1020	940	$\cdots$	950	$\cdots$	990	1000	1000	-
Std_λ	51.64	49.11	48.40	$\cdots$	39.02	$\cdots$	-	-	-	**41.11**

α-λ Accuracy The α-λ metric is a binary index which considers whether the predicted RUL at time t_λ lies within the $\pm\alpha$ interval stating whether the requirements of prediction accuracy is met at a given time t_λ. As being illustrated in Figure 3.9, lying within the α-λ accuracy zone is described by Equation (3.18):

$$\alpha Ac_\lambda = p\left(\alpha_\lambda^- \leq \widehat{RUL}_\lambda \leq \alpha_\lambda^+\right) \tag{3.18}$$

The binary index is shown in Table 3.5, the α-λ Accuracy index is computed as the probability of the number of "true" over the number of all elements in the metric. Higher value represents better performance.

Precision The Precision index Prc_λ computes the relative width of the prediction interval, which is defined by:

$$Prc_\lambda = \frac{\widehat{RUL}_\lambda^{CI+} - \widehat{RUL}_\lambda^{CI-}}{RUL_\lambda^*} \tag{3.19}$$

where $\widehat{RUL}_\lambda^{CI+}$ and $\widehat{RUL}_\lambda^{CI-}$ are the upper and lower bounds of the Confidence Interval (CI) of the predicted RULs distribution (*e.g.* CI=50%) while RUL_λ^* is the corresponding true RUL. Smaller values of Prc_λ indicate more precise predictions.

Table 3.5: α-λ accuracy results (α=0.2)

t_λ	300	320	340	$\cdots$	600	$\cdots$	920	940	960	% of "true"
$\widehat{RUL}_\lambda$	750	700	600	$\cdots$	350	$\cdots$	70	60	40	-
$RUL_\lambda^{*\alpha+}$	816	792	768	$\cdots$	456	$\cdots$	72	48	24	-
$RUL_\lambda^{*\alpha-}$	544	528	512	$\cdots$	304	$\cdots$	48	32	16	-
α-λ metric	true	true	true	$\cdots$	true	$\cdots$	true	false	false	**88%**

Table 3.6: Precision results (CI=80%)

t_λ	300	320	340	$\cdots$	600	$\cdots$	920	940	960	Average
$\widehat{RUL}_\lambda^{CI+}$	910	890	870	$\cdots$	400	$\cdots$	110	120	80	-
$\widehat{RUL}_\lambda^{CI-}$	560	540	510	$\cdots$	290	$\cdots$	40	30	10	-
RUL_λ^*	680	660	640	$\cdots$	380	$\cdots$	60	40	20	-
Prc_λ	0.51	0.53	0.56	$\cdots$	0.29	$\cdots$	1.17	2.25	3.50	**0.62**

Risk The Risk index Rsk is the probability of obtaining an estimated RUL larger than the true RUL:

$$Rsk_\lambda = p(\widehat{RUL}_\lambda > RUL_\lambda^*) \tag{3.20}$$

This index indicates the probability of receiving a later notification of a failure such that scheduling a maintenance after the failure is risky. Lower values represent the lower risk, which means better performance.

Table 3.7: Risk results

t_λ	300	320	340	$\cdots$	600	$\cdots$	920	940	960	% of "true'
RUL_λ^*	680	660	640	$\cdots$	380	$\cdots$	60	40	20	-
$\widehat{RUL}_\lambda$	750	700	600	$\cdots$	350	$\cdots$	70	60	40	-
Rsk metric	false	false	true	$\cdots$	true	$\cdots$	false	false	false	**50%**

Coverage The Coverage index Cvg_λ is a binary index which considers whether the true RUL lies within the RUL prediction interval at time index λ for each trajectory:

$$Cvg_\lambda = p\left(\widehat{RUL}_\lambda^{CI-} \leq RUL_\lambda^* \leq \widehat{RUL}_\lambda^{CI+}\right) \tag{3.21}$$

The value of Cvg close to 80% indicates a good representation of the uncertainty [49].

We can see that by applying different metrics on the prognostic performance, the Acc and Prc become weaker close to the EOL due to the relatively smaller RUL^*, whereas the Std avoids this inconvenient. High value of Cvg index is relatively easier to achieve than other indexes whereas the Rsk index is the most difficult.

Table 3.8: Coverage results (CI=80%)

t_λ	300	320	340	$\cdots$	600	$\cdots$	920	940	960	% of "true'
$\widehat{RUL}_\lambda^{CI+}$	910	890	870	$\cdots$	400	$\cdots$	110	120	80	-
$\widehat{RUL}_\lambda^{CI-}$	560	540	510	$\cdots$	290	$\cdots$	40	30	10	-
RUL_λ^*	680	660	640	$\cdots$	380	$\cdots$	60	40	20	-
Cvg metric	true	true	true	$\cdots$	true	$\cdots$	true	true	true	**97%**

3.5 Conclusion

In this chapter, the particle filtering-based approach has been presented with a numerical example. The RUL prognosis results are evaluated by a synthesis of the prognostic performance metrics. The metrics are mainly based on the assessment of predictions accuracy, as well as their uncertainties. Uncertainty information is particularly difficult to evaluate, and we need to think about how they are presenting uncertainty and how different representations can lead to different decision-making strategies. Along with detailed discussions and illustrations, it has been shown that the prognostic approach and the synthesis of those metrics could be applied to a PEMFC system. Therefore, this approach is ready to be deployed in the following chapters.

Chapter 4

RUL Prognostics for PEMFC

In the previous chapter, we have presented the PF-based prognostic approach. In this chapter, this approach is implemented on the experimental data sets of PEMFC stacks measurements. First, a simple approach is applied for the degradation path estimation to obtain the RUL prediction. Then the PEMFC RUL prognosis is improved by taking into account the knowledge of stack SOH characterization. The work reported in this chapter is based on the work presented in the 3rd IFAC Workshop on Advanced Maintenance Engineering, Service and Technology, October 19-21, 2016, Biarritz [97].

Contents

4.1 RUL Prognosis on Stacks Output Power

4.1.1 Degradation Data

For the application test, two long-term experiment data sets of two identical stacks (refer to FC1 and FC2) measurements will be used. Figure 4.1 shows stack power drop signal [13] over time in both nominal and dynamic operating conditions. Several peaks at certain time instances can be observed. In practice, characterization measurements (polarization and EIS) take place each week. These measurements lead to the observed sudden drops in power, and then the power jumps back getting recovered thanks to the reversibility of the stack. This

behavior of PEMFC stack can be assessed based on the internal characterizations of the stack's State of Health (SOH), such as the polarization curves and the Electrochemical Impedance Spectroscopy (EIS), this issue will be addressed in the following section.

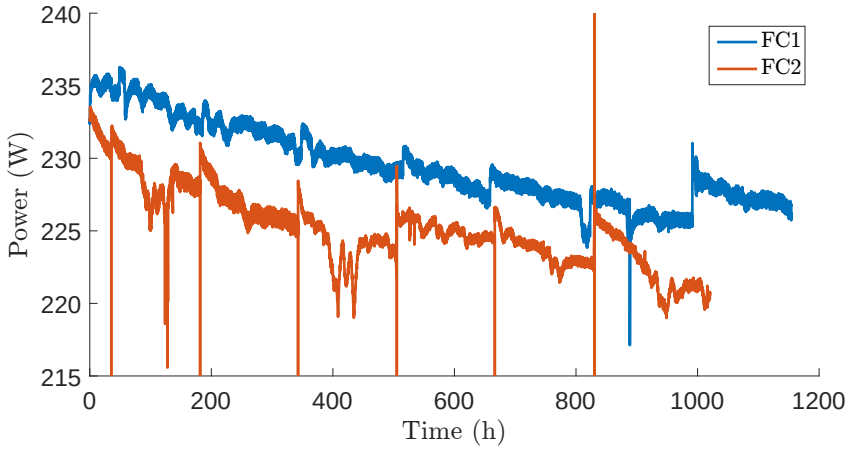

Figure 4.1: Power degradation in stack FC1 and FC2.

4.1.2 Adaptation of PF to PEMFC

As being discussed in Chapter 2, the stack's output power is chosen as the indicator of the performance degradation of the PEMFC stacks. The degradation models described previously refer to the empirical models for degradation trends, *i.e.* linear, polynomial, exponential and logarithm models, *etc.*, are commonly used in prognostics [37]. By comparing RUL prediction errors in literature, the 2nd order polynomial decreasing model proposed in [74] is chosen for the degradation trend. Given the measurement data and the problem framework, the following equations are adapted:

$$\begin{aligned} x_k =& \alpha \cdot (t_k - t_{k-1})^2 + \beta \cdot (t_k - t_{k-1}) + x_{k-1} + \omega_k, \quad \omega_k \sim \mathcal{N}(0, \sigma_\omega^2) \\ z_k =& x_k + \nu_k, \quad \nu_k \sim \mathcal{N}(0, \sigma_\nu^2) \end{aligned} \tag{4.1}$$

where x_k is the current state, α and β are the polynomial degradation model parameters, t_k is the current time step, t_{k-1} is the previous time step, σ_ω and σ_ν are the process noise and the measurement noise, respectively. It is necessary to note that, for the measurement function z_k, it is assumed that z_k is the same as the output power including measurement noise ν_k. The unknown model parameters thus are $\Theta = [\alpha, \beta, \sigma_\omega, \sigma_\nu]$.

The model is trained by PF with the measurement data until half of life time. The training is processed until the prediction time t_λ reached which has been set to 600 hours. A sensitivity analysis mentioned in [37] shows $N = 2000$ particles and one measurement each 15 hours is enough to help to learn the model and then giving good results. To ensure a better prediction, the number of $N = 5000$ particles is chosen in this implementation, and the critical stack voltage value (96% of its initial power) is defined as the Failure Threshold (FT).

Since there is no available prior information, it is assumed that the initial distributions of the system state x and the unknown parameters Θ are uniformly distributed between their lower and upper bounds:

$$\begin{aligned} x_0 &\sim \mathcal{U}(x_0^-, x_0^+) \\ \Theta_0 &\sim \mathcal{U}(\Theta_0^-, \Theta_0^+) \end{aligned} \tag{4.2}$$

The bounds of x_0 are set to ± 5 W around FC1 initial power (represented by the first measurement) and the measurement noise variance $\sigma_{\nu 0}^2$ in PF is set accordingly to ensure a good estimation of the noisy measurement. The value for process noise variance is found through successive tuning as $\sigma_\omega^2 = 10^{-2}$, to obtain a smooth, desirable estimation. The parameters Θ_k evolving unknown process that is independent of the state x_k should be estimated by PF as well. We need to assign some types of evolution to the parameters to realize the estimation. The typical solution is to add a random walk [95]. Here we assign the same process noise ω_k as the random walk to unknown parameters $\Theta_k = \Theta_{k-1} + \omega_{k-1}$ where ω_{k-1} is sampled from a zero-mean Gaussian distribution.

4.1.3 Results on Stationary Regime (FC1)

The output power degradation of FC1 over 1000 hours is estimated by PF. The RUL of a PEMFC stack is predicted regarding to its output power Failure Threshold (FT). The FT of the stack is defined as certain portions of its initial output power (*e.g.* 96% of its power at $t = 0$ h). Figure 4.2 shows the estimation of degradation path at prediction time $t_\lambda = 600$ hours for FC1. The predicted RUL with its uncertainty are illustrated in Figure 4.3. The predicted RUL at $t_\lambda = 600$ hours is [130 200 330] of 80%CI whereas the true RUL is 210 hours.

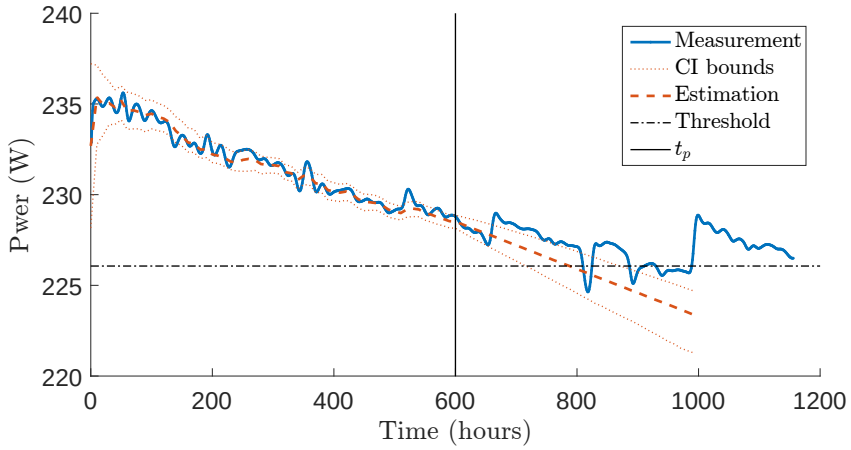

Figure 4.2: Degradation estimation for FC1.

Several RUL predictions are applied at different time s to evaluate the average performance. 25 predictions are made through time index t_λ from 300 hours to the End of Life (EOL) at

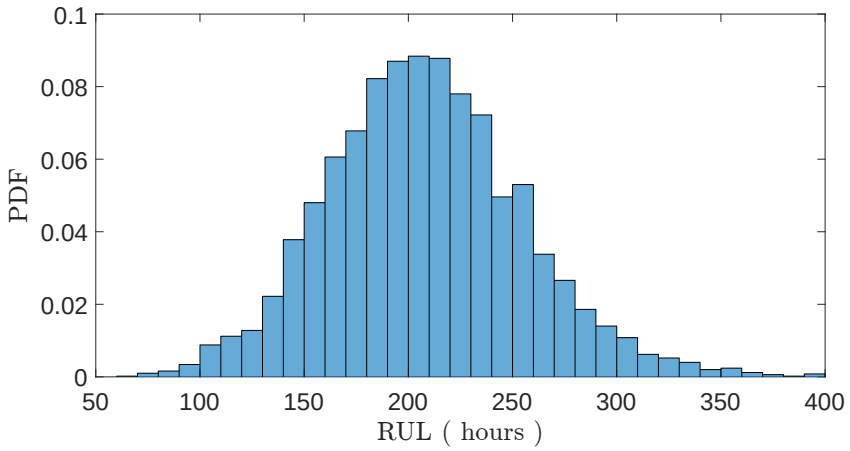

Figure 4.3: Predicted RUL PDF for FC1 at t_λ=600 hours.

every 20 hours. The boxplot in Figure 4.4 shows the predicted RUL uncertainties with $\alpha = 0.2$ and $CI = 50\%$ bounds. It can be seen that the predicted RULs at earlier time steps (*e.g.* $t_\lambda = 200$ hours) are far from the true values. Then the prediction accuracy is improved with more new incoming measurements (*e.g.* $t_\lambda = 400 \sim 600$ hours).

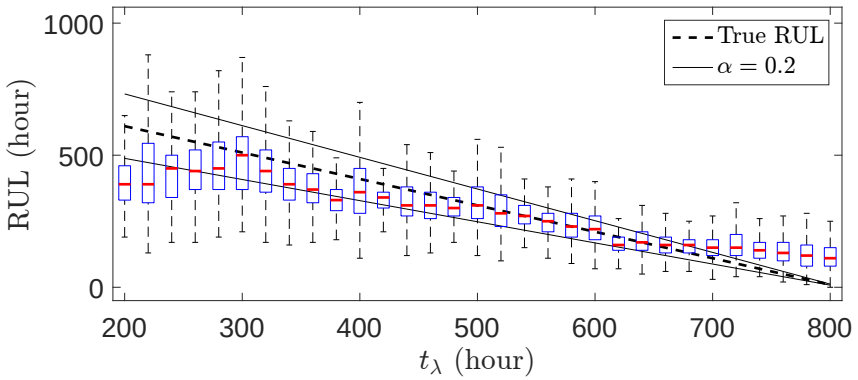

Figure 4.4: Predicted RULs for FC1.

4.1.4 Results on Dynamic Regime (FC2)

The output power degradation of FC2 over 1000 hours is estimated by PF for all the models. The RUL of a PEMFC stack is predicted regarding to its output power Failure Threshold ($FT = 95\%$). Figure 4.5 shows the estimation of degradation path at prediction time $t_\lambda = 600$ hours for FC2. The predicted RUL with its uncertainty are illustrated in Figure 4.6. The predicted RUL at $t_\lambda = 600$ hours is [130 220 390] of $80\%CI$ whereas the true RUL is 340 hours.

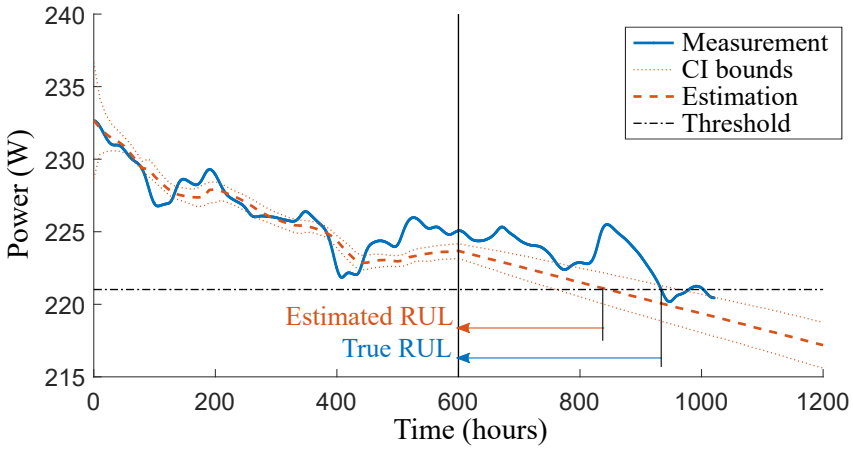

Figure 4.5: Degradation estimation for FC2.

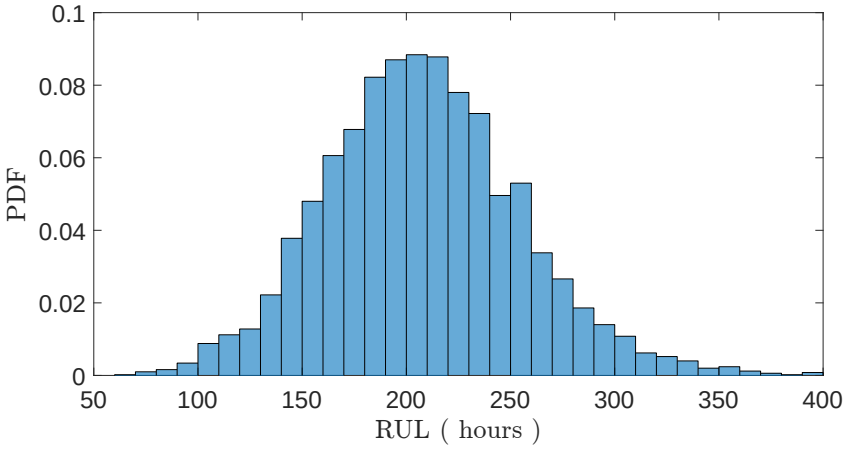

Figure 4.6: Predicted RUL PDF for FC1 at $t\lambda = 600$ hours.

38 RUL predictions are applied with time index t_λ from 300 hours to the End of Life (EOL) at every 20 hours, to evaluate the average performance.

The boxplot in Figure 4.7 shows the predicted RUL uncertainties with $\alpha = 0.2$ and $CI = 50\%$ bounds. It can be seen that around $t_\lambda = 380$ to $t_\lambda = 600$ hours, the predictions are abnormally inaccurate. By looking at the degradation trend in Figure 4.5, it can be found that there are a sudden drop and a strong recovery during that period. The recovery behavior strongly impacts the prediction accuracy.

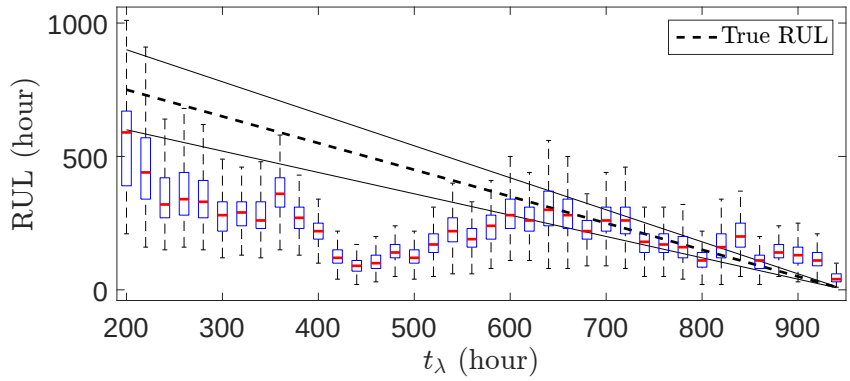

Figure 4.7: Predicted RUL PDF for FC2.

4.2 RUL Prognosis Considering Recovery Phenomena

Thus the prognostic algorithm has to face a specific difficulty, *i.e.*, the power trend is not only a degradation indicator but also include reversible phenomena. However, the irreversible degradation of the PEMFC stack can be assessed based on the internal characterizations of the stack's State of Health (SOH), such as the polarization curves and the Electrochemical Impedance Spectroscopy (EIS). These characterizations are detailed as follows.

4.2.1 PF Algorithm with recovery phenomena

The algorithm is then adapted to take into account the EIS and polarization measurements, which occur at characterization time step $C = [c_1, c_2, \dots]$. At these time steps, the degradation model Equation (5.1) is then replaced by a model including recovery phenomena (x_c). The Algorithm 1 is modified such as: (*line 5*) is replaced by Algorithm 3.

Algorithm 3 PF Modification

1: **if** $k = c_1$ or $k = c_2, \cdots$
2: Draw particles $x_c^i \sim p(x_c^i | x_{k-1}^i, \omega_{k-1}^i, \Theta_k^i, \Theta_c^i)$
3: $x_k^i = x_c^i$
4: **else**
5: Draw particles $x_k^i \sim p(x_k^i | x_{k-1}^i, \omega_{k-1}^i, \Theta_k^i)$ using Equation (5.1)
6: **end if**

4.2.2 Degradation Models

4.2.2.1 Degradation Trend Models

The degradation model described in Equation (4.1) is chosen for the main degradation trend. Several models in Table 4.1 are tested to adapt the recovery trends. x_c is the state including recovery phenomena. In Model 1, α_0 is the average recovery amplitude of power increase after each characterization. In Model 2, the model parameters fit the shape of the recovery phenomena with two parameters: the recovery amplitude α_1 and its trend β_1.

Table 4.1: Trend models

N^0	Model
classical	x_k
1	$x_c = x_k + \alpha_0$
2	$x_c = x_k + \alpha_1 \cdot exp(\beta_1 \cdot (t_k - t_{k-1}))$

The drawback of Model 2 is that the amplitude of the recovery phenomena changes with the SOH of the fuel cell and tends to higher peaks with aging. For that reason, the model is improved in the next section by linking the parameters with the SOH of the fuel cell.

4.2.2.2 Recovery Phenomena Model from EIS

As being discussed in Chapter 2, the EIS represents the dynamic behavior of the PEMFC stacks, which can be interpreted by fitting the Equivalent Circuit Model (ECM) to the spectrum (Figure 4.8).

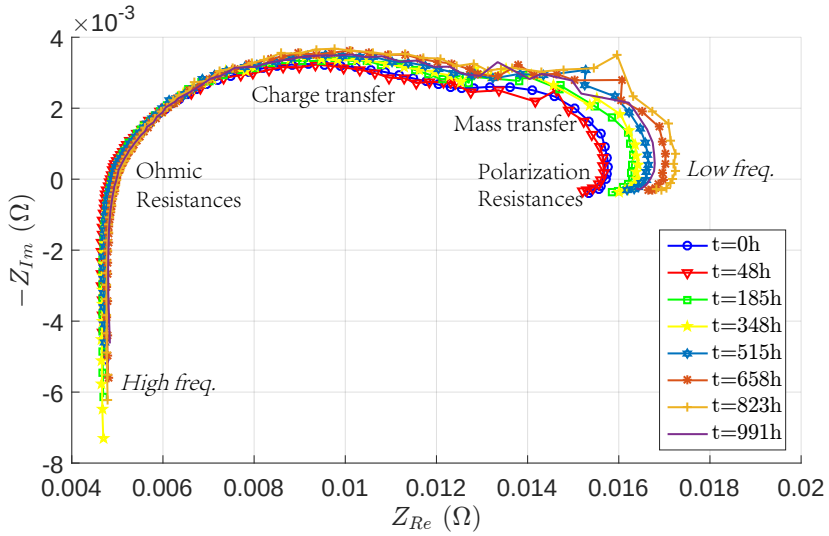

Figure 4.8: EIS of FC1 at different time stages.

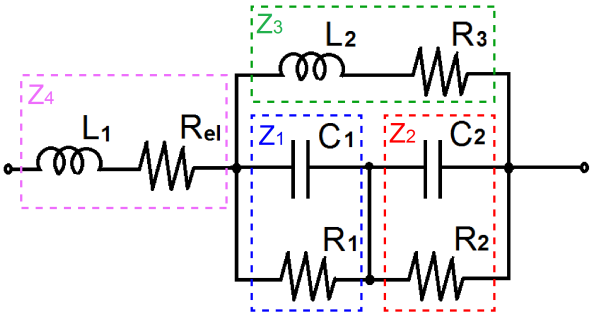

Figure 4.9: An ECM for PEMFC stacks.

Figure 4.9 shows an ECM proposed in [22]. The equivalent impedance of the PEMFC can be thus described as:

$$Z_{eq} = \frac{(Z_1 + Z_2) \cdot Z_3}{Z_1 + Z_2 + Z_3} + Z_4 \tag{4.3}$$

The first stage is to determine which parameter from EIS is the most representative of the SOH degradation. The identification results issued from [22] show that only the internal resistances are taken into account because other parameters do not have significant changes to degradation such as the capacitance C_1 and C_2, the inductance L_1 and L_2. Besides the polarization resistance is calculated as:

$$R_{pol} = \frac{(R_1 + R_2) \cdot R_3}{R_1 + R_2 + R_3} + R_{el} \tag{4.4}$$

The fitting is realized by a nonlinear programming solver which searches for the minimum of the error model estimated spectrum and experimental data.

A fitting example is shown in Figure 4.10. The results of the parameter identification on FC1 and FC2 measurements [13], are listed in Table 4.2.

Table 4.2: ECM parameters identification

FC1		FC2	
t (h)	$R_{pol}(m\Omega)$	t (h)	$R_{pol}(m\Omega)$
48	14.8	35	15.2
185	15.4	182	15.7
348	15.5	343	16.2
515	15.9	515	17.2
658	16.2	661	16.9
823	16.5	830	17.4
991	16.1	1016	18.6

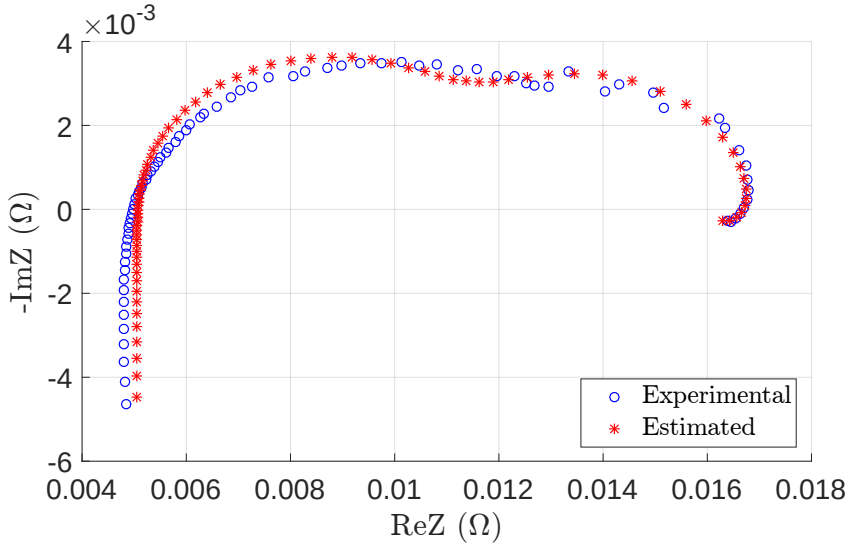

Figure 4.10: ECM fitting result of FC1 at 991 hours.

It can be seen that the resistances generally increase in time, which enables the feasibility of using R_{pol} as aging indicator. For each characterization time, the polarization resistance can be estimated from the polarization curve. Figure 4.11 pinpoints the correlation between R_{pol} and *Power* degradation.

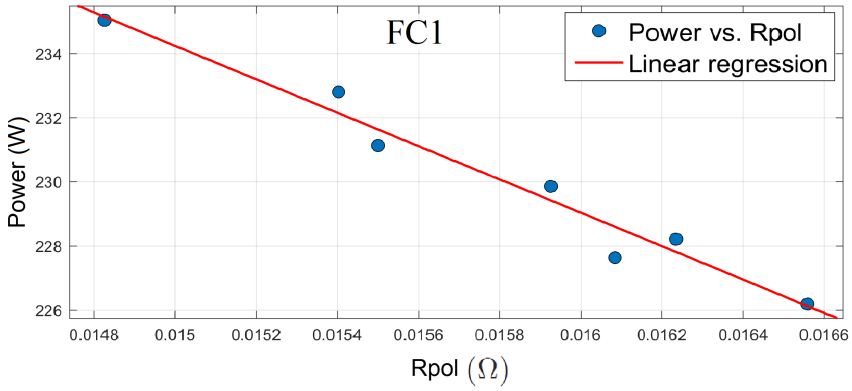

Figure 4.11: Correlation between *Power* and R_{pol}.

The R-squared measure of goodness of the linear regression is 0.966 for FC1 and 0.969 for FC2, which shows that these data follow a strong linear function for both stacks. The stack power value drops as the resistance increases. The challenge is now to find relevant relations between α_1 and R_{pol}, β_1 and R_{pol}. The variable parameter R_{pol} can thus be included in a new model (Model 3) as:

$$x_c = x_k + \alpha_2(R_{pol}) \cdot exp(\beta_2(R_{pol}) \cdot \Delta t) \tag{4.5}$$

With longer ageing progress the reversible amplitude parameter α_1 and the trend parameter β_1 become greater. The idea is to add the variability/evolution regarding R_{pol}. So the coefficient

can be set to a value close to 1 that will not effect the parameters significantly whereas they still can be adapted by R_{pol}. Thus we assume that:

$$\begin{aligned} \alpha_2(R_{pol}) &= \alpha_1 \cdot \frac{R_{pol}(k)}{R_{pol}(1)} \\ \beta_2(R_{pol}) &= \beta_1 \cdot \frac{R_{pol}(k)}{R_{pol}(1)} \end{aligned} \tag{4.6}$$

where $R_{pol}(1)$ is the value of R_{pol} at $k = 1$.

4.2.2.3 PF Settings

The estimation performed by PF (*e.g.* in Figure 4.12), is realized with $N = 5000$ particles. The bounds of x_0 are set to ± 5 W around FC1 initial power (represented by the first measurement), and the measurement noise variance $\sigma_{\nu_0}^2 \in (0, 5)$ is set accordingly to ensure a good estimation of the noisy measurement. The value for process noise variance is found through successive tuning as $\sigma_\omega^2 \in (0, 0.04)$.

4.2.3 Results on Stationary Regime (FC1)

The output power degradation of FC1 over 1000 hours is estimated by PF for all the models. The RUL of a PEMFC stack is predicted regarding its output power Failure Threshold (FT). The FT of the stack is defined as a given portion of its initial output power (*e.g.*, 96% of its power at $t = 0$ h).

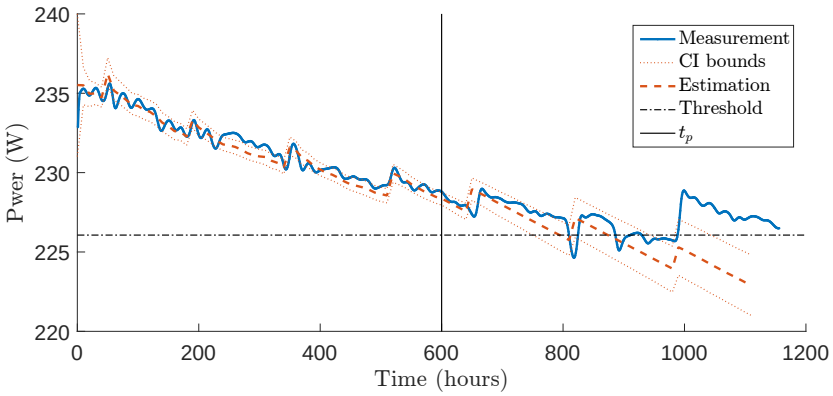

Figure 4.12: Degradation estimation for FC1 (Model 3).

Figure 4.12 shows an example of the estimation of degradation path at prediction time $t_\lambda = 600$ hours for Model 3. One can see the recovery phenomenon has been adapted both in learning and prediction phases. The predicted RUL with its uncertainty is depicted in

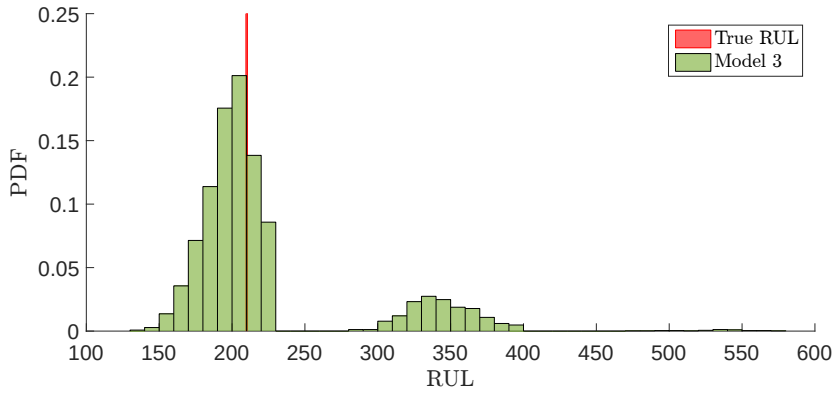

Figure 4.13: Histogram of the predicted RUL for FC1 at 600 hours (Model 3).

Figure 4.13. The predicted RUL at $t_\lambda = 600$ hours is 200h with $80\%CI$ in [170 330] whereas the true RUL is 210 hours.

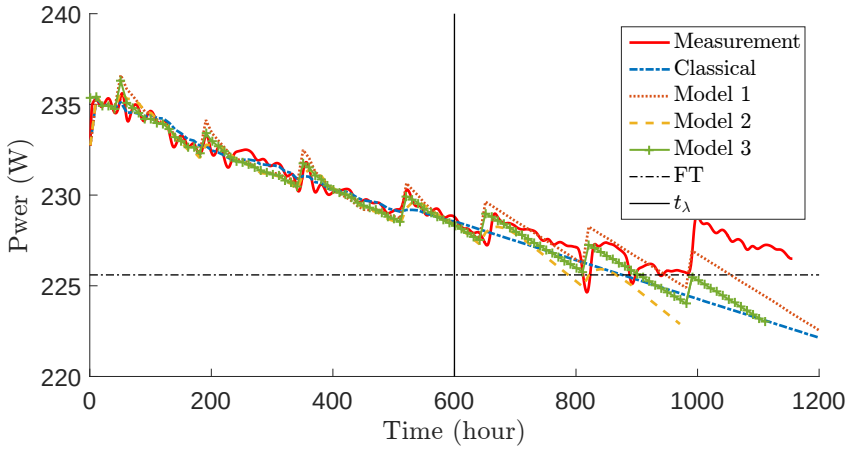

Figure 4.14: Degradation estimations with different models for FC1 at 600 hours.

Figure 4.14 shows the degradation estimations with different models for FC1 at prediction time $t\lambda = 600$ hours. There is no significant difference among the estimations with all models except the classical model. The recovery phenomena have been adapted both in learning and prediction phases with Model 1, Model 2 and Model 3. Figure 4.15 shows the corresponding predicted RUL uncertainties at $t\lambda = 600$ hours. We can see that the RUL PDFs of all models are centered around the true values. It is difficult to tell which model has the best performance. Therefore, to evaluate the average performance of each model, the RUL predictions are then applied with time index t_λ from 200 hours to the End of Life (EOL) at every 20 hours. The boxplot in Figure 4.16 shows the predicted RUL uncertainties with $CI = 50\%$ bounds, where $\alpha = 0.2$.

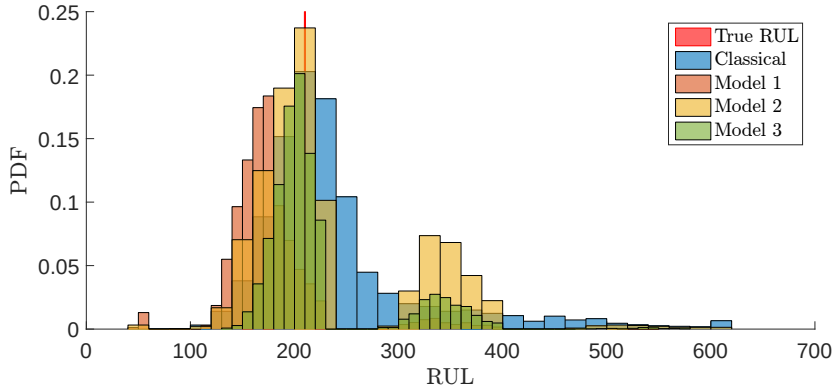

Figure 4.15: RUL predictions with different models for FC1 at 600 hours.

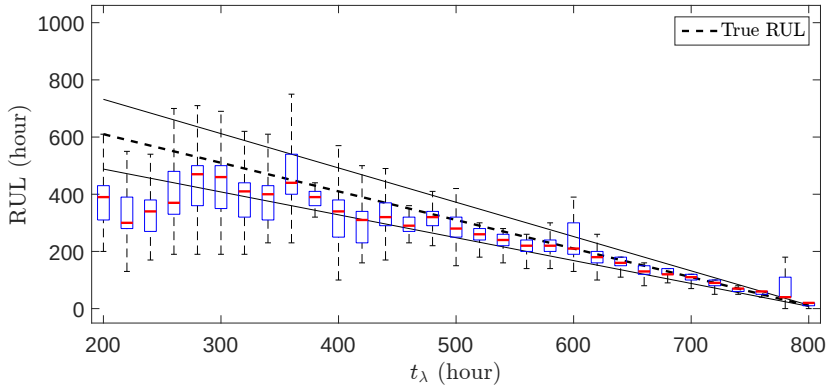

Figure 4.16: Model 3 RUL predictions with uncertainties for FC1 ($\alpha = 0.2$ and $CI = 50\%$).

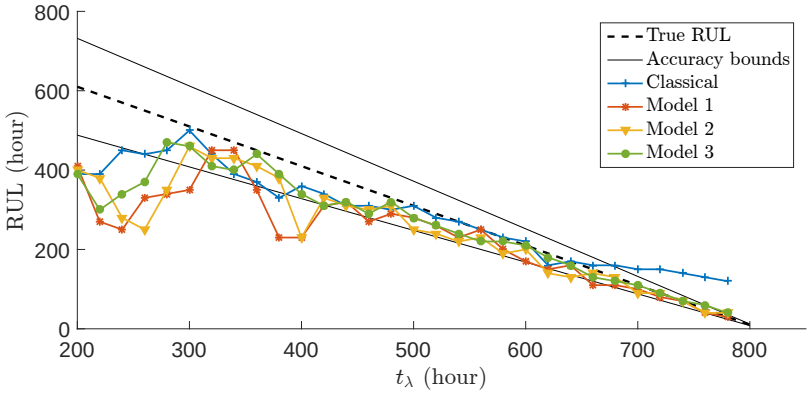

Figure 4.17: RUL predictions with different models for FC1 ($\alpha = 0.2$).

Figure 4.17 shows the RUL predictions with α bounds of all models. It can be seen that the results of Model 3 are better suited in the bounds than the others. The performances evaluated by the prognostic metrics for FC1 are compared in Table 4.3.

Table 4.3: Prognostic performance for FC1 ($\alpha = 0.2$,$CI = 80\%$)

	Classical	Model 1	Model 2	Model 3
Acc	0.670	0.780	0.807	**0.858**
α-λ	0.645	0.516	0.677	**0.774**
Prc	0.888	0.892	0.702	**0.683**
Cvg	0.742	0.581	0.581	**0.774**
Std	0.063	0.091	0.074	**0.060**
Rsk	0.710	**0.936**	**0.936**	0.903

Model 3 shows better performances on α-λ Accuracy and *Acc* indexes which imply that this model gives more accurate predictions than the other two models. Such a model also has better performances on *Prc* (the lowest value) and *Cvg* (the closest to 80% [98]), which indicates that it provides more precise RUL predictions while maintaining a better coverage performance than other models. For the risk index *Rsk*, Model 1 and Model 2 have the best performance. In practice, different accuracy criteria might be required. We thus look at a more strict scenario, where the accuracy $\alpha = 0.1$ is required and the confidence interval $CI = 50\%$.

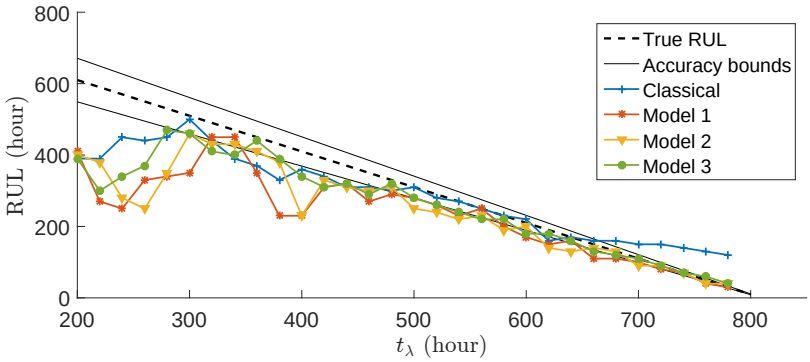

Figure 4.18: RUL predictions with different models for FC1 ($\alpha = 0.1$).

As being shown in Figure 4.18, the median values of predicted RULs do not change compared with Figure 4.17, but the shrinking accuracy zone is narrower, which leads to the result that some predictions will no longer fall in the zone. Consequently, the evaluated performance will show a lower performance in accuracy zone related metric. The evaluated results are listed in Table 4.4. We can see that the α-λ accuracy decreases compared with the those in Table 4.3. However, Model 3 still shows the best performance.

As being stated in [43] that $\alpha = 0.1$ can meet most industrial systems, we use this criterion for the rest of this section.

Table 4.4: Prognostic performance for FC1 ($\alpha = 0.1$,$CI = 80\%$)

	Classical	Model 1	Model 2	Model 3
Acc	0.670	0.780	0.807	**0.858**
α-λ	0.290	0.258	0.290	**0.420**
Prc	0.888	0.893	0.702	**0.683**
Cvg	0.742	0.581	0.581	**0.774**
Std	0.063	0.091	0.074	**0.060**
Rsk	0.290	**0.064**	**0.064**	0.097

4.2.4 Results on Dynamic Current Regime (FC2)

The same algorithm is applied on the other stack FC2.

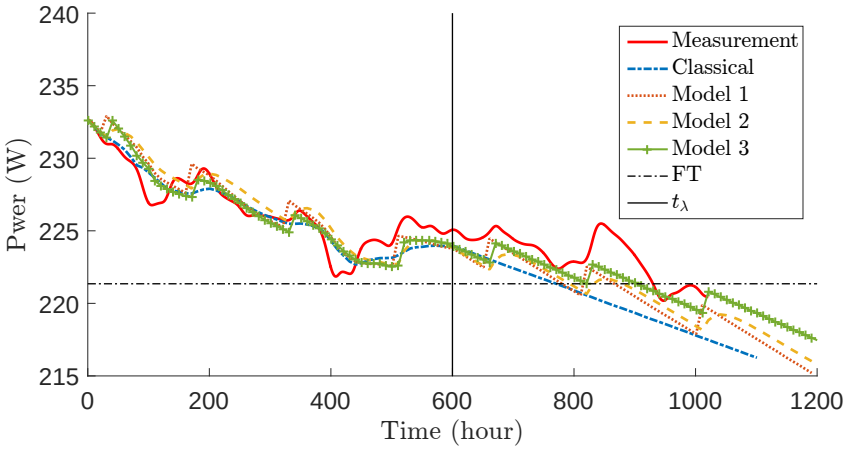

Figure 4.19: Degradation estimations with different models for FC2 at 600 hours.

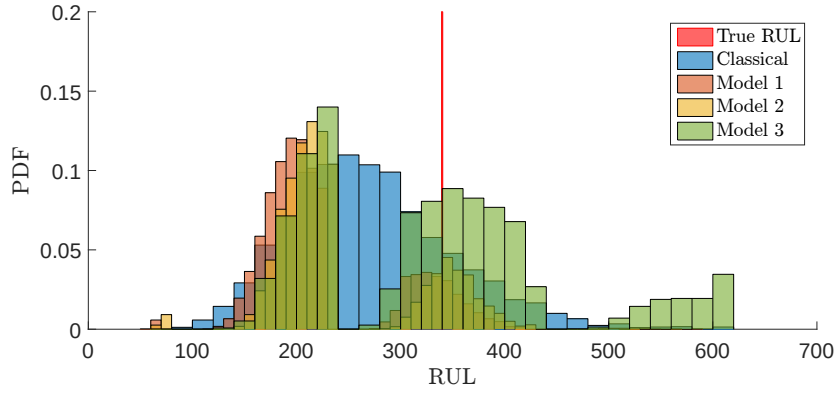

Figure 4.20: RUL predictions with different models for FC2 at 600 hours.

An example of degradation estimations at $t_\lambda = 600$ hours for FC2 are shown in Figure 4.19. It suggests that:

- The classical model gives a realistic RUL prediction, but this prediction may not be robust to other experiments, as the characterization moments are not taken into account.
- For the Models 1 and Model 2, the characterization moments are taken into consideration, but the magnitude and the rate are estimated during data training. Thus, the prediction RUL is too short.
- For Model 3, taking into account the polarization resistance allows adapting the magnitude and the degradation rate. The RUL prediction is thus accurate. However, it can be seen that the peak at time 850 hours cannot be predicted without additional information on this event.

The corresponding RUL PDFs (*e.g.* at $t_\lambda = 600h$) by all models are shown in Figure 4.20. We can see that the distribution of RULs is narrower of Model 3. The boxplot in Figure 4.21 shows the predicted RUL uncertainties with Model 3. This figure highlights that the dramatic drop between $t = 400h$ and $t = 500h$ induce difficulties in the RUL prediction. Figure 4.22 shows the RUL predictions with α bounds of all models and classical PF. We can see that Model 3 gives better predictions after $t = 500h$.

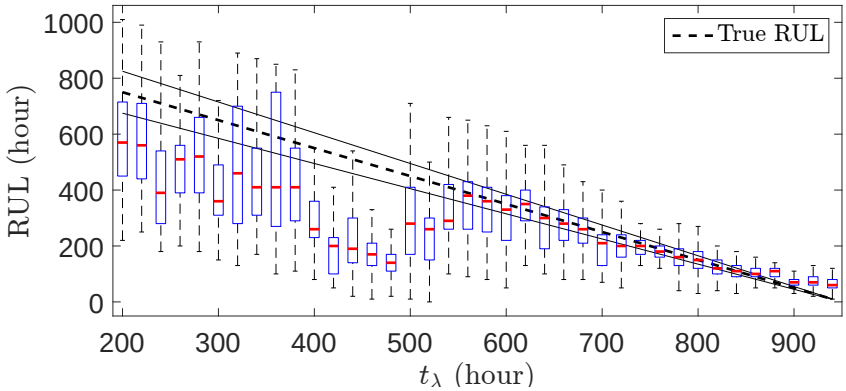

Figure 4.21: Model 3 RUL predictions with uncertainties for FC2 ($\alpha = 0.1$ and $CI = 80\%$).

Table 4.5 reports all performance metrics obtained when using all models for FC2. It can be noticed that the performances on FC2 are globally worse when compared with those on FC1. The classical PF provides in this case more precise predictions but lack of accuracy. Model 3 shows better performances on α-λ Accuracy, Acc , Cvg and Rsk indexes. The poor performance of Prc index for Model 3 is due to the fact that the predicted RUL distribution does not converge as fast as with the classical PF because of the adaption to the recovery phenomena.

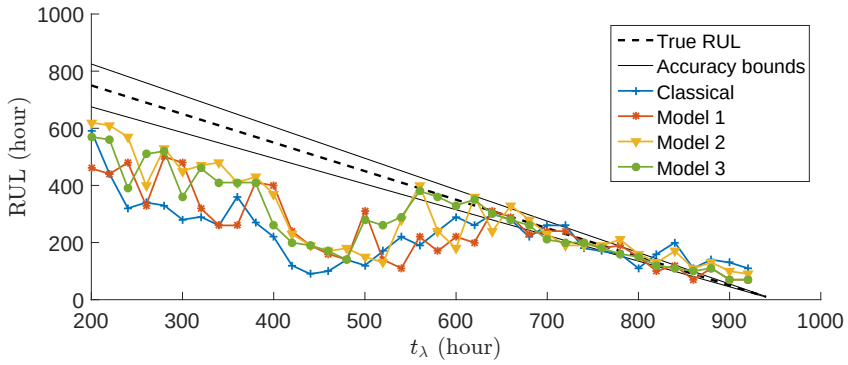

Figure 4.22: RUL predictions with different models for FC2 ($\alpha = 0.1$).

Table 4.5: Prognostic performance for FC2 ($\alpha = 0.1$,$CI = 80\%$)

	Classical	Model 1	Model 2	Model 3
Acc	0.478	0.631	0.639	**0.718**
α-λ	0.105	0.211	0.211	**0.342**
Prc	**0.690**	0.767	0.946	0.745
Cvg	0.316	0.553	0.658	**0.790**
Std	0.170	0.128	**0.114**	0.120
Rsk	0.237	0.184	0.342	**0.158**

4.3 Conclusion

In this study, the PF-based RUL prognosis was adapted to the available information from two completed tests of the PEMFC platform. Other tests, especially the tests involve varying operating conditions, will be investigated once they are available. For this end, the prognostics data on accelerated aging tests carried out in FCLAB could be a promising direction. Indeed, this involves the varying operating (current) profile that can be used for both development and validation of prognostics algorithms. The parameter of polarization resistance estimated from EIS helped to improve the RUL prediction accuracy. The proposed model gives the best performance among all the tested models, especially for long-term predictions. This study brings an idea of integrating SOH characterization into RUL prediction, which leads to a better performance of RUL predictions. In the following chapters, the use of available information regarding the SOH characterization will be further explored.

Chapter 5

Multi-level Prognostics Using On-line Inspection of Degradation Covariates

Through the RUL prognosis in the previous chapter, it suggests that the degradation processes in general change with time, as do the functioning of the system due to external operating conditions (*e.g.* environmental causes, input profiles, *etc*) or internal causes (*e.g.* modification of a system parameter, *etc*). The degradation behavior might be accessible thanks to internal and external covariates which are usually difficult to access owing to expensive measurement cost or technological difficulties. The main obstacles to this adaptation are that the covariates effects might not be directly accessible from the current degradation indicator and that the link between the degradation process and covariates may differ in different cases. If there is a possibility to gather information on the hidden or "deep" covariates, it might be interesting to inspect them from time to time to improve the state of knowledge on the system for a better prognostics, even though the inspections are very costly. The mitigation of the impacts of known degradation covariates can help to improve the precision in durability assessment. This chapter aims to propose a multi-level prognostics approach for systems whose degradation covariates at different levels are accessible. The work reported in this chapter is based on the work presented in the IFAC 2017 World Congress, 9-14 July 2017, Toulouse [99].

Contents

5.1 Problem Formulation

The degradation evolution of a system under operation may not be well estimated because either external conditions or internal modifications can modify the degradation behavior: if these degradation covariates are unknown, it can be difficult to identify their effect from the observation of the degradation alone. Classic Bayesian estimation-based prognostic methods lack the ability to accommodate the unexpected changes in degradation evolution due to these underlying covariates. A possible solution to this issue could be to investigate the degradation covariates through indicators gathered at other levels of the system and to update the parameters of used degradation model to accommodate the changes in degradation evolution for a better estimation.

5.1.1 General Modeling Assumptions

Consider a system under operation subject to degradation from new till its EOL. Its performance level is constantly monitored to reveal the degradation of its State of Health (SOH) ($0 \leq \text{SOH} \leq 100\%$). Assume that the evolution of this degradation (SOH decrease) follows a process, which can be described by a discrete-time state transition model :

$$x_k = f_k(x_{k-1}, \omega_{k-1}, \Theta_{k-1}) \tag{5.1}$$

where k is the time step index, x is the system state representing the system performance, f is the state transition function (degradation model, *e.g.* the evolution of the degradation path in Figure 5.1), ω is the system noise and Θ is the vector of the model parameters ($\Theta = [\theta_1, \theta_2, ...]$).

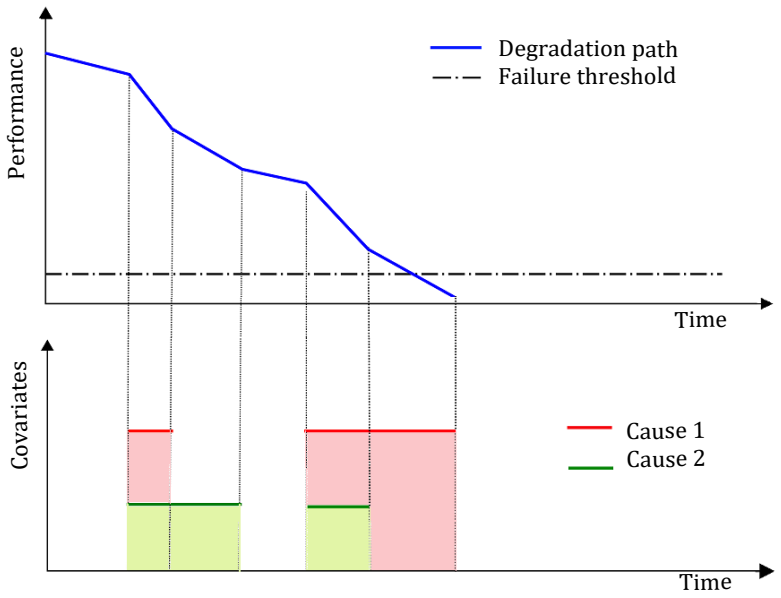

Figure 5.1: Degradation path and covariates.

The degradation of the SOH of the system can be due to its intrinsic imperfection and also, to the effect of both external or internal degradation covariates. Here we assume that some covariates, denoted c, can impact the degradation behavior by affecting the model parameters:

$$\Theta_k = g_k(c_k) \tag{5.2}$$

Where g is the function describing the effect of the degradation covariates on the degradation model parameters. The covariates, shown in Figure 5.1, are supposed to be measurable. We also assume that the model parameters and the covariate are known.

5.1.2 Objectives of the work

Traditional Bayesian estimation-based prognostic methods lack the ability to accommodate the unexpected changes in degradation evolution due to these underlying and unmonitored covariates. On the other hand, when the causes of the changes are accessible, with a multi-level approach, those changes can be adapted faster by inspecting the degradation covariates and by adapting accordingly the parameters of the prognosis filter. Figure 5.2 presents an example of degradation path with degradation covariate. For instance, a classical Particle Filtering (PF) method (green dashed line in Figure 5.2) can estimate the degradation path but when there are significant changes in the evolution trend of the path, the PF can not immediately response. It needs a certain period to adapt the changes. On the other hand, with the help of inspecting the covariate and update the model accordingly, the estimation can be adapted better (red dashed point line in Figure 5.2).

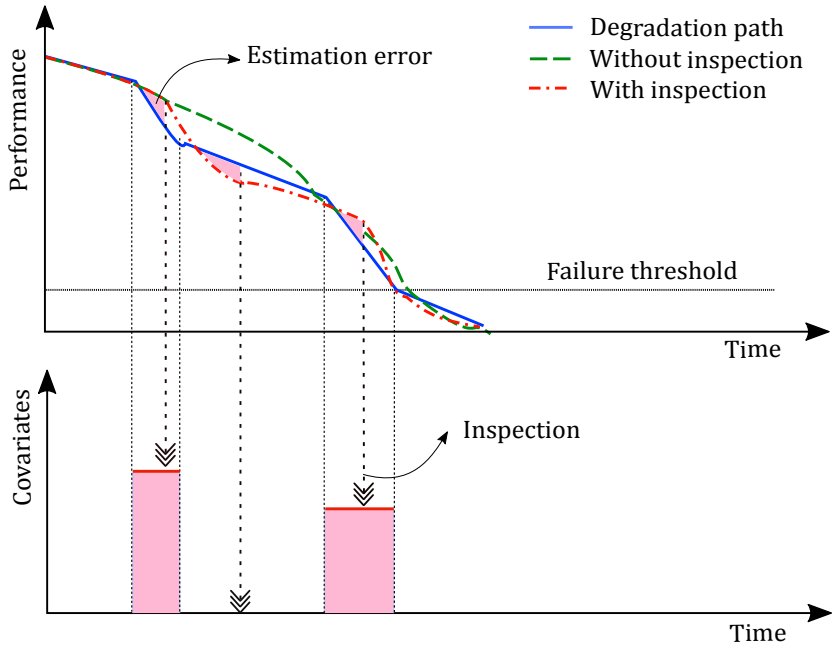

Figure 5.2: Principle of degradation estimation with inspection policy.

The objective here is then to develop a method to predict the future system degradation and RUL, using both the degradation information (easily accessible, but incomplete when

considered alone) and, when necessary, the information on the degradation covariates (deeper information, accessible with a cost). Since getting the information on the underlying covariates is costly, they cannot be measured continuously. We propose a procedure to optimize the measurements and the use of the covariates in two steps [99]:

- the issue is first to build a covariate inspection policy so that the covariates are measured only when necessary to minimize an overall cost function for the prognosis procedure and to find an optimal balance between the covariate monitoring cost and the quality of the degradation estimation and RUL prediction ;
- within a PF-based prognosis procedure, when the measure of the covariates values is available, it can be used to adapt the parameters of the filter to improve the estimation and the prediction.

We propose in the next section an implementation of this approach.

5.2 Multi-Level Prognosis Approach

In this section, we detail the inspection policies and present the algorithm of multi-level prognostic approach.

5.2.1 Inspection of the Covariates

The question is how and when to inspect. Assuming that the covariates impacts on the degradation level can be quantified and modeled, two types of inspection policies can be implemented:

- Periodic inspections: the covariates are inspected periodically, with a fixed time period, performed every τ time steps;
- Online Triggered Inspections: the covariates can be inspected only when it is necessary, when the degradation estimation accuracy is no longer satisfying. At each estimation step k, the estimation error is calculated online:

$$\hat{\epsilon}_k = \frac{\sum_{k-L}^{k} \|z_k - \hat{x}_k\|}{L} \tag{5.3}$$

where z_k is the online measurement, $\hat{x}_k$ is the estimated current state and $\hat{\epsilon}$ is the current estimation error with a time window of size L. An inspection is triggered whenever $\hat{\epsilon}_k$ reaches preset error threshold $ET : \hat{\epsilon}_k \geq ET \rightarrow inspection$. The online inspection policy is also illustrated in Figure 5.2. The inspections are triggered when the estimation error are accumulated to a certain limit.

5.2.2 Integration of the Covariates Information in the Prognostic Algorithm

The information on the covariates values delivered by the inspection has to be integrated into the prognosis scheme. If the covariates measured by the inspection are the same as the covariates assumed in the prognosis filter, nothing is done. If the measured covariates are different, then the parameters of the degradation model are updated according to Equation (5.2). Integrating the periodic inspection procedure into the PF prognosis algorithm leads to Algorithm 4:

Algorithm 4 PF estimation with periodic inspection.

1: **for** $k = 1 : t_\lambda$
2: **for** $i = 1, ..., n$
3: Draw new particles x_k^i from the prior density $p(x_k|x_{k-1}^i)$
4: Calculate the corresponding weight of each particle: $w_k^i = L(z_k|x_k^i)$
5: Normalize the weights: $w_k^i = w_k^i / \sum_{i=1}^{n} w_k^i$.
6: Calculate the cumulative sum of normalized weights:
$Q_k = CumulativeSum\left[\{w_k^i\}_{i=1}^N\right]$
7: Draw a random value u^j from the uniform distribution $U[0, 1]$
8: State and parameters estimation:
$\hat{x_k} = MedianValue\left[\{x_k^{i*}\}_{i=1}^N\right]$
$\hat{\Theta}_k = MedianValue\left[\{\Theta_k^{i*}\}_{i=1}^N\right]\ j = 1$
9: **while** $Q_k \geq u^j$
10: $j = j + 1$.
11: **end while**
12: Assign particles: $x_k^{i*} = x_k^j$, $\Theta_k^{i*} = \Theta_k^j$.
13: **if** $k = \tau, 2\tau, ...$ **then**
14: inspect c_k and update the parameters if necessary using the model $\Theta_k = g_k(c_k)$
15: **end if**
16: Go back to step 1
17: **end for**
18: **end for**

The PF estimation will sequentially processed until the prediction time step t_λ is reached. The covariate c is inspected when the time step reaches a scheduled inspection time interval τ (Algorithm 4, *line* 13). If we integrate the online inspection procedure into the scheme, it gives Algorithm 5, where the covariate c is checked only when the estimation error reaches a threshold ET (Algorithm 5, *line* 13).

5.2.3 Decision Variables for the Inspections Policies

The covariates inspection policy can be optimally tuned using one of the decision variables (either the inter-inspection period τ or the error threshold ET) to ensure the best estimation

Algorithm 5 PF estimation with online inspection.

for $k = 1 : t_\lambda$
  for $i = 1, ..., n$
    Draw new particles x_k^i from the prior density $p(x_k|x_{k-1}^i)$
    Calculate the corresponding weight of each particle: $w_k^i = L(z_k|x_k^i)$
    Normalize the weights: $w_k^i = w_k^i / \sum_{i=1}^{n} w_k^i$.
    Calculate the cumulative sum of normalized weights:
    $Q_k = CumulativeSum\left[\{w_k^i\}_{i=1}^N\right]$
    Draw a random value u^j from the uniform distribution $U[0, 1]$
    State and parameters estimation:
    $\hat{x_k} = MedianValue\left[\{x_k^{i*}\}_{i=1}^N\right]$
    $\hat{\Theta_k} = MedianValue\left[\{\Theta_k^{i*}\}_{i=1}^N\right]$ $j = 1$
    while $Q_k \geq u^j$
      $j = j + 1$.
    end while
    Assign particles: $x_k^{i*} = x_k^j$, $\Theta_k^{i*} = \Theta_k^j$.
    if $\hat{\epsilon}_k \geq ET$ **then**
      inspect c_k and update the parameters if necessary using the model $\Theta_k = g_k(c_k)$
    end if
    Go back to step 1
  end for
end for

accuracy and to minimize the overall estimation cost. The estimation cost J in this study is defined as the combination of two parts: the cost (or penalty) resulting from the estimation error, and the cost of inspections represented by the number of performed inspections. We assign those costs with an arbitrary unit.

$$J = \alpha \cdot \hat{\epsilon} + \beta \cdot N_{ins} \tag{5.4}$$

Where $\hat{\epsilon}$ is the average estimation error on the system degradation on its whole life, N_ins is the number of inspections performed on the system life and α and β are the respective corresponding cost coefficients. From the estimation accuracy's point of view, the more inspections are carried out; the better accuracy can be achieved. On the other hand, implementing too many inspections leads to higher costs. The objective here is to balance the quality of the degradation estimation and the number of inspections on the whole system life. Note that for a periodic inspection policy:

$$N_{ins} = \frac{EOL}{\tau}. \tag{5.5}$$

5.3 Application & Numerical Experiments

Due to the limitation of real experimentation, this section shows the implementation of the approach with a simulated case.

5.3.1 Degradation Simulation

The degradation paths are simulated using an exponential state transition function described in [100]:

$$x_k = x_{k-1} \cdot exp(-b(c_k) \cdot \Delta t) + \omega_k \tag{5.6}$$

An additive zero-mean Gaussian noise $\omega_k \sim \mathcal{N}(0, \sigma_\omega^2)$ is used to represent the system (process) noise. The initial state value x_0 is equal to 100% of SOH. We consider in this simulation only one degradation covarate, the presence of covariate c (Figure 5.1) impacts the degradation behavior, which is represented by the change in trend parameter b in Equation (5.6):

$$b(c_k) = \begin{cases} b_0, & if \quad c_k = 0 \\ b_0 \cdot (1 + 3c_k), & else \end{cases} \tag{5.7}$$

The covariate c is generated by a Markov process with two values: $c = 0$ and $c = 1$ (Figure 5.3). b_0 is set to 10^{-3}.

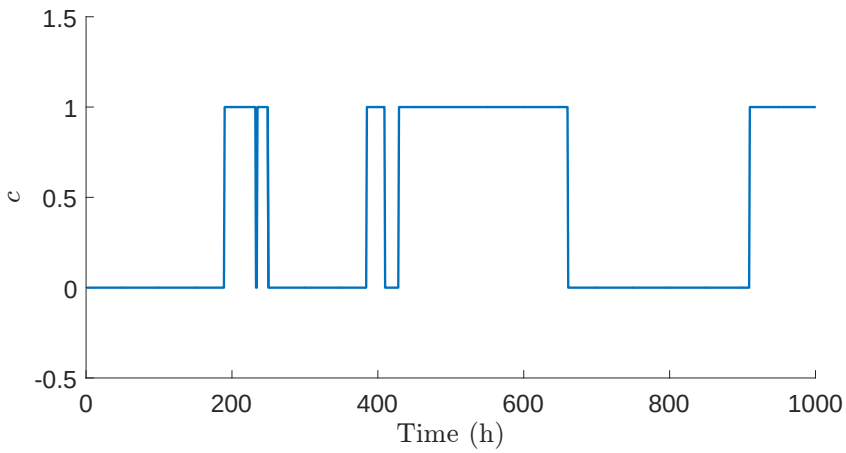

Figure 5.3: Covariate simulated by Markov process.

The measurement is generated by adding a zero-mean Gaussian noise (measurement noise) $\nu_k \sim \mathcal{N}(0, \sigma_\nu^2)$ at each step:

$$z_k = x_k + \nu_k \tag{5.8}$$

The degradation is shown in Figure 5.4 with performance degrades from 0% to 100%, and time from 0 hour to 1000 hours.

5.3.2 Degradation Estimation without Inspection

First, a PF-based estimation method is applied on the degradation path without any inspection on the covariate c.

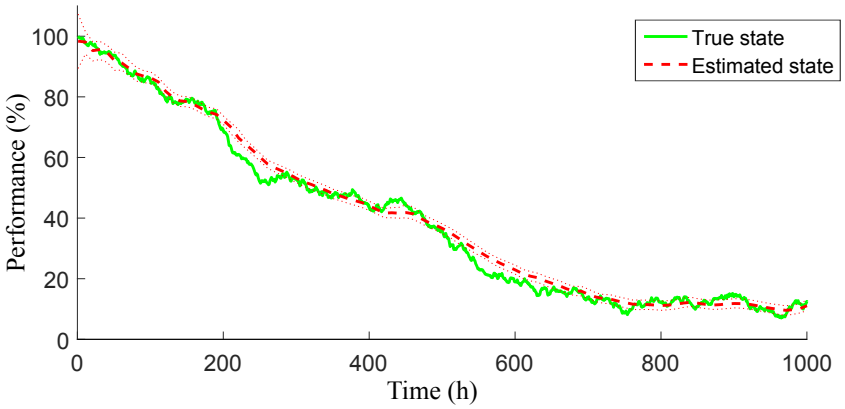

Figure 5.4: State estimation without inspection.

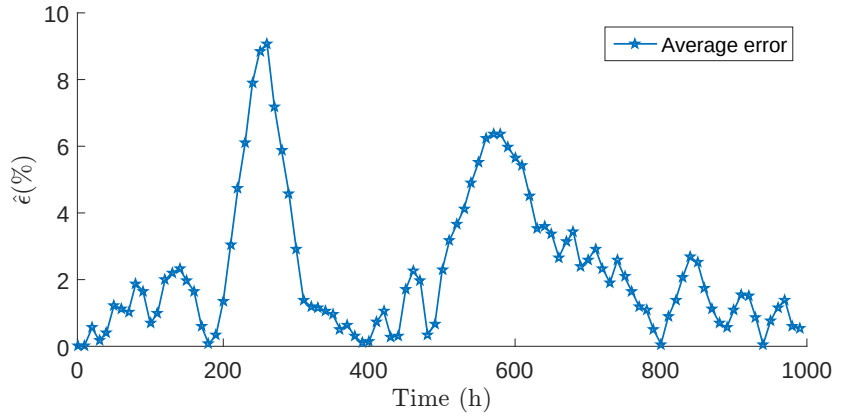

Figure 5.5: Estimation error without inspection.

Figure 5.4 shows the degradation estimation by a classic PF without inspection. The PF filter does not adapt rapidly to the sudden changes due to covariate changes. Figure 5.5 shows the average error corresponding to the estimation without inspection that reaches a maximum around 10%.

5.3.3 Estimation with Periodic Inspection of the Covariate

A degradation estimation procedure with periodic inspection of the covariate is considered here. The inspection period τ is optimally tuned to minimize the criterion cost J combing the estimation accuracy and inspection costs introduced in Section 5.2.3. Assuming the cost of estimation (un-)accuracy ($\alpha \cdot \hat{\epsilon}$) is more important than the cost of inspection action ($\beta \cdot$

N_{ins}), we choose for example $EOL = 1000$ hours, $\alpha = 10$ and $\beta = 1$ with arbitrary unit in Equation (5.4). To determine the optimal inspection period, 50 different values of τ are tested from 10 hours to 500 hours.

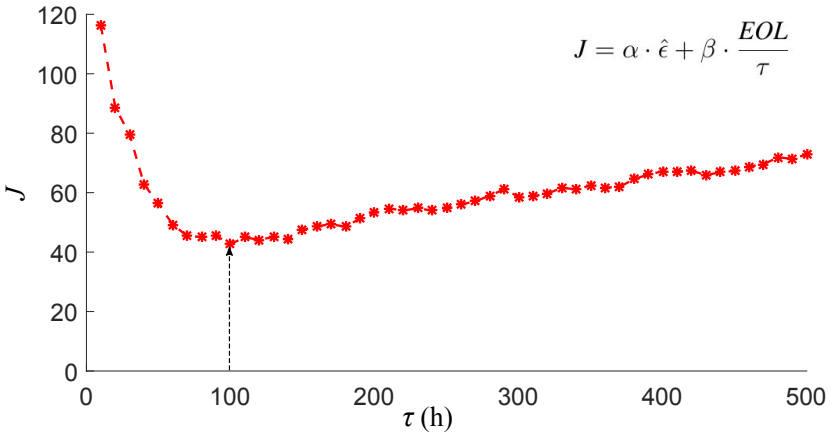

Figure 5.6: Cost for different lengths of inspection intervals.

Figure 5.6 shows the cost for different inspection periods τ and a minimum cost is found for $\tau^* \simeq 100$ hours. Figure 5.7 shows the estimation with the minimum cost interval τ^*. It can be seen in Figure 5.8 that the degradation estimation procedure is able to integrate the covariate information delivered by inspections to adapt the degradation estimation as shown in Figure 5.7. It can also be noticed that the state model does not always need to be updated. The black circles (Figure 5.7 and Figure 5.8) without a central cross (mode switch) imply that these inspections are not necessary since the used mode is the same as the true mode. Figure 5.9 shows the estimation error with periodic inspection for $\tau^* = 100$ hours. The error remains at a lower level than the one without inspection. Nevertheless, to avoid unnecessary inspections, a decision has to be made on whether to carry them out or not.

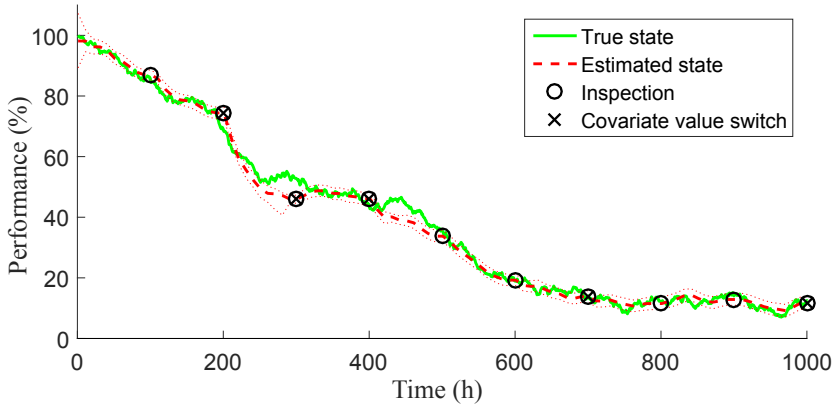

Figure 5.7: State estimation with periodic inspection ($\tau^* = 100$ hours).

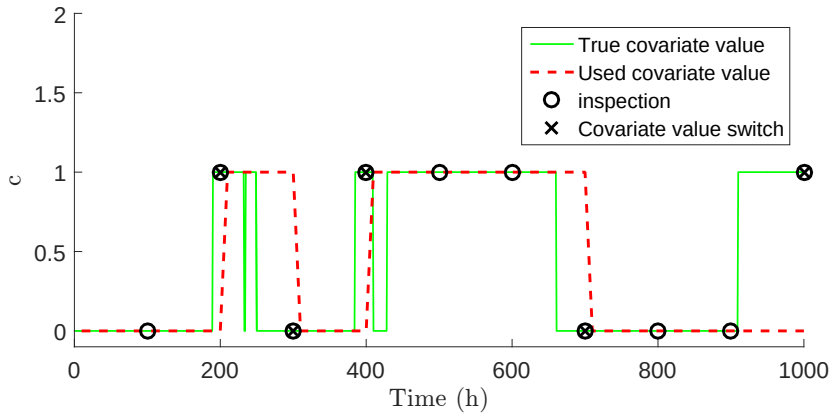

Figure 5.8: Periodic inspection for covariates ($\tau^* = 100$ hours).

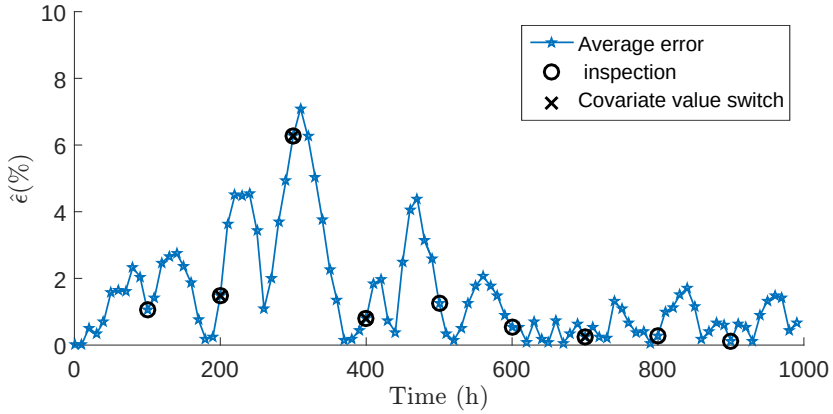

Figure 5.9: Estimation error of periodic inspection ($\tau^* = 100$ hours).

5.3.4 Estimation with Online Triggered Covariate Inspection

Consider now the procedure for the degradation estimation with online triggered covariate inspection. Three decision variables have to be tuned for this procedure: i) the time window size L to filter the estimation error; ii) the threshold ET on the estimation error to trigger the inspection; iii) the minimum waiting time τ_h between two inspections to avoid unnecessary inspections. These variables are tuned according to:

- Window size L: A preliminary sensitivity analysis on L in Equation (5.3) has shown that a window size of $L \geq 50$ hours does not alter the estimation accuracy nor the number of inspections. Thus L is set at 50 hours.
- Error threshold ET: When the estimation error reaches the threshold ET, a covariate inspection is triggered to decide whether it is necessary to update the degradation model parameters. The estimation error is calculated as in Equation (5.3) as the average distance between estimated value and the observation on a moving window of size L. In the presented example, values of ET are tested from 1% to 15%.

- Waiting time τ_h: Different values of the minimum waiting time between two inspections τ_h are tested from 10 hours to 500 hours.

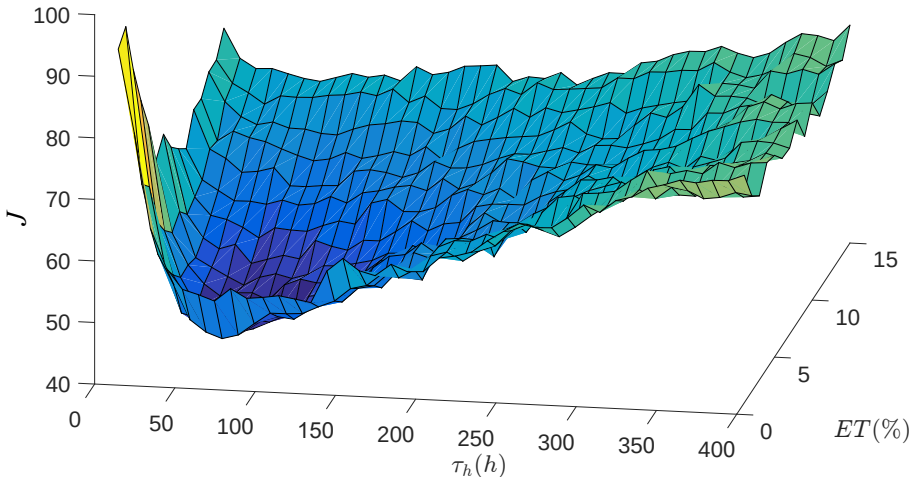

Figure 5.10: Estimation cost surface for online triggered covariate inspection $J(ET, \tau_h)$

Figure 5.10 shows the cost surface for the estimation with online triggered inspections of a covariate as a function of two decision variables, ET and τ_h. The minimum cost is found at $ET^* = 4\%$ and $\tau_h^* = 50$ hours.

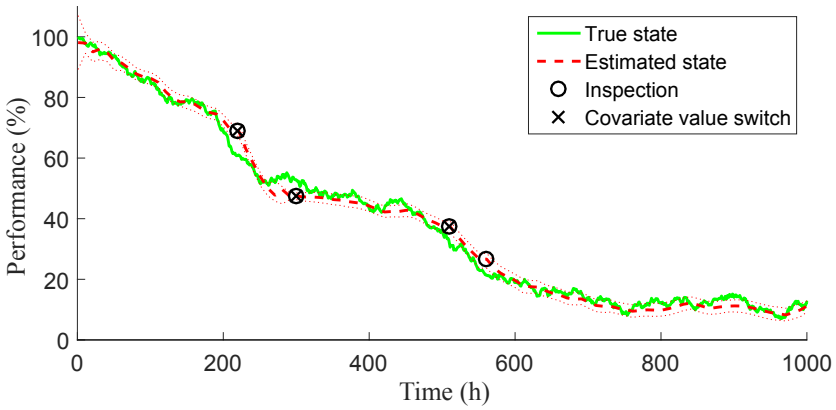

Figure 5.11: State estimation with online triggered covariate inspection

Figure 5.11 shows the estimation for the optimally tuned decision variables. In Figure 5.13, when the estimation error reaches ET, inspections on covariate c are triggered and corrections can be decided (Figure 5.12). The number of unnecessary inspections is reduced compared with periodic inspection, which permits a lower cost as shown in Table 5.1. The results are the average of 100 estimations.

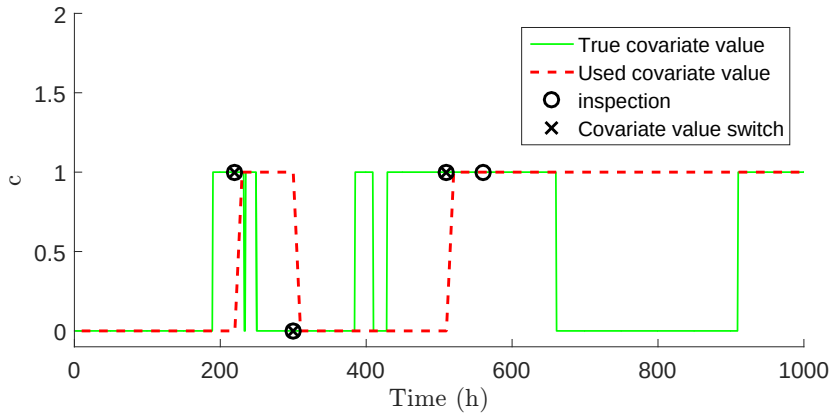

Figure 5.12: Online triggered inspection for covariates.

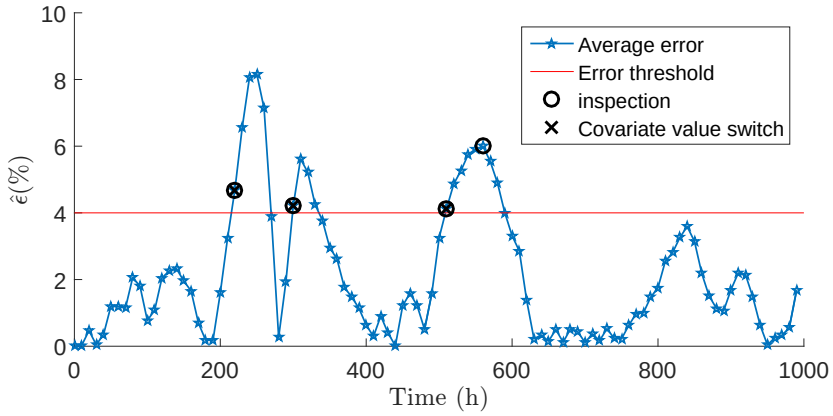

Figure 5.13: Estimation error with online triggered covariate inspection.

5.3.5 RUL Prognosis and Performance Analysis

The PF is used to train the state transition model during the estimation phase until prediction time t_λ, then the particles are propagated through the estimated model. Figure 5.14 shows the RUL prediction example at 600 hours. The RUL histogram represents the time indexes distribution of all particles reaching a preset failure threshold.

To evaluate the prognostic performance, several RUL predictions with different prediction time steps (range from $t_\lambda = 300$ hours to 740 hours, where the true EOL is at 745 hours) are made and assessed using the prognostic performance metrics.

Figure 5.15, Figure 5.16 and Figure 5.17 shows the predicted RULs with uncertainties at different prediction times of three cases with different inspection policies: 1) without any inspection; 2) with periodic inspection; and 3) with online inspection, respectively. We can visually observe that the PH of periodic inspection is the longest (Figure 5.16) which implies the best prognostic performance. When there is no inspection applied, the RUL predictions

Table 5.1: Estimation cost for different covariate inspection schemes

	Without	Periodic	Online
ϵ (%)	5.91	3.47	3.51
N_{ins}	0	10	7
J	59	45	42

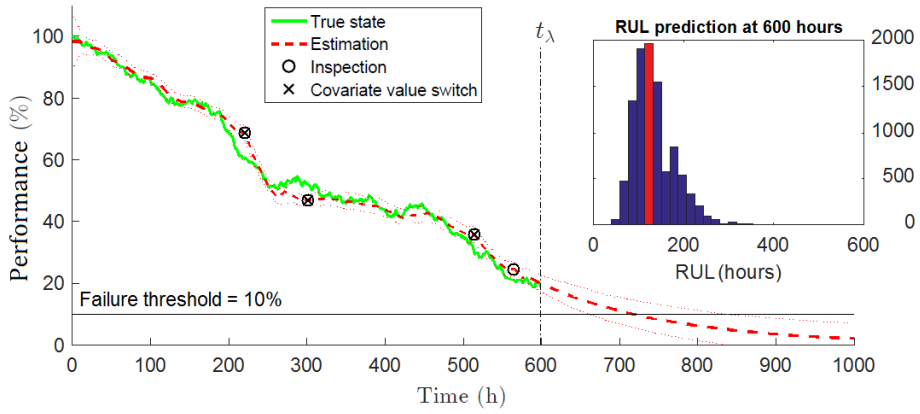

Figure 5.14: Degradation estimation with online triggered inspections and RUL prediction at 600 hours.

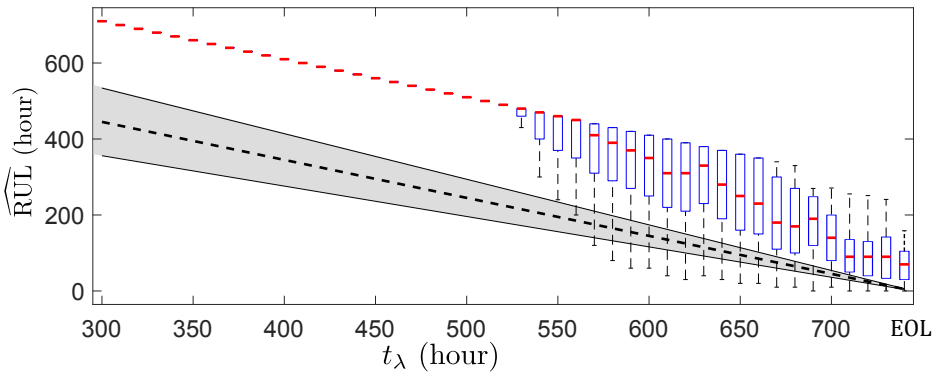

Figure 5.15: RUL predictions without inspection.

can hardly enter the accuracy zone (Figure 5.15). The RUL predictions with online inspection (Figure 5.17) enter the zone later than the ones with periodic inception due to the frequency of inspections applied. The performance for those three cases are listed in Table 5.2. In this study, we focus on the metrics of accuracy only.

We can see that the predictions with periodic inspection scheme give the best performance in both Acc and αAcc indexes, which indicates that the predictions are more accurate thanks to the information delivered by the inspections and associated the model update. Meanwhile, the frequent inspections incur a higher cost of inspection (larger number of inspections N_{ins}).

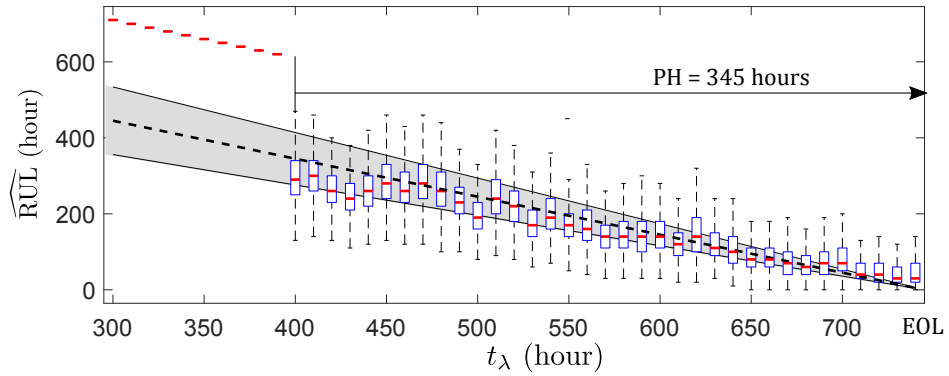

Figure 5.16: RUL predictions with periodic inspections.

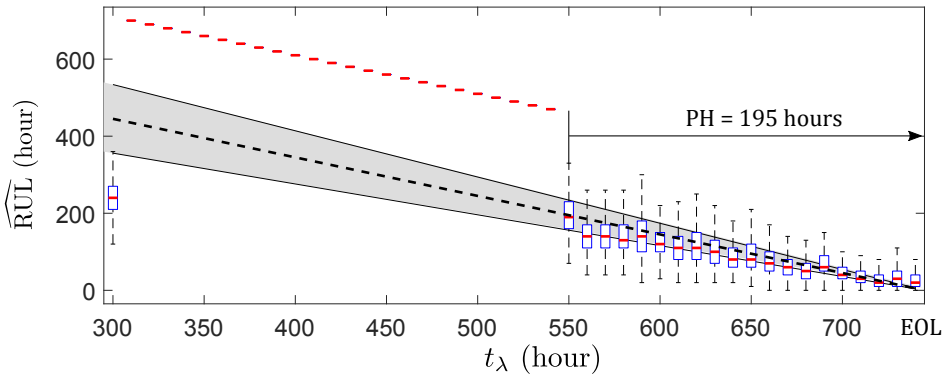

Figure 5.17: RUL predictions with online triggered inspections.

Online inspections can provide better predictions than the one without inspection and incur a lower cost than periodic inspections.

In this study, it has been found that the estimation error decreases when the standard deviation of process noise ω in (5.1) increases. With a smaller noise, the PF-based estimation is constrained thus the degradation trend cannot be followed which leads to a larger error. With a larger noise, the particles have more freedom to adapt the degradation changes which reduces the estimation error. From the estimation accuracy point of view, a better estimation can be achieved by increasing the process noise. However, the prognostics approach is devoted to predicting RUL. Thus the necessity and benefit of inspection should also be discussed in the view of RUL prediction. In a numerical experiment, 100 estimations are repeated with different σ_ω.

It is shown in Figure 5.18 that, with very small noise (around 0), the PF-based prognostic approach is not able to perform an RUL prediction. For a process noise with a large variance (*e.g.* σ_ω=10), both predictions without inspection and with online inspections are the same. It indicates that when the noise is great, the inspection is no longer activated. The model is thus not trained by the true state process but its noise, which results in a lack of reliable/accurate predictions. On the other hand, prediction with periodic inspection will continue to check the

Table 5.2: Prognostic performance & cost

	Without	Periodic	Online
Acc	0	**0.54**	0.27
αAc	0	**0.53**	0.36
$\epsilon_{pre}(\%)$	69.19	**20.73**	28.91
N_{ins}	0	215	110
J	692	422	**399**

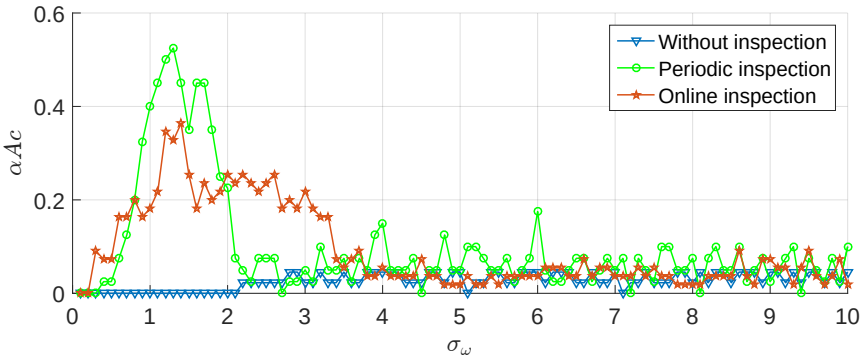

Figure 5.18: Prognostic performances with different σ_ω.

covariates at preset time step which helps the model to learn the useful information and make predictions at higher accuracy although being impacted by the noise. Figure 5.18 shows that the best prediction performance for periodic inspection is obtained with $\sigma_\omega = 1.3$, and with $\sigma_\omega = 1.4$ for online inspection, which is the value used in our approach.

5.4 Conclusion

The proposed study on a simulated deteriorating system shows that the multi-level prognostics can be improved by applying online inspections. The covariates are investigated which allows the PF-based prognostics approach to give better predictions for RUL prognosis at a lower cost. To become commercially interesting, the inspection has to be done only when the minimum of the cost criteria J is reached to avoid unnecessary inspection costs. Note that the definition of J will impact the choice of inspection schemes. Another way of using information of degradation covariates at the different level will be proposed in next chapter.

Chapter 6

Multi-level Prognostics Using An Ensemble of Models for Integrating Dependent Sources of Information

This chapter presents a prognostic approach based on an ensemble of two models for the RUL prediction of a fuel cell stack. Two different prognostic models are used, and the prognostic procedure is implemented using particle filters and fed by measurements taken at different levels in the system. The filter for the first model receives a signal directly observable and related to the fuel cell output voltage which can be frequently and easily measured, but it relies on a simplified model of the degradation trend. The second particle filter is fed by measurements from the physical characterization of the stack, which are seldom acquired by periodic inspections, and uses a model of the SOH evolution, from which the degradation state is estimated. The outcomes of the two prediction filters are aggregated to obtain the ensemble predictions. The work reported in this chapter has been presented at the 10th International Conference on Mathematical Methods in Reliability (MMR) held in Grenoble in July 2017 [101].

Contents

6.1 Problem Formulation

During the research on prognostic approaches for PEMFC, we should not ignore, indeed, that there are many works on prognostics for other industrial systems as well. We found special interests in the approaches of the ensemble of models which uses prediction outcomes of different degradation models and gives the prognostic result as a combination. With a prognostic tool (*e.g.* Particle Filtering), the RUL predictions can be carried out based on several degradation measurements. The idea is to combine those indicators that complement each other by leveraging their strengths and overcoming their drawbacks. To this end, solutions based on an ensemble of models, instead of a single model, have shown promising results for the prognostics of industrial systems [49], [60], [98], [102]; indeed, they provide a way to use jointly several models to aggregate information from different measurements. However, this kind of approach is usually based on a significant amount of historical run-to-fail data, such as fuzzy similarity, which has not been applied in the field of PEMFC due to the high cost of large quantities of the run-to-failure test. Although it is not yet ready to apply for PEMFC in practice by far, we rather consider the ensemble of models a possible solution to PEMFC prognostics since the focus on the prognostics for PEMFC are growing.

6.1.1 Fuel Cell Degradation

Performance degradation is unavoidable but can be minimized by proper operation and maintenance, based on a comprehensive understanding of degradation mechanisms. PEMFC degrades due to calendar aging, which can occur even under constant optimal conditions, start and stop cycles and inadequate operating conditions such as temperature, pressure and poor water management. In a fuel cell, the aging process reduces the component performance and modifies its material physical properties. Figure 6.1 shows the evolution of the stack voltage degradation. The decreasing trend represents the irreversible degradation, whereas the voltage jumps represent the reversible behavior caused by operating conditions modification.

During the lifetime of a PEMFC, its "health" and performance gradually deteriorate, due to irreversible physical and chemical changes, which take place with usage and with aging, until the moment the stack is no longer usable. As explained in Chapter 2, the SOH (*e.g.* from its Begin Of Life (BOL) status of 100% performance to its End Of Life (EOL) status of 0%) provides an indication (not an absolute measurement) of the performance which can be expected from the PEMFC in its current condition and of the amount of lifetime already spent by the component.

Any parameter significantly changing with age, such as cell impedance, can be used for indicating the SOH of the cell. These parameter changes are typically identified by performing

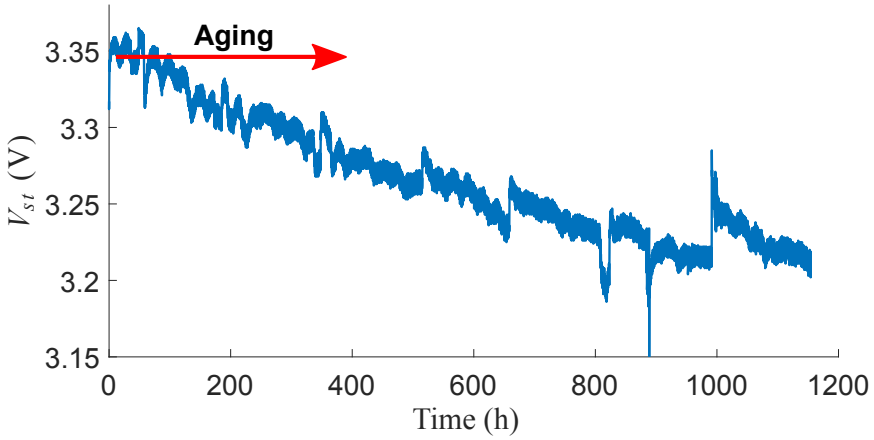

Figure 6.1: Voltage degradation with aging (under constant current density) [13].

characterization measurements such as polarization curves. The polarization curve describes the working performance of PEMFC. The variations of internal parameters, including physical and empirical ones, have great impact on the polarization characteristic. Figure 6.2 shows the variation of the polarization curves under aging. In this work, physical and empirical parameters are used to predict the performance of the fuel cell. We will consider two indicators of the PEMFC degradation: the stack voltage and the SOH. The stack voltage V_{st} can be measured at a high frequency ($\approx 0.6s$) and the SOH are characterized every week in practice.

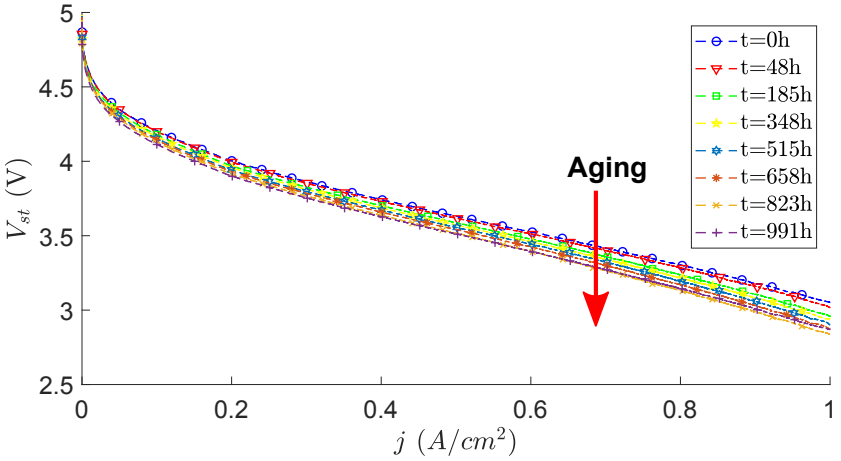

Figure 6.2: Polarization curves during aging [13].

6.1.2 Models Description

6.1.2.1 Voltage Model

Being electrochemical cells, fuel cells obey to thermodynamic and kinetic laws. The static voltage of a fuel cell stack, depicted in Figure 6.2, is given by [77]:

$$V_{st} = n \cdot (E - V_{ohm} - V_{act} - V_{trans}) \tag{6.1}$$

where V_{st} is the stack voltage, n is the number of cells in the stack, E is the open circuit voltage (OCV), V_{act} is the activation polarization, V_{ohm} represents the ohmic losses (due to the electrical resistance of individual components and their contact), and V_{trans} is the concentration polarization (due to mass transport limitation). For a stack operating at a current density j [103]:

$$V_{st} = n \cdot \left(E - r \cdot j - A \cdot ln(\frac{j}{j_0}) - m_1 \cdot exp(m_2 \cdot j) \right) \tag{6.2}$$

where r is the internal resistance, j is the operating current density, A is the Tafel coefficient, j_0 is the exchange current density, m_1 and m_2 are the mass-transfer constants. Considering different current current density values, a static polarization curve is obtained.

6.1.2.2 SOH Degradation Model

A limitation of the stack voltage is that it does not allow separating the effect of the load variation, which causes current density variations, from that of the stack inner degradation, which influences the OCV [3] and the global resistance parameters [79], [80]. Since physical laws describing the effects of the degradation on E and r are not known, in this work we adapt linear equations for simplicity of illustration and without loss of generality of the proposed approach. The changes in the two parameters are coupled by variable $\gamma(t)$, which reflects the SOH degradation:

$$\begin{aligned} r(t) &= r_0(1 + \gamma(t)) \\ E(t) &= E_0(1 - \gamma(t)) \end{aligned} \tag{6.3}$$

where r_0 and E_0 are the initial values of r and E. Since it has been proven in [79], [80] that the SOH indicator $\gamma(t)$ can be estimated from polarization curves, in this work we assume the availability of the procedure which returns the SOH degradation estimation $\gamma(t)$ from characterization measurements of the PEMFC stack. Thus, $\gamma(t)$ can be taken as an input for our prognostic procedure.

6.1.2.3 Prognostic Models for RUL Prediction

Two stochastic state transition models are used for describing the SOH deterioration $\gamma(t)$ and the stack voltage degradation $V_{st}(t)$.

6.1.3 Problem Statement

When the fuel cell stack experiences variable operating conditions, a single degradation indicator is not able to provide a precise and robust RUL prediction. The stack voltage does not directly measure the component degradation but it is only related to degradation symptoms, which are significantly affected by operating conditions. The SOH provides aging information but it can only be measured at low frequency in industrial applications.

In this work, we consider prognostics based on two different measurements of the stack degradation:

- An external signal, such as the stack voltage, which is easily accessible and frequently measured, but of "poor quality", *i.e.* its measurement is affected by significant noise.
- A signal which provides an internal characterization of the component, such as the stack SOH, which is seldom measured due to the complexity and cost of the measurement procedure that requires to take the fuel cell stack out of service for the measurements.

The objective is to combine the predicted RUL outcomes based on the two signals.

6.2 Ensemble-based Prognostics

6.2.1 PF-based RUL prediction

It has been proven that Bayesian estimation techniques provide a framework which can deal with high uncertainties in degradation processes [104]. Bayesian estimation with particle filters is not limited by either linearity or Gaussian noise assumption. PF-based approaches are more and more deployed for prognostics purposes, and are thus chosen for the degradation path estimation in this study.

In a PF framework [92], the filtering step for the estimation of the degradation state at present is based on the prior Probability Density Function (PDF) of the degradation state and the model parameters provided by the experts; then the Bayesian update is processed sequentially. In the prediction phase, the posterior PDF of the state and model parameters are used for the estimation of the future degradation evolution. The RUL PDF can be obtained when the degradation state reaches the preset failure threshold FT by being propagated along the estimated degradation evolution (Figure 6.3).

6.2.2 Prognostic Models for RUL prediction

For the PF-based estimation stage, the following simplified state models are used for the SOH deterioration $\gamma(t)$ and the stack voltage degradation trend $V_{st}(t)$:

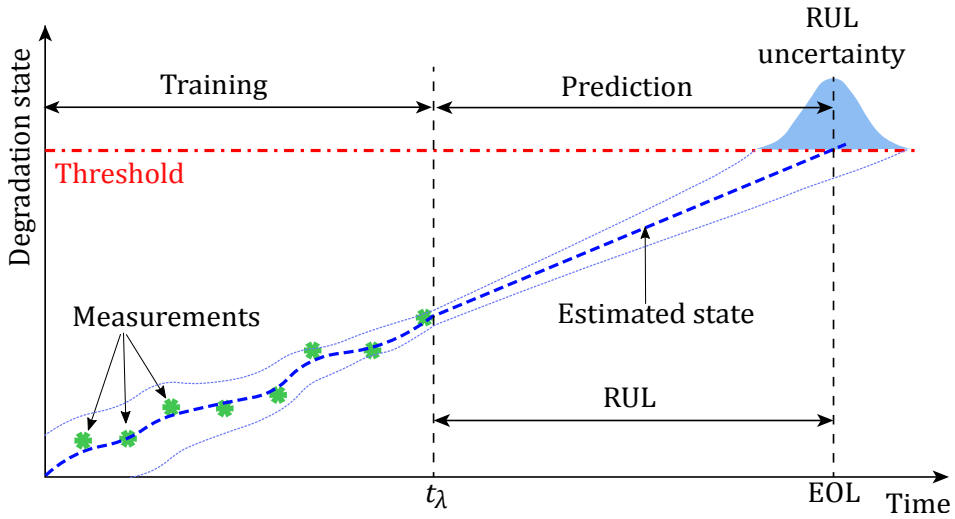

Figure 6.3: RUL prediction with PF.

- $\gamma(t)$ represents the SOH degradation. It assumes values from 0 (healthy) to 100% (failed), following a linear model:

$$\gamma(t+1) = c^{(1)}(t) \cdot \gamma(t) \tag{6.4}$$

  where $c^{(1)}(t)$ is the time-dependent SOH degradation model parameter [79].

- $V_{st}(t)$ represents a symptom of the stack degradation, which, according to Equation (6.4), follows a linear trend:

$$V_{st}(t+1) = c^{(2)}(t) \cdot V_{st}(t) \tag{6.5}$$

  where $c^{(2)}(t)$ is the time-dependent voltage degradation parameter

The two linear degradation models of Equation (6.4) and (6.5) are used in two different particle filtering algorithms to provide the RUL predictions $\widehat{RUL}_t^{(m)}$ (m=1, 2), respectively. Model 1 in Equation (6.4) uses measurements of good quality, but not frequently acquired, whereas Model 2 in Equation (6.5) uses measurements that are regularly available, whose quality can be poor due to higher measurements noise and lower correlation with the true health states. The objective is, then, to combine the individual estimates $\widehat{RUL}^{(1)}$ and $\widehat{RUL}^{(2)}$, taking into account their "local" qualities.

6.2.3 Ensemble of Models

Fusing the outputs of an ensemble of diverse prognostic models can improve overall prediction accuracy [105]. Local aggregation dynamically assigns weights to each model according to its local performance, typically evaluated on the available historical patterns [106]. For prognostics, local aggregation requires the computation of the local performances of the individual models on a set of run-to-failure degradation trajectories.

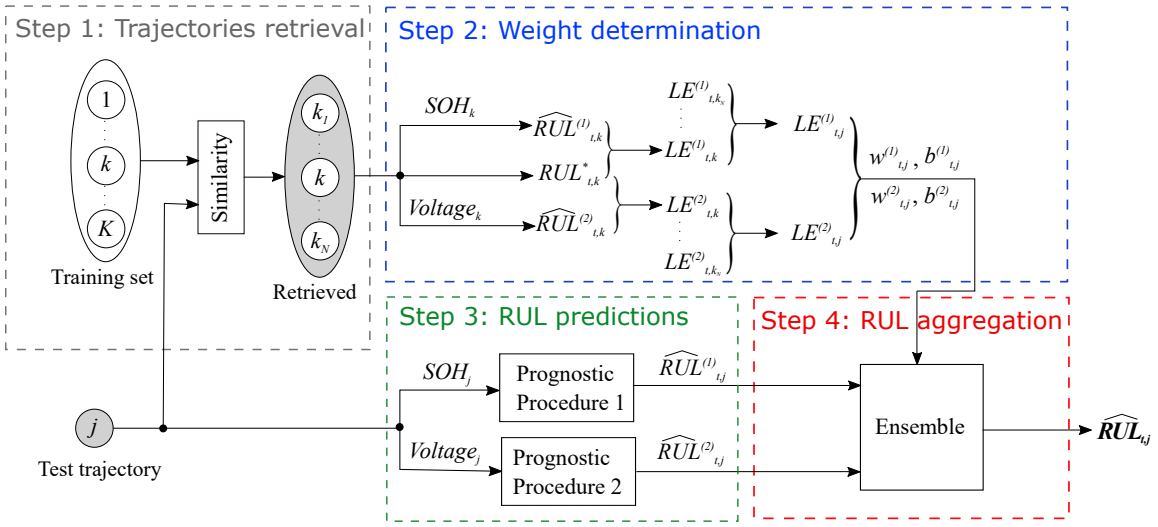

Figure 6.4: Scheme of proposed prognostic approach.

Figure 6.4 presents the scheme of an ensemble-based prognostic approach. As mentioned previously, we assume the availability of the measurements of the signals $x^{(1)} = \gamma$ and $x^{(2)} = V_{st}$ collected during the life of K identical fuel cell stacks:

$$\{x_k^{train}\}_{k=1}^{K} = \{(x_k^{(1),train}, x_k^{(2),train})\}_{k=1}^{K} \tag{6.6}$$

These run-to-failure trajectories form a training set, which is also used within the ensemble approach for the aggregation of the individual model outcomes. The local fusion approach for the aggregation of the individual model outcomes is based on the following steps:

1. Identify among the training trajectories the most similar to the test trajectory x^{test}, by computing the minimum Euclidean Distance (ED) [106]:

$$d_t^{(m)} = min\{ED\left(x_{(t-L):t,k}^{(m),train}, x_{(t-L):t}^{(m),test}\right)\}_{k=1}^{K} \tag{6.7}$$

   where $d_t^{(m)}$ is the minimum ED of the test trajectory for the m^{th} model at present time t, L is the time window modifier. Then, select N nearest (*i.e.* most similar) trajectories among the K training trajectories of each measurements for future analysis.

2. The local weights of each model of the ensemble are computed based on their local performances of RUL prediction accuracy on the N selected training trajectories [98]. The performance of the m^{th} model is here measured as the average of the local error between the ground truth RUL and the estimation:

$$LE_t^{(m)} = \frac{1}{N}\sum_{k=1}^{N} |RUL_{t,k}^{*} - \widehat{RUL}_{t,k}^{(m)}| \tag{6.8}$$

   where the time step $t \in T$, $LE_t^{(m)}$ is the local error representing the local performance for the m^{th} model at time step t, $RUL_{t,k}^{*}$ is the corresponding ground truth RUL and

$\widehat{RUL}_{t,k}^{(m)}$ is the estimated RUL of the k^{th} trajectory predicted by the m^{th} model, respectively. For a large LE, a small weight is associate. The weight is computed as the reciprocal of the local error [98]:

$$w_t^{(m)} = \frac{1/LE_t^{(m)}}{\sum_{m=1}^{M}\left(1/LE_t^{(m)}\right)} \tag{6.9}$$

where M is the number of models (in our case $M = 2$). The local weights $w^{(m)}$ are non-negative and sum to 1. Note that the weights are "local" in the sense that the RUL estimation $RUL_t^{(m)}$ is evaluated at different time steps dynamically. Before aggregating the RUL predictions with their corresponding weights, a bias correction $B_t^{(m)}$ of the i^{th} model is subtracted:

$$B_t^{(m)} = \frac{1}{N}\sum_{k=1}^{N}\left(RUL_{t,k}^{*} - \widehat{RUL}_{t,k}^{(m)}\right) \tag{6.10}$$

This quantity represents the accuracy of the RUL predictions obtained by each m^{th} model on the N selected training trajectories. The reason of introducing the bias correction is that at the early prediction stage, due to insufficient available observations, the prognostic algorithm usually provides predictions characterized by large variability. Exploiting the historical data, the average variation can be learned from the training trajectories and used as an offset.

3. Predict the RULs for the test trajectory using the PF method described in Section **??**, based on the M models.

4. Aggregate RUL predictions based on the individual models and weighted based on prognostic performances:

$$\widehat{RUL}_t = \sum_{i=1}^{M} w_t^{(m)} \cdot \left(\widehat{RUL}_t^{(m)} - B_t^{(m)}\right) \tag{6.11}$$

where $\widehat{RUL}_t^{(m)}, m = 1, 2, \ldots, M$ is the predicted RUL of the test trajectory x^{test} and $B_t^{(m)}$ is the bias correction evaluated on all N training trajectories.

The ensemble approach allows obtaining the PDF density of the predicted RUL. Various mathematical methods and approaches for combining probability distributions are discussed in [107]. Among them, in this work, we consider the Linear Opinion Pool (LOP):

$$p(\widehat{RUL}_t) = \sum_{i=1}^{M} w_t^{(m)} \cdot p\left(\widehat{RUL}_t^{(m)}\right) \tag{6.12}$$

where $p(\widehat{RUL}_t)$ represents the merged probability distribution, and $p(\widehat{RUL}_t^{(m)})$, represent the RUL distributions predicted by the M particle filters.

6.3 Data Generation

We aim at simulating a realistic evolution of the signals $\gamma(t)$ and $V_{st}(t)$, properly accounting for the dependence between the two signals. By "realistic", we mean that both signals should be correlated, but not fully equivalent or exchangeable with respect to the degradation information they carry. Given the unavailability of real data describing the degradation of a fleet of similar PEMFC stacks, the degradation trajectories are generated by applying the physics-based models of Equation (6.2). This procedure allows obtaining the SOH and the voltage degradation paths of similar stacks, realistically taking into account their dependence by resorting to stochastic Gamma processes. The simulated degradation trajectories are divided into a training set made by K trajectories and a test set made by J trajectories.

6.3.1 Gamma Process

A Gamma process is a stochastic process with independent, non-negative increments following a Gamma distribution. If x_t is a Gamma process, then:

$$\Delta x_t = x_{t_2} - x_{t_1} \sim \Gamma(\alpha(t_2) - \alpha(t_1), \beta) \tag{6.13}$$

where $x_0 = 0$, with probability equal to 1, Δx_t are independent, $\Gamma(\alpha(t), \beta)$ denotes the Gamma distribution with the shape parameter $\alpha(t)$ and the scale parameter β. Over a time interval t, the average degradation rate (slope) is $\overline{x} = \alpha \cdot \beta$, the process variance $Var = \alpha \cdot \beta^2$. Therefore, the choice of α and β allows to model various degradation behaviors, from almost-deterministic to very chaotic. Given the degradation measurements, both parameters can be estimated using classical statistical methods such as maximum likelihood method, moment method, Bayesian statistics method, *etc.*

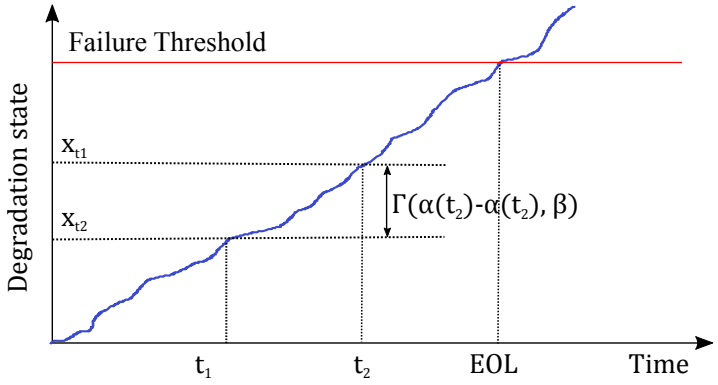

Figure 6.5: Illustration of a gamma process degradation path.

One advantage of using this process for degradation modeling is that the required mathematical calculations are relatively straightforward. The RUL can be thus obtained in an analytic form. Another advantage of this model is that its physical meaning is easy to understand. Gamma process-based degradation models can take the temporal variability into

account [108]. The Gamma process is suitable to model gradual damage monotonically accumulating over time in a sequence of tiny increments, such as wear, fatigue, corrosion, crack growth, degrading health index, etc [85]. Thus it is chosen here for simulating the irreversible degrading SOH of the PEMFC stack.

6.3.2 Signal Simulation

6.3.2.1 SOH Simulation

The degradation path of $\gamma(t)$ is generated by a Gamma process, which accounts for the randomness of the degradation process. The failure threshold FT_γ, here set to the value of 0.15, is obtained by estimating the internal resistance from EIS characterization [22]. Figure 6.6 shows one simulated degradation path. The average Gamma process $\overline{\gamma}$ classifies the type of fuel cell stack, and the variation from stack to stack is represented by drawing different realizations from $\overline{\gamma}$. The average End Of Life ($\overline{EOL}$) can be found at the time point when $\overline{\gamma}$ crosses the threshold FT_γ:

$$\overline{EOL} = \frac{FT_\gamma}{\alpha \cdot \beta} \tag{6.14}$$

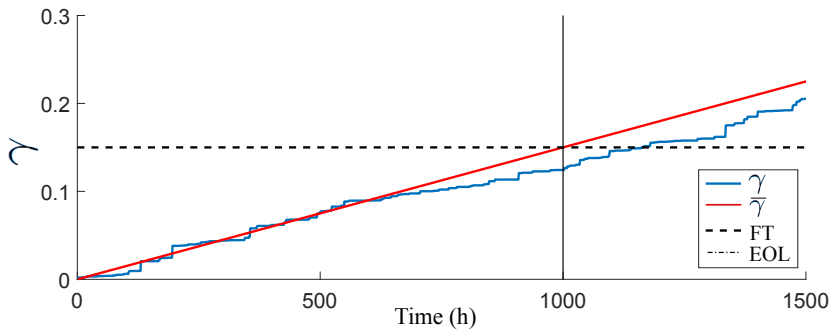

Figure 6.6: Simulated average SOH degradation $\overline{\gamma}$ and one realization of signal γ representing one stack.

6.3.2.2 Stack Voltage Simulation

According to Equation (6.2), the stack voltage is influenced by the loading current density j, which is here simulated by a Markov process [109]. It is used here to simulate the operating conditions during stack usage (Figure 6.7).

From a given γ, the degradation path of V_{st} is simulated using Equation (6.2) where the failure threshold $FT_{V_{st}}$ is obtained by substituting $t = \overline{EOL}$ (Figure 6.8). Note that this failure threshold is deduced from the failure time $\overline{EOL}$.

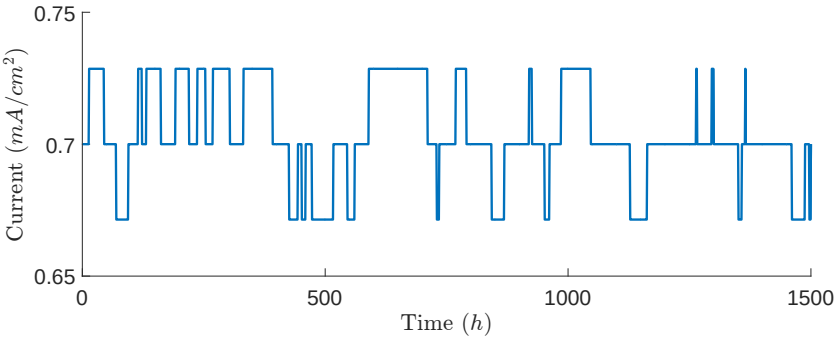

Figure 6.7: Loading current density j of one stack.

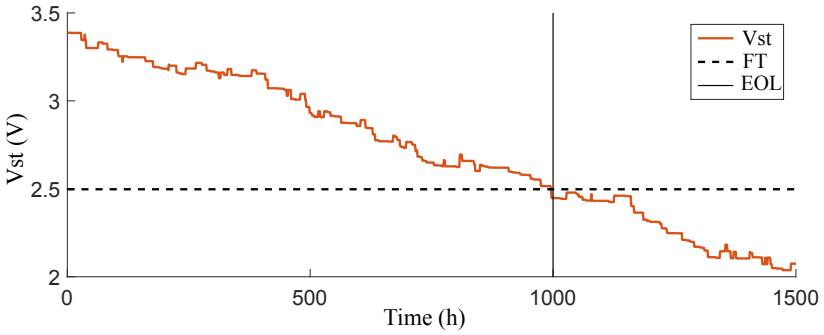

Figure 6.8: Voltage state V_{st} of one stack.

6.3.2.3 Observation

The two γ and V_{st} trajectories simulated above are considered as the ground truth. Since measurements revealed by sensors are affected by noises, we randomly sample their values by adding to the ground truth states zero-mean Gaussian noises:

$$\gamma_{meas} = \gamma + \mathcal{N}(0, \sigma_{\gamma}^2) \tag{6.15}$$

$$V_{stmeas} = V_{st} + \mathcal{N}(0, \sigma_{V_{st}}^2) \tag{6.16}$$

where γ and V_{st} are the system true states, γ_{meas} and V_{stmeas} are the measurement readings, σ_{γ} and $\sigma_{V_{st}}$ are the standard deviations of those two types of measurements, respectively. Note that $\sigma_{\gamma} < \sigma_{V_{st}}$ given that the SOH measurements γ_{meas} is more precise than the voltage measurements V_{st}.

6.3.2.4 Data Availability

As mentioned in the previous section, the stack voltage can be measured more frequently than the SOH degradation. Thus, the measurement data of SOH degradation are constrained such that they are available only every 100 hours, whereas the measurement data of stack voltage

are available every hour. The γ and V_{st} measurements for one single stack are shown in Figure 6.9. For computational convenience, ten-time steps between two successive measurements are considered for the measurements of V_{st}.

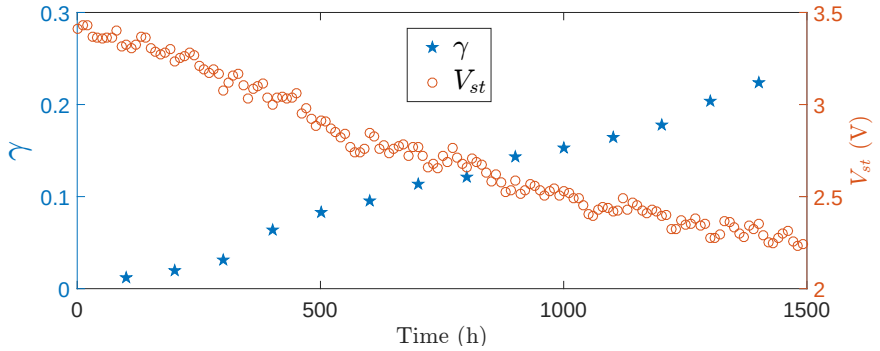

Figure 6.9: SOH degradation γ and voltage V_{st} measurements of one stack.

6.3.3 Degradation Simulation Procedure

The algorithm described in the previous section models the uncertainty in the measurements but it does not take into account the dependence between γ and V_{st}. It can be seen from Equations (6.2) and (6.3) that $V_{st}(t)$ is a symptom of the degradation $\gamma(t)$, the deterioration levels of the two indicators are correlated. To properly produce realistic simulations of the degradation trajectories that model the different sources of variability, randomness, and dependence between the signals, we propose two data simulation approaches:

6.3.3.1 Approach 1

The two indicators V_{st} and γ are generated from the same realization of a Gamma degradation process, with different additive noises. Different parameters α^i are used for the i^{th} stack. The objective of the simulation procedure is to represent stack-to-stack variability around the average behavior given by:

$$\overline{\gamma}(t) = \overline{\gamma}(t-1) + \Gamma(\overline{\alpha}\Delta t, \overline{\beta}) \tag{6.17}$$

The average values of the Gamma process parameters $\overline{\alpha}$ and $\overline{\beta}$ are preset according to our knowledge of PEMFC stack degradation in the following way. The failure threshold FT_γ (degradation rate) is set to 0.15, the average End of Life $\overline{EOL}$ is set to 1000 hours, and the slope of the degradation path is fixed to the computed value of $\overline{\alpha} \cdot \overline{\beta} = \frac{FT_\gamma}{\overline{EOL}}$, whereas the degradation variance is the value of $\overline{\alpha} \cdot \overline{\beta}^2$. Thus, for the i^{th} PEMFC stack:

$$\gamma^i(t) = \gamma^i(t-1) + \Gamma(\alpha^i \Delta t, \beta^i) \tag{6.18}$$

where α^i is drawn from a normal distribution of $\overline{\alpha}$ with 5% variation. The measurements data are simulated according to Algorithm 6.

Algorithm 6 Data simulation Approach 1

1: Choose $FT_\gamma, \overline{EOL}, \overline{\alpha}, \overline{\beta}$
2: **for** i = 1 : number of simulations
3: Draw α^i, β^i, from distributions with average values $\overline{\alpha}$ and $\overline{\beta}$
4: Generate realization $\gamma^i(t)$ of a Gamma process with parameters (α^i, β^i)
5: Add noises to $\gamma^i(t)$ to obtain the SOH degradation indexes for building the signals for Model 1 and Model 2:
$\gamma_1^i(t) = \gamma^i(t) + \mathcal{N}(0, \sigma_1^2(t))$
$\gamma_2^i(t) = \gamma^i(t) + \mathcal{N}(0, \sigma_2^2(t))$
6: Generate V_{st}^i index via Equations (6.2) and (6.3) using $\gamma_2^i(t)$
7: Add measurement noises:
$\gamma_{meas}^i(t) = \gamma_1^i(t) + \mathcal{N}(0, \sigma_{meas,1}^2(t))$
$V_{st}{}_{meas}^i(t) = V_{st}^i(t) + \mathcal{N}(0, \sigma_{meas,2}^2(t))$
8: **end for**

6.3.3.2 Approach 2

The two indicators V_{st} and γ are simulated from two different degradation processes, dependent by construction. To this aim, a bivariate dependent Gamma process is constructed by trivariate reduction in the case of bivariate Gamma random vectors [110].

Let us first recall that an univariate Gamma process [111] with parameters (α, β) (where α, $\beta > 0$) is a subordinator such that for every $t \geq 0$, the random variable $G(t)$ is Gamma-distributed $(\alpha t, \beta)$ with PDF:

$$f(x; \alpha, \beta) = \frac{\beta^\alpha x^{\alpha-1} e^{-\beta x}}{\Gamma(\alpha)} \quad for \quad x, \alpha, \beta > 0 \tag{6.19}$$

The random variable $G(\alpha t, \beta)$ is the increment of the Gamma process at time t:

$$\Delta\gamma_t = G_t(\alpha t, \beta) \tag{6.20}$$

Starting from three independent univariate Gamma processes g_t^j with (a_j, b_j) for $j = 1, 2, 3$, one can build two dependent Gamma processes (or a bivariate dependent Gamma process) by trivariate reduction:

$$\begin{aligned} G_{1,t} &= g_{1,t} + g_{3,t} \\ G_{2,t} &= g_{2,t} + g_{3,t} \end{aligned} \tag{6.21}$$

The process $G_t = (G_{1,t}, G_{2,t})$ is, then, a bivariate subordinator [112] with Gamma marginal processes and marginal parameters (α_j, β_j) where $\alpha_j = a_j + a_3$ for $j = 1, 2$. The linear correlation between the two random variables $G_{1,t}$ and $G_{2,t}$ is independent of time t and described by the Pearson's correlation coefficient [112], [113]:

$$\rho = \frac{a_3}{\sqrt{\alpha_1 \alpha_2}} \tag{6.22}$$

where ρ is the Pearson's correlation coefficient, α_1 and α_2 are the marginal gamma parameters. Consequently, we have the following link between the two parametrizations (a_1, a_2, a_3) and $(\alpha_1, \alpha_2, \rho)$:

$$\begin{aligned} a_1 &= \alpha_1 - \rho\sqrt{\alpha_1\alpha_2} \\ a_2 &= \alpha_2 - \rho\sqrt{\alpha_1\alpha_2} \\ a_3 &= \rho\sqrt{\alpha_1\alpha_2} \end{aligned} \tag{6.23}$$

where $0 \leq \rho \leq \frac{min(\alpha_1,\alpha_2)}{\sqrt{\alpha_1\alpha_2}}$.

This link allows to choose a_1, a_2 and a_3 so as to generate a bivariate Gamma process with desired α_1, α_2 and ρ. Within the range $0 \leq \rho \leq \frac{min(\alpha_1,\alpha_2)}{\sqrt{\alpha_1\alpha_2}}$, trivariate reduction leads to one of the fastest algorithms known to date for bivariate Gamma distributions [110], which is described in Algorithm 7.

Algorithm 7 Data simulation Approach 2

1: Choose $FT_\gamma, \overline{EOL}$
2: Given α_1, α_2 and β for marginal Gamma distributions
3: Given ρ, $0 \leq \rho \leq \frac{min(\alpha_1,\alpha_2)}{\sqrt{\alpha_1\alpha_2}}$
4: **for** i=1 : number of simulations
5: Generate the realizations of Gamma process with parameters
$a_1 = \alpha_1 - \rho\sqrt{\alpha_1\alpha_2}$, $a_2 = \alpha_2 - \rho\sqrt{\alpha_1\alpha_2}$, $a_3 = \rho\sqrt{\alpha_1\alpha_2}$, $b = \beta$:
$g_1^i = \Gamma(a_1, b)$
$g_2^i = \Gamma(a_2, b)$
$g_3^i = \Gamma(a_3, b)$
6: Return $(G_1^i = g_1^i + g_3^i, G_2^i = g_2^i + g_3^i)$ by trivariate reduction
7: Generate SOH indexes:
$\gamma_1^i(t) = \gamma_1^i(t-1) + G_1^i$
$\gamma_2^i(t) = \gamma_2^i(t-1) + G_2^i$
8: Generate V_{st}^i index via Equations (6.2) and (6.3) using $\gamma_2^i(t)$
9: Add measurement noises:
$\gamma_{meas}^i(t) = \gamma_1^i(t) + \mathcal{N}(0, \sigma_{meas,1}^2(t))$
$V_{st}{}_{meas}^i(t) = V_{st}^i(t) + \mathcal{N}(0, \sigma_{meas,2}^2(t))$
10: **end for**

6.4 RUL Prognosis Results & Performance Evaluation

Considering that in real industrial applications we expect to have available a limited number of PEMFC stacks degradation trajectories. We simulate 100 trajectories of which we use each type of measurement: $K = 50$ for training and $J = 50$ for testing. By performing a sensitivity analysis regarding the prediction accuracy and the computation time, we have set the number of nearest trajectories in the training set to $N = 5$ and the time window for the similarity calculation to $L = 100$ hours.

6.4.1 RUL Prognosis for Data Simulation Approach 1

The variance of the degradation process, $\alpha\beta^2$ depends on the choice of the Gamma process parameters α and β. It stands for the similarity in degradation behavior of identical PEMFC stacks. As being discussed in Section 6.3.3.1, the objective of introducing the variance is to represent stack-to-stack variability around the average behavior. Figure 6.10 shows three examples of degradation paths with different levels of variance: 1) low variance ($\alpha = 0.6, \beta = 2.5e{-}4$); 2) medium variance ($\alpha = 0.1, \beta = 1.5e{-}3$); 3) high variance ($\alpha = 0.03, \beta = 5.0e{-}3$).

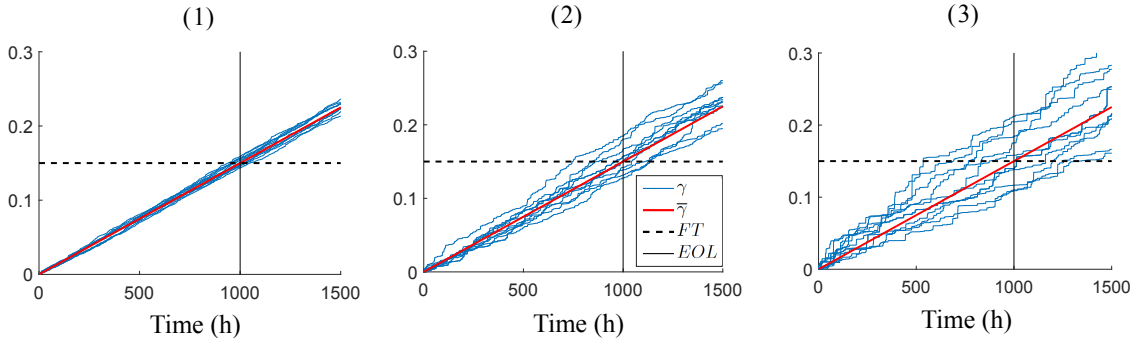

Figure 6.10: Data simulation with three levels of variance: (1) Low variance; (2) Medium variance; (3) High variance.

The RUL predictions for all the degradation trajectories are carried out by the Particle Filtering-based approach described in Chapter 3. For each trajectory in the test set ($J = 50$ trajectories), the RUL predictions are made every 100 time steps with Model 1 and every 10 time steps with Model 2. The RUL predictions based on Model 1 are less frequent than the ones based on Model 2, because the measurements that feed Model 2 are intermittently taken. Thus, to have a fair comparison between the two models, the missing predictions of Model 1 are reconstructed by linear interpolation. The simulation is carried out with the data dependence generation of Approach 1 and Gamma process with medium variance.

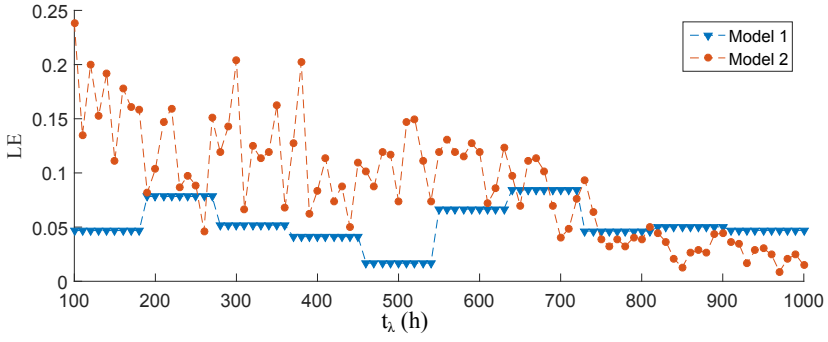

Figure 6.11: Local error evaluated over 50 training trajectories for test trajectory №40.

Figure 6.11 shows the Local Error (LE) at different prediction time steps obtained for a

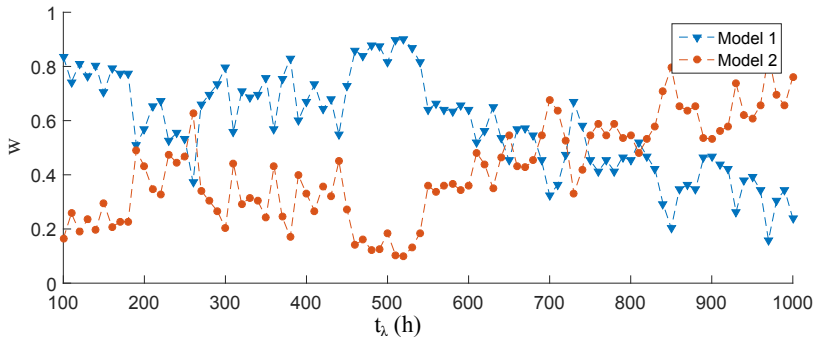

Figure 6.12: Weight assigned to each model for test trajectory №40.

single test trajectory (№40). Figure 6.12 shows the corresponding weights which are dynamically assigned to the two models according to their local error evaluated at each time step. Notice that:

- Model 1 weights are larger at the beginning of the component life compared to that of Model 2. This can be justified by the fact that Model 1 is fed by more precise SOH measurements and it is not influenced by loading current variations.
- Model 2 weights are larger than those of Model 1 after approximately 600 hours. This can be justified by the fact that Model 2 is trained by using more data. Thus, its prediction performance is improved much faster than the one of Model 1, especially near the end of life when Model 1 is no longer updated due to lack of new incoming measurements.

6.4.1.1 RUL Aggregation

The RUL predictions based on both models are aggregated according to Equation (6.11).

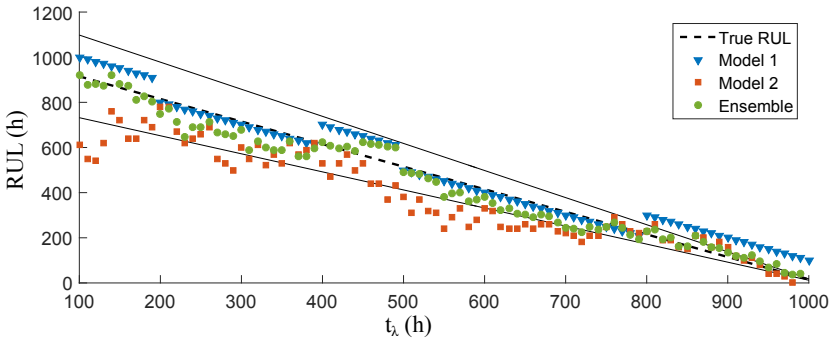

Figure 6.13: RUL predictions aggregation for trajectory №40.

Figure 6.13 shows the RUL predictions and the aggregation for one test trajectory. The ensemble RUL predictions take advantage of the complementary behaviors of individual models. Indeed, the analysis of Figure 6.13 suggests that:

- The predictions provided by the two models are comparable, even if Model 1 [1] provides more accurate RUL predictions at the early life stages of the stack №40, Model 2 provides more accurate predictions when this stack approaches the EOL.
- The ensemble of the two models allows obtaining more accurate predictions throughout the RUL predictions of stack №40 than each individual model.

Figure 6.14 provides a global view of the average local error for all 50 test trajectories. Since each trajectory (stack) has different EOL, we normalized the time index considering the EOL ratio $\lambda_j = \frac{t_\lambda}{EOL_j}$. Globally, Model 1 prediction errors are lower at earlier life stages, whereas Model 2 errors gradually decrease thanks to the updating by sufficient incoming measurements and finally becomes lower.

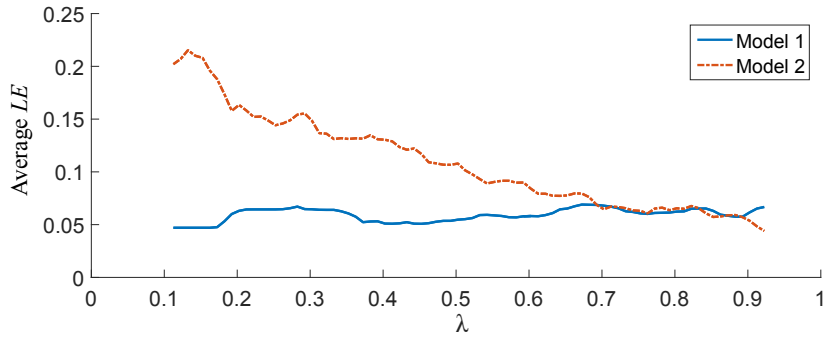

Figure 6.14: Average local error from 50 test trajectories.

Figure 6.15 shows the average prediction error for each test trajectory. It is the average local error of each trajectory along the entire prediction horizon (from 100 hours to 1000 hours): we can see that the ensemble gives the smallest prediction error for almost all the test trajectories.

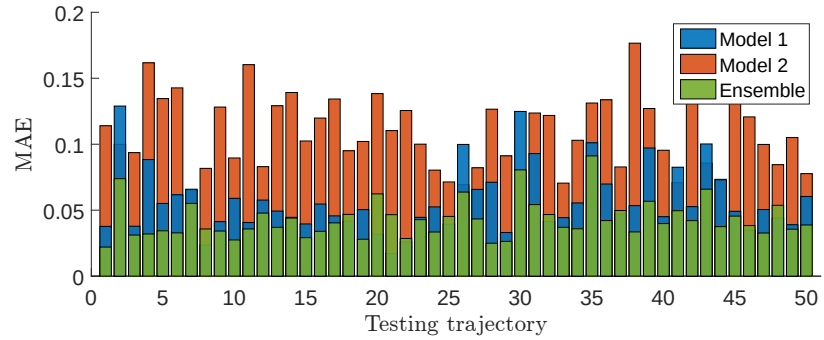

Figure 6.15: Mean absolute error for 50 test trajectories.

[1] Here "Model 1" stands for "the prognostic approach based on Model 1", "Model 2" for "the prognostic approach based on Model 2", and "Ensemble" for "the prognostic approach based on the ensemble of models". This simplification is to avoid the wordy expression, and is used in the rest of the paper.

6.4.1.2 RUL Uncertainty Aggregation

Figure 6.16 shows the 25^{th} and 75^{th} percentiles of the RUL PDF provided by the ensemble, which is obtained by merging the RUL PDFs of Model 1 and Model 2 according to Equation (6.12), for trajectory №40.

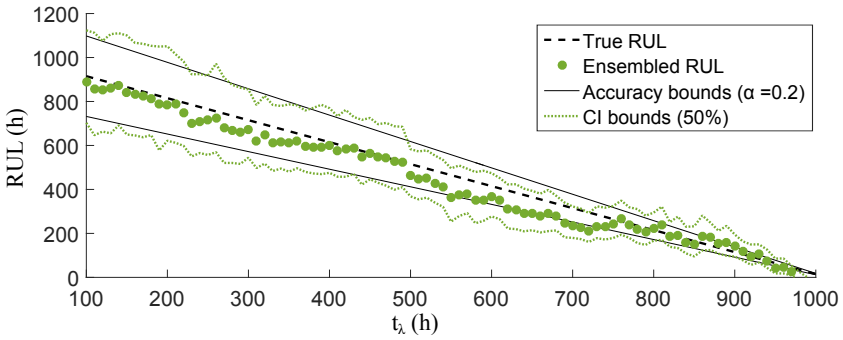

Figure 6.16: Aggregated RUL predictions with uncertainty for trajectory №40 with accuracy and CI.

By aggregating the two PDFs, we obtain not only the RUL but also the uncertainty of the predictions, which is very important for maintenance decision making. As expected, the prediction becomes closer to the ground truth RUL and the uncertainties (PDFs) of the ensemble become smaller when approaching the end of life.

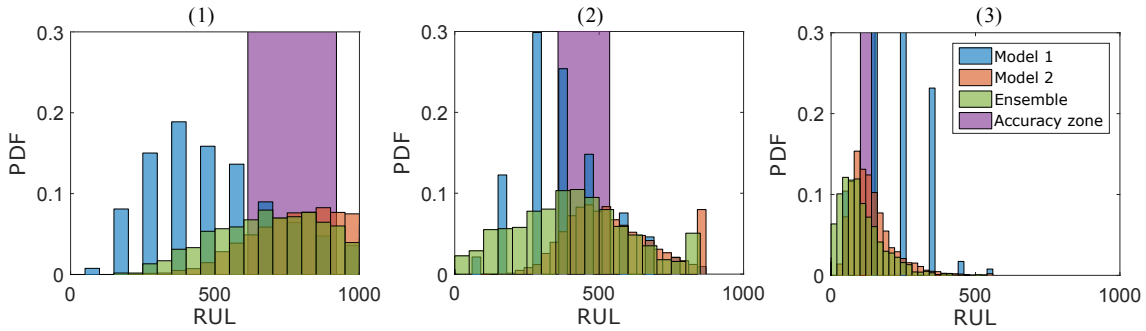

Figure 6.17: Histogram of aggregated RUL uncertainties for trajectory №40 at different prediction time steps: (1) $t_\lambda = 200$ hours; (2) $t_\lambda = 500$ hours; (3) $t_\lambda = 800$ hours.

Figure 6.17 depicts the RUL uncertainty at different life stages: at the early prediction time of 200 hours (Figure on the left), at half-life of 500 hours (Figure in the middle) and near the EOL of 800 hours (Figure on the right). All three models become less spread and centered to the true RUL accuracy zone when the prediction time approaches the end of life. The less spread distribution indicates the RUL predictions become more accurate and more precise when more observations become available, which meets our expectation.

To quantify the performance, the results of all models are evaluated by the prognostic performance metrics.

6.4.1.3 Prognostic Metrics

We recall the definitions of the prognostic performance metrics. In order to evaluate the average performance of RUL predictions, the common way is to apply several RUL predictions at different time steps to obtain a sequence of predicted RULs [42], [43]. To evaluate the quality of prognostic outcomes, a synthesis of the prognostic metrics is used [44], [45], [47]–[49].

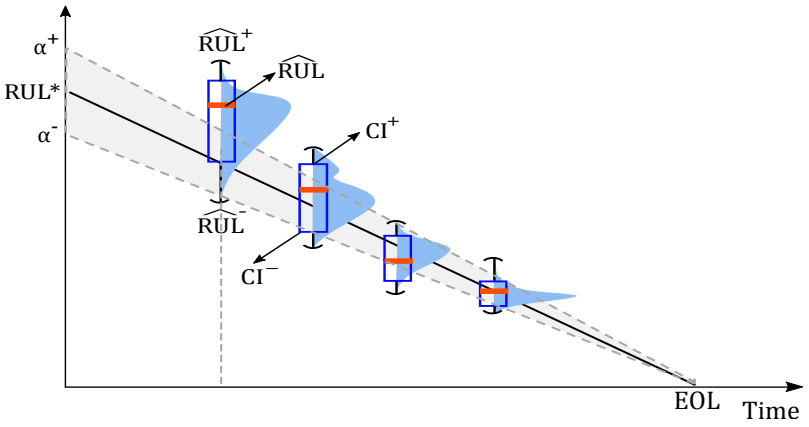

Figure 6.18: RUL predictions at different prediction time t_λ.

Figure 6.18 illustrates the RUL predictions with uncertainties at different prediction time steps t_λ. The uncertainties are represented by the Probability Density Function (PDF). The accuracy bounds of a width of 2α shrinks with the prediction time index t_λ, which creates the α-λ accuracy zone covering the true residual life RUL^*. The upper bounds and the lower bounds of the α-λ accuracy zone:

$$\begin{aligned} \alpha^+ &= RUL_t^* \cdot (1+\alpha) \\ \alpha^- &= RUL_t^* \cdot (1-\alpha) \end{aligned} \tag{6.24}$$

$\widehat{RUL}^+$ and $\widehat{RUL}^-$ are the upper and lower bounds of the predicted RUL uncertainties, whereas CI^+ and CI^- are the bounds of the confidence interval.

Based on those characteristics, different metrics are described as the follows:

- The accuracy index Acc_t directly reflects the prediction errors relative to the true RUL:

$$Acc_t = 1 - \frac{|RUL_t^* - \widehat{RUL}_t|}{RUL_t^*} \tag{6.25}$$

  where RUL_t^* the true RUL and $\widehat{RUL}_t$ the median value of predicted RULs at prediction time t_t. Larger value of Acc_t indicates better accuracy.

- The α-λ metric considers whether the predicted $\widehat{RUL}$ lies within the $\pm\alpha$ interval stating whether the required accuracy is met at a given time t_λ. As being illustrated in

Figure 6.18, the probability of lying within the α-λ accuracy zone is described by Equation (6.26):

$$\alpha Ac_t = p\left(\alpha_t^- \leq \widehat{RUL}_t \leq \alpha_t^+\right) \tag{6.26}$$

where α_t^+ and α_t^- are the upper and lower bounds of the accuracy zone. Higher value represents better performance.

- The coverage index Cvg_t considers whether the true RUL lies within the RUL prediction interval at time index λ for each trajectory:

$$Cvg_t = p\left(\widehat{RUL}_t^{CI-} \leq RUL_t^* \leq \widehat{RUL}_t^{CI+}\right) \tag{6.27}$$

  The value of Cvg close to 80% indicates a good representation of the uncertainty [49].

- The precision index Prc_t computes the relative width of the prediction interval, which is defined by:

$$Prc_t = \frac{\widehat{RUL}_t^{CI+} - \widehat{RUL}_t^{CI-}}{RUL_t^*} \tag{6.28}$$

  where $\widehat{RUL}_t^{CI+}$ and $\widehat{RUL}_t^{CI-}$ are the upper and lower bounds of the Confidence Interval (CI) of the predicted RULs distribution (*e.g.* CI = 50%) while RUL_t^* is the corresponding true RUL. Smaller values of Prc_t indicate more precise predictions.

- The steadiness index Std_t measures the variance of the estimated value of the End of Life (EOL) when new measurements become available. It is defined as:

$$Std_t = \frac{\sqrt{var(\widehat{EOL}_{(t-L):t})}}{EOL^*} \tag{6.29}$$

  where L is the length of a sliding time window filtering the variances of the predicted EOL. Smaller values of Std_t indicate better performance.

- The risk index Rsk_t is the probability of obtaining an estimated RUL larger than the true RUL:

$$Rsk_t = p(\widehat{RUL}_t > RUL_t^*) \tag{6.30}$$

  This index indicates the probability of receiving a later notification of a failure such that scheduling a maintenance after the failure is risky. Lower values represent the lower risk, which means better performance.

6.4.1.4 Prognostic Performance Evaluation

The quality of the RUL predictions of the individual models and the ensemble are evaluated using the prognostic performance metrics in Table 6.1, which reports the average performances over $J = 50$ test trajectories and all t_λ time steps.

The values in Table 6.1 suggest that:

Table 6.1: Prognostic performance metrics (Approach 1, medium variance)

Average Performance	Model 1	Model 2	Ensemble Point	Ensemble PDF
Acc	0.52	0.12	0.55	**0.56**
αAc	0.31	0.24	**0.54**	0.49
Std	0.16	0.14	**0.07**	**0.07**
Rsk	**0.34**	0.49	0.44	0.36
Prc	**0.25**	0.27	–	0.32
Cvg	0.48	0.37	–	**0.74**

- The Ensemble shows better performance than any individual model with respect to Acc, αAc, Std and Cvg indexes.
- Model 1 shows better performance in Rsk index, which means that the RUL predictions based on Model 1 are early notifications. This does not mean that all early predictions are good predictions: an early notification which is too far from the true failure time leads to unnecessary maintenance, which incurs extra cost. The Rsk performance needs to be considered jointly to the accuracy indexes (Acc and αAc). The Rsk of the Ensemble is between Model 1 and Model 2, with respect to both point values and uncertainty.
- The Prc index of the Ensemble is the weakest, whereas its Cvg index is the strongest. This is due to the fact that the PDFs of the Ensemble merges Models 1 and 2 PDFs. The spread of its distribution is, thus, broader than the individual models, but it provides a larger coverage.

Above all, in this example of Approach 1 with medium variance, we can conclude that the Ensemble-base approach globally provides the best prognostic performance.

6.4.2 RUL Prognosis for Data Simulation Approach 2

Similarly to what has been done for the data simulation Approach 1, three different levels of process variance are simulated. Furthermore, for each level of variance, seven different levels of processes dependence between $\gamma(t)$ and V_{st} are considered to represent the underneath correlation between the two signals.

6.4.2.1 Parameters Used for the Simulated Examples

The parameters used for the generation of the simulated examples of dependent Gamma processes are reported in Table 6.2. The correlation coefficient ρ ($0 \leq \rho \leq \rho_{max} = \frac{min(\alpha_1,\alpha_2)}{\sqrt{\alpha_1 \alpha_2}}$) indicates the dependence level of the two final degradation processes after the trivariate reduction.

Table 6.2: Parameters used for the simulated examples ($\rho_{max} = 0.9128$)

ρ	α_1	α_2	β	a_1	a_2	a_3
0	0.60	0.50	4.00	0.60	0.50	0
$10\%\rho_{max}$	0.60	0.50	4.00	0.55	0.45	0.05
$25\%\rho_{max}$	0.60	0.50	4.00	0.47	0.38	0.13
$50\%\rho_{max}$	0.60	0.50	4.00	0.35	0.25	0.25
$75\%\rho_{max}$	0.60	0.50	4.00	0.22	0.13	0.38
$90\%\rho_{max}$	0.60	0.50	4.00	0.15	0.05	0.45
ρ_{max}	0.60	0.50	4.00	0.10	0	0.50

6.4.2.2 Prognostic Performance Evaluation

Figures 6.19 and 6.20 show the performance improvements of the Ensemble with respect to the two individual models, considering different dependence scenarios, for point values and uncertainty, respectively. The improvements of performance metrics are computed in terms of percentage increased in the metrics' values, for example:

$$\begin{aligned} Acc(gain) &= \frac{Acc_{Ensemble} - max\left(Acc_{Model1}, Acc_{Model2}\right)}{max\left(Acc_{Model1}, Acc_{Model2}\right)} \\ Std(gain) &= \frac{min\left(Std_{Model1}, Std_{Model2}\right) - Std_{Ensemble}}{min\left(Std_{Model1}, Std_{Model2}\right)} \end{aligned} \tag{6.31}$$

The values indicate the improvements of the Ensemble with respect to the best between Model 1 and Model 2. Gains above 0 indicate that the Ensemble performance is more satifactory than that of the individual models.

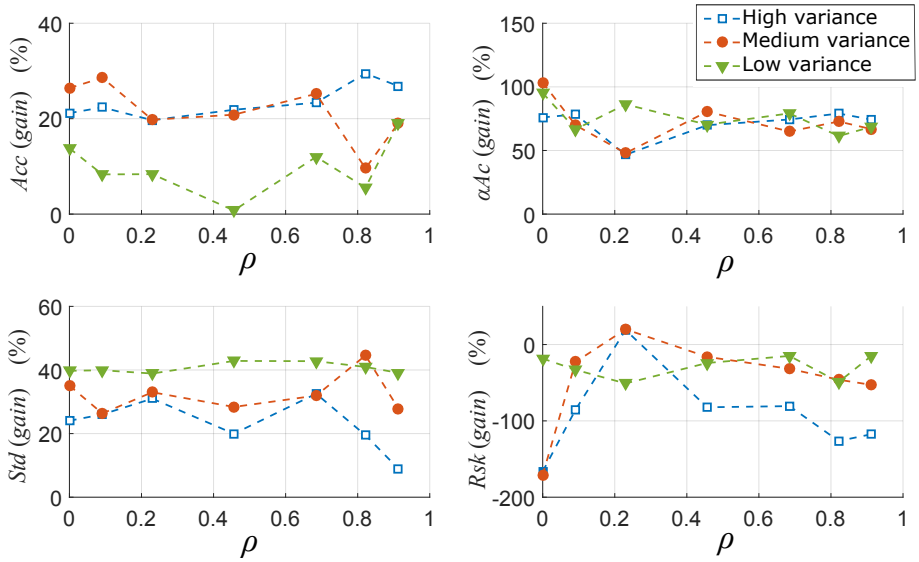

Figure 6.19: Point values aggregation: prognostic performances gains vs. dependence.

With respect to the point values, notice that:

- Considering the *Acc*, αAc and *Std* metrics, the Ensemble always outperforms any of the individual models. Therefore, we can conclude that the Ensemble is more accurate than Models 1 and 2. Larger process variance, the larger the Ensemble gain.
- Similar to the case of data simulation Approach 1, he *Rsk* index of the Ensemble trends to decay, which means that the Ensemble provides RUL predictions exceeding the ground truth RUL, even though they are located in the accuracy zone.

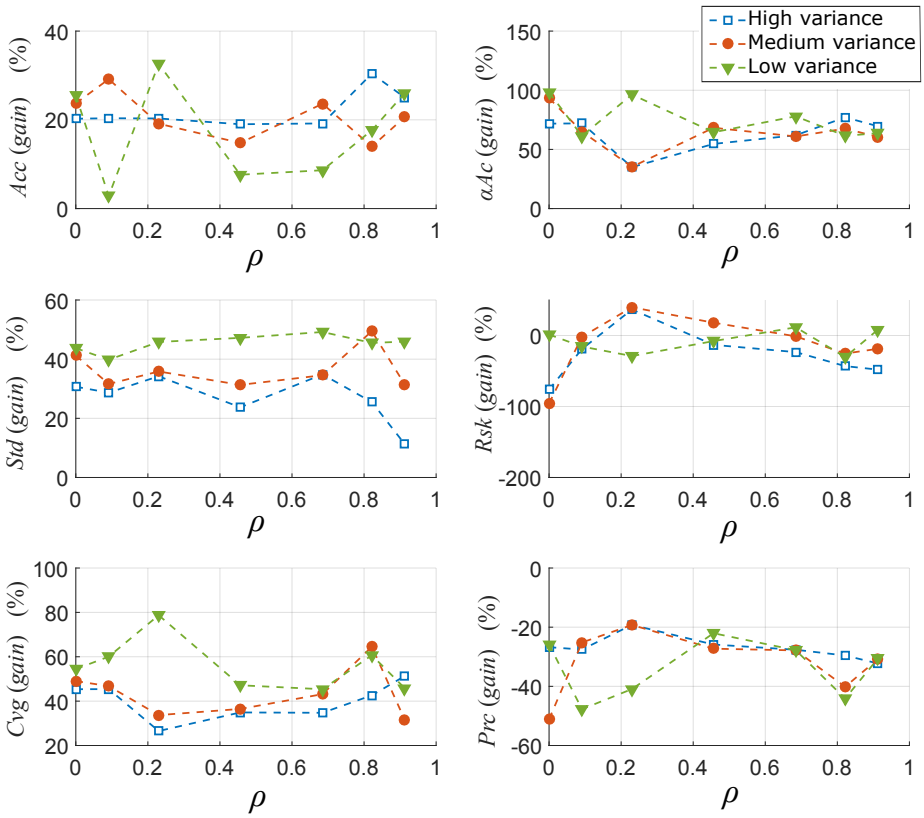

Figure 6.20: Uncertainties aggregation: prognostic performances gains vs. dependence.

For the uncertainties aggregation, the analysis of Figure 6.20 indicates that:

- Considering the *Acc*, αAc and *Std* metrics, the Ensemble model with any process dependence outperforms any of the individual models. The gains of *Std* are nearly the same as the one with point values.
- The *Rsk* index for low variance processes is sometimes improved. It can also be noticed that this index is better than the one with point values aggregation, which indicates that with complete information (uncertainties), some "risky" predictions can be avoided.
- Not surprisingly, the *Prc* index of the Ensemble is the weakest and, on the other hand, its *Cvg* index is the strongest. It is because that the PDFs of the Ensemble are the merge of the ones of Model 1 and Model 2. The spread of the distributions are, thus,

broader than those of the individual models, which provide for a large coverage.

Hence, the Ensemble can largely improve the prognostic performance for degradation processes with different variances and different dependencies.

6.5 Conclusion

In this work, the coexistence of two kinds of degradation measurement (estimation) data at different levels were considered: 1) the external output voltage measurements; 2) the SOH degradation estimated from internal characterization measurements, which is assumed the covariate of voltage drop. We developed an ensemble approach that combines the RUL predictions from the two different sources at different levels. The RUL predictions of both models are dynamically aggregated according to their local weights. The weights of models were defined by the prognostic performance that evaluated on a set of historical data. The results showed that the prediction accuracy was improved by overcoming both models' drawbacks and leveraging their strengths. The performance of proposed model outperforms over individual models. However, in our approach, the weights were computed on the basis of offline historical run-to-fail data. Consequently, a large quantity of historical data was required. The feasibility of the deployment in PEMFC when data requirement is met or other solutions of weights definition are found which are less dependent on the quantity of historical data. Moreover, Without limiting ourselves in the framework of the PEMFC systems, the developed approaches could be adapted and extended to different systems in industries.

General Conclusion

Summary of work

The objective of this work was to develop prognostic methodologies for the RUL prognosis adapted to the complexity of PEMFCs. Indeed, the PEMFC is a multi-scale and multi-physics system, and various challenges were faced:

1. The definition of SOH to build a degradation indicator.
2. The coexistence of both reversible and irreversible degradation phenomena.
3. Taking into account different degradation causes and effects of operating conditions.

First, to apply the prognosis, degradation-related measurements are required. One of the most commonly used degradation indicator is the stack voltage (or power). This indicator is usually monitored continuously online and is thus a good candidate for the online prognostic purpose. However, the coexistence of reversible and irreversible degradation phenomena gives this candidate significant limitations. In Chapter 3, we developed a particle filtering based prognostic algorithm for PEMFC and applied it to the measurements of output power, which is most commonly used way in this field to interpret the PEMFC degradation. The first results showed that the prognosis algorithm is disturbed by the existing reversible degradation. It revealed the limitation that with a single degradation indicator, it is difficult to handle multiple degradation behaviors. Therefore, we paid attention to looking for additional degradation indicators. Since the research in the prognostics for PEMFC are scarce at the beginning of the thesis, we have paid special attention to prognostics of Li-ion batteries because it shares some features with PEMFC: first, they are both electrochemical cells; second, research on batteries in the prognostics field is much maturer. Finally, we found interests in characterization measurements: the EIS and polarization curves of the stack. The drawbacks of those measurements are their availability, intrusiveness, and costs. To overcome this inconvenience, we proposed an RUL prognosis using multiple indicators. The irreversible degradation can be estimated thanks to characterization measurements.

Therefore in Chapter 4, we adapted & extended prognostic algorithm to take into account two degradation indicators: the output power degradation, and the SOH degradation estimated from EIS characterization. We tested different models of the reversible degradation trend. To compare the prognostic performances, the prediction results of the previous approach and the extended algorithm (with different reversible models) are evaluated by different prognostic performance metrics. The evaluation results showed the interest of the proposed approach. The parameter of polarization resistance estimated from EIS helped to improve the RUL prediction accuracy. The proposed model gives the best performance among all the tested models, especially for long-term predictions. This study brings an idea of integrating SOH characterization into RUL prediction, which leads to a better performance of RUL predictions. This approach used usual measurements of the stack (power and EIS) and was able

to distinguish reversible and irreversible degradation behaviors. The particle filtering used in the approach was also a common prognostic tool. So we can expect that the proposed method would fit other PEMFC and easy to tune. The proposed approach is ready to be tested with other PEMFC stacks when new data are available. Moreover, the SOH degradation (polarization resistance decay) can also be estimated through other models from polarization curves. A short-term perspective is to take into account the estimation results from polarization curves, which could involve the operating conditions [79], [80].

Then, we tried to define a more general problem for prognostics based on the knowledge of PEMFC, which can be used for other applications. We proposed a case study in which we have two signals: a regularly measured degradation signal (similar to PEFMC output power) but with incomplete or poor information of SOH; in a first approach, another degradation signal we have is an intermittent measurement of a degradation covariate, which can provide relevant information of SOH but was only accessible from time to time. Thus, in Chapter 5, the problem was addressed from a more theoretical point of view. Indeed, a system's degradation behavior is often correlated with internal and external covariates which are usually difficult to access owing to expensive measurement cost. We proposed a degradation covariate inspection scheme to gather additional degradation information when necessary to reach an optimal trade-off between performance (accuracy and precision) and cost (monitoring cost due to inspections) for the degradation estimation and RUL prediction. To become commercially appealing, the inspection has to be done only when the minimum of the cost criteria J is reached to avoid unnecessary inspection costs. We expected that information from deeper levels can provide more relevant information of true SOH. Therefore, the perspective is to inspect/investigate possible available covariates at different (deeper) levels, *e.g.*, a covariate that modifies even the behavior of SOH degradation, which could be the operating conditions.

In another approach, the intermittent measurement was considered as a signal of SOH, assuming the availability of a procedure which returns an estimation of SOH from characterization measurements. Thus in Chapter 6, the coexistence of two kinds of degradation measurement (estimation) data at different levels were considered: 1) the external output voltage measurements; 2) the SOH degradation estimated from internal characterization measurements, which is assumed the covariate of voltage drop. We developed a model ensemble approach that combines the RUL predictions from the two different sources at different levels. The RUL predictions of both models are dynamically aggregated according to their local weights. The weights of models were defined by the prognostic performance that evaluated on a set of historical data. The results showed that the prediction accuracy was improved by overcoming both models' drawbacks and leveraging their strengths. The performance of proposed model outperforms over individual models. However, in our approach, the weights were computed on the basis of offline historical run-to-fail data. Consequently, a large quantity of historical data was required. The feasibility of the employment in PEMFC when data requirement is met or other solutions of weights definition are found which are less dependent on the historical data.

Perspectives

In the thesis, we have paid special attention to the possible use of degradation covariates, and we have focused our work on proposing solutions to perform RUL predictions using the information at different levels to tackle the problem raised by the existence of reversible degradation vs. irreversible degradation. We extend the problem to multi-level prognostics and explore new possibilities, which open new aspects for future research on PEMFC lifetime prognosis and management. Shortly, some extensions could be envisaged to overcome the limitations of the presented works.

In Chapter 4, the PF-based RUL prognosis was adapted to the available information from two completed tests of the PEMFC stacks. Other tests, especially the tests involve varying operating conditions, will be investigated once they are available. For this end, the prognostics data on accelerated aging tests carried out in FCLAB could be a promising aspect. Indeed, this involves the varying usage (current) profile that can be used for both development and validation of prognostics algorithms.

In Chapter 6, the ensemble approach was developed based on the knowledge of PEMFC, it is also developed in a general purpose regarding the possibility to apply on other industrial systems where sufficient historical data is easy to access. Moreover, with the growth of (available) run-to-fail tests of the PEMFC stacks in the community, implementing the ensemble approach on PEMFCs will become technically feasible.

Another point that could be extended concerns the multi-level inspection in Chapter 5. Indeed, while constructing the inspection schemes, we assumed that the degradation was monotonic and only one degradation covariate impacted degradation evolution. Such assumption could help to facilitate the RUL estimation tasks, but it also limits the application range of the models. For example, in continuous production industries, maintenance interventions are regularly implemented to prevent machines from high damaged states. Under the effects of these actions (*e.g.* the polarization characterization for PEMFC), the degradation processes could be no longer monotonic (*e.g.* the peak values in output voltage/power). Extension to non-monotone could help to take into account such real situations in degradation modeling. This theoretical perspective can be also referred to the simulation in Chapter 6. Furthermore, the inspection schemes were designed based on a simple cost function, where the consideration of real-life impacts is not complete. In fact, the definitions of the prognostic cost function can be further investigated. Other aspects such as the timeliness could be taken into account in the cost model as well. It could be two folds: 1) the cost of simulation elapsed time; 2) feedback loses its value over time since it is superseded by new data, the frequency of reporting can also contribute to the cost model.

Indeed, although the data from an experimental platform (*e.g.* the PHM2014 Data Challenge) and case studies were studied in this thesis, it still does not refer to real-life industrial application (or system) data. For a long-term perspective, a validation of the developed approaches with real-life data should be envisaged to become commercially attractive. Also, the approaches developed in this thesis are from the knowledge of electrochemical cells but not

constrained in this domain. They could be hence adapted for the RUL prognosis of other kinds of systems. Therefore, without limiting ourselves in the framework of the PEMFC systems, in the future, the developed approaches ought to be adapted & extended to different systems in industries.

Appendix A

Résumé en Français

Contexte et motivation

Dans le contexte de la transition énergétique, la pile à combustible est l'une des sources d'énergie alternatives les plus prometteuses. Récemment, la recherche a mis l'accent sur les piles à combustible, et plus particulièrement sur celle à membrane échangeuse de protons (Proton Exchange Membrane Fuel Cell ou Polymer Electrolyte Membrane Fuel Cell ou PEMFC) qui est l'une des meilleures candidates pour les applications stationnaires et de transport. Même si cette technologie évolue constamment, elle n'est pas encore prête pour un déploiement industriel à grande échelle en raison de sa durabilité et de sa fiabilité limitées. Le "Prognostics and Health Management" (PHM) est une approche récente pour gérer et prolonger la durée de vie des systèmes. Les techniques de pronostic sont capables de fournir une estimation de l'état de santé (State of Health ou SOH) des piles à combustible et une prédiction de leur durée de vie résiduelle (Remaining Useful Life ou RUL) afin d'aider les fabricants à gérer la durée de vie de ces systèmes.

Les travaux développés dans cette thèse portent sur le développement d'approches pronostiques pour la prédiction de la durée de vie résiduelle (RUL) des piles à combustible de type PEMFC, en tenant compte du plus d'information possible.

Pronostic

L'objectif de l'approche PHM est de maximiser le retour sur investissement des équipements en :

1. augmentant la disponibilité du système et réduisant les coûts d'exploitation pour en optimiser la maintenance ;
2. améliorant la sécurité du système ;
3. améliorant le processus décisionnel pour augmenter la durée de vie de l'équipement.

Le principal outil utilisé par les méthodes de pronostics est l'estimation du temps de fonctionnement avant défaillance et le risque d'existence ou d'apparition ultérieure d'un ou de plusieurs modes de défaillance. Cela permet de définir la durée de vie résiduelle (RUL). Le

RUL est l'estimation du temps écoulé entre le moment actuel et le moment où le système est considéré comme étant en panne.

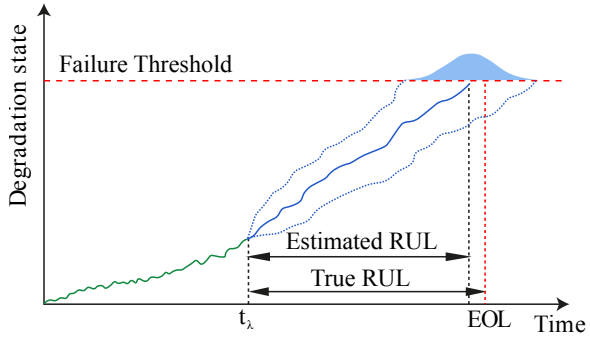

Figure A.1: Estimation de l'état de dégradation.

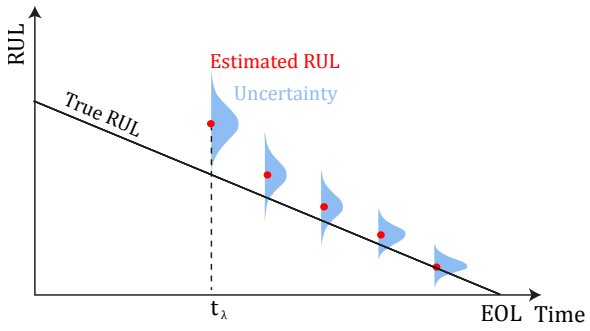

Figure A.2: Prédictions des RULs.

La Figure A.1 montre l'évolution temporelle typique d'un indicateur de la dégradation. Les mesures de l'indicateur de dégradation sont utilisées dans une phase d'apprentissage jusqu'à l'instant de prédiction t_λ. A partir de cet instant, le comportement appris de l'évolution de la dégradation est utilisé pour prédire l'évolution future. L'instant où l'indicateur de dégradation atteint le seuil de défaillance est appelé fin de vie (End Of Life - EOL). Le RUL est la prédiction du temps mis par le système pour atteindre l'EOL à partir de l'instant de prédiction. Comme le montre la Figure A.2, il peut être intéressant de représenter l'évolution des RUL prédites et leurs incertitudes pour différents instants de prédiction. Des indicateurs de performances peuvent être établis à partir des résultats de ces prédictions en les comparants avec le vrai RUL.

Problématique

Les piles de type PEMFC sont des systèmes multi-échelle et multi-physique très complexes dont les composants fonctionnent avec des conditions opératoires variées. De nombreux défis doivent être relevés pour prédire la durée de vie résiduelle (RUL). Une des difficultés est liée au choix des mesures de dégradation en tant qu'indicateur de vieillissement. On utilise le plus souvent la puissance fournie par la pile. Cet indicateur est généralement surveillé en permanence en ligne et est donc un bon candidat pour le pronostique en ligne. Cependant la dégradation observée est en fait le résultat de la combinaison d'une dégradation matérielle d'origine diverses et de l'effet temporaire de conditions opératoires inappropriées (souvent appelés «défauts»), ce qui conduit à la coexistence de phénomènes réversibles et irréversibles (Figure A.3). La coexistence des ces phénomènes de dégradation réversibles et irréversibles confère à cet indicateur des limitations importantes.

La prédiction de la vie résiduelle (RUL) d'une pile PEMFC s'effectue en deux grandes étapes, chacune d'entre elles entraînant des défis scientifiques spécifiques :

1. Choix d'un indicateur de dégradation pertinent et développement d'un modèle de dégradation. Les indicateurs pertinents doivent refléter l'état de santé de la pile (State Of

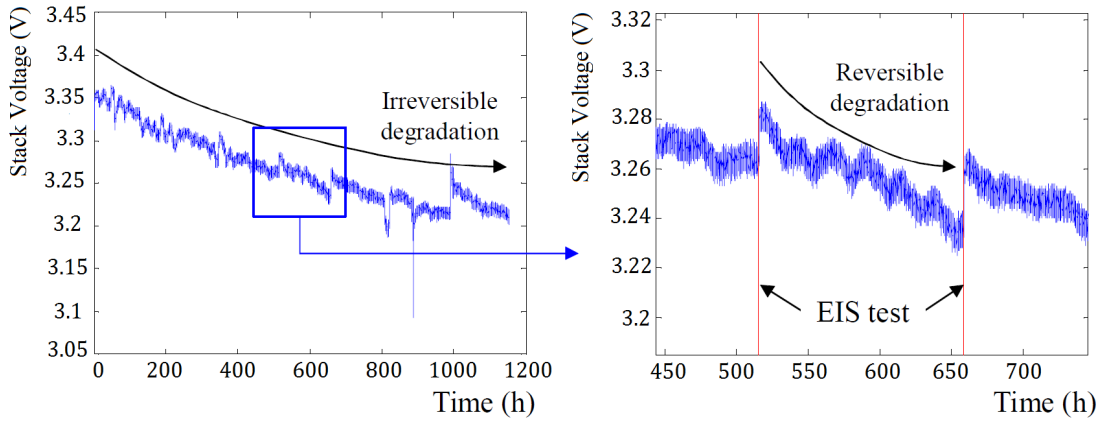

Figure A.3: Dégradation réversible et irréversible des performances d'une pile PEMFC.

Health, SOH) et divers indicateurs de vieillissement sont examinés : tension de la pile, puissance, mais également les courbes de polarisation et de spectroscopie d'impédance (EIS). A partir de l'indicateur choisi, un modèle de dégradation est établi.

2. La méthode de prédiction de la durée de vie résiduelle sera établie à partir du modèle de dégradation de la pile, incluant les informations disponibles en ligne sur son état interne.

Ces points nous ont amené à relever les défis suivants :

1. Bien que diverses mesures soient disponibles, il n'existe pas de définition unique d'un indicateur de bonne santé d'une pile PEMFC à des fins de pronostique. Toutes les mesures ne sont pas intéressantes pour prédire la durée de vie. Notre point de départ - et le premier sujet de recherche - est d'identifier les indicateurs de dégradation potentiellement pertinents de la PEMFC.
2. Les courbes de dégradation de la pile mesurées par la puissance de la pile comprennent des dégradations réversibles et irréversibles. Les dégradations réversibles conduisent à des chutes temporaires de la puissance, mais elles peuvent également entraîner une dégradation pérenne des performances et contribuer à la dégradation irréversible. Dans ce travail de recherche, l'objectif est de distinguer les comportements de dégradation irréversibles de ceux qui sont réversibles dans la prédiction de la RUL afin de la rendre plus performante.
3. Un défi supplémentaire est d'appliquer le pronostic pour des conditions opératoires dynamiques des PEMFC. Des causes multiples ou covariables peuvent conduire à des mécanismes de dégradation complexes sur lesquelles nous avons peu ou pas de connaissance. Par conséquent, un seul niveau d'information ne suffit pas pour établir un modèle de dégradation approprié. Notre objectif est d'étudier et d'explorer différentes façons d'utiliser des covariables de dégradation disponibles à différents niveaux, comme par exemple les courbes de spectroscopie d'impédance et de polarisation, de sorte que différentes sources puissent être fusionnées et contribuer au pronostic de la durée de vie résiduelle (RUL).

Résumé des chapitres

Nous avons développé dans ce mémoire plusieurs approches qui sont présentées ci-après.

Chapitre 1 à 3

Ces chapitres présentent les piles à combustibles, les méthodes de pronostic et une étude bibliographique des applications PHM sur les piles à combustible. Etant donné la complexité d'une pile, et le peu de mesures disponibles, nous avons prêté attention à la recherche d'indicateurs de dégradation supplémentaires. Nous avons accordé une attention particulière au pronostic des batteries Li-ion. En effet, ces dernières sont également des cellules électrochimiques et la recherche sur les batteries dans le domaine du pronostic est beaucoup plus mature. Cependant les indicateurs utilisés ne sont pas transposables aux piles. Toutefois nous avons trouvé des points communs intéressants dans les courbes de caractérisation de spectroscopie d'impédance et de polarisation. Les inconvénients de ces mesures sont leur disponibilité et leurs coûts.

Chapitre 4

Nous sommes partis de courbes de dégradations réelles (challenge IEEE 2014) pour appliquer la prédiction de la RUL à partir de méthodes à filtres à particules (Particle Filtering). Les résultats obtenus en utilisant uniquement la puissance de la pile montrent que celle-ci ne permet pas de distinguer les dégradations réversibles de celles qui sont irréversibles, entrainant des résultats insuffisants. Nous avons donc adapté la méthode de pronostic pour prendre en compte deux indicateurs de dégradation: la dégradation de la puissance de la pile et la dégradation du SOH estimée à partir de la résistance de polarisation identifiée à partir de la caractéristique EIS. La Figure A.4 montre les prédictions RUL avec les tolérances limites α de tous les modèles.

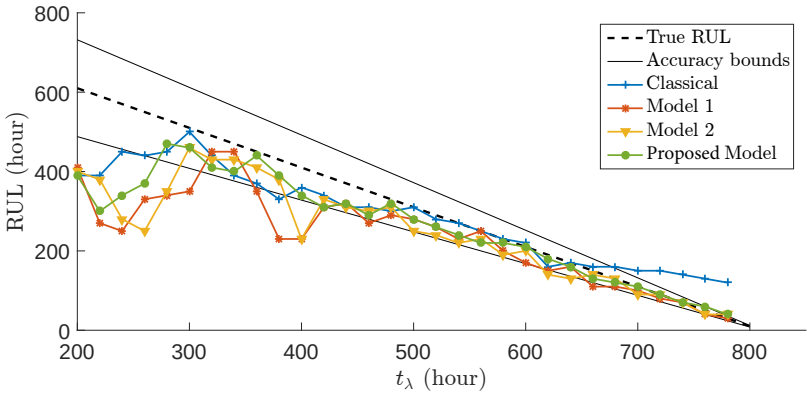

Figure A.4: Performances pronostiques de différents modèles réversibles.

Les performances de prédiction de la RUL sont évaluées grâce à des indicateurs de per-

formance. Les résultats montrent l'intérêt de l'approche proposée par rapport à l'utilisation uniquement de la puissance de la pile. Le paramètre de la résistance de polarisation estimé à partir de la courbe d'EIS a contribué à améliorer la précision de la prévision RUL. Le modèle proposé donne les meilleures performances parmi tous les modèles testés, en particulier pour les prévisions à long terme.

Pour comparer les performances pronostiques, les résultats de prédiction de l'approche précédente et l'algorithme étendu (avec différents modèles réversibles) sont évalués par différentes métriques de performance pronostique. Les résultats de l'évaluation ont montré l'intérêt de l'approche proposée. Le paramètre de la résistance de polarisation estimé à partir d'EIS a contribué à améliorer la précision de la prévision RUL. Le modèle proposé donne les meilleures performances parmi tous les modèles testés, en particulier pour les prévisions à long terme.

Chapitre 5

Ce chapitre aborde le problème d'un point de vue plus théorique. Le comportement de dégradation d'un système est souvent corrélé avec des covariables internes et externes qui sont généralement difficiles d'accès. Lorsque les causes des changements sont accessibles, elles ne le sont que de manière ponctuelle et les coûts de mesure sont élevés. Nous avons proposé un système d'inspection périodique de ces covariables de dégradation pour collecter des informations supplémentaires sur la dégradation pour obtenir un compromis optimal entre performance (précision et précision) et coût (contrôle des coûts dû aux inspections) pour l'estimation de la dégradation et la prévision RUL. Les méthodes traditionnelles de prévision basées sur l'estimation bayésienne doivent être adaptées à une approche multi-niveaux. Les changements de vitesse de dégradation peuvent être reconnus rapidement en inspectant les covariables de dégradation et en adaptant en conséquence les paramètres du filtre de pronostic. La Figure A.5 présente un exemple la courbe de dégradation temporelle avec une covariable de dégradation. Par exemple, une méthode classique de filtrage de particules (PF) (ligne pointillée verte sur la Figure A.5) peut estimer l'évolution de la dégradation mais quand il y a des changements significatifs dans la vitesse d'évolution, le PF ne peut pas répondre immédiatement. Il lui faut un certain temps pour s'adapter aux changements. L'autre courbe montre qu'avec l'aide de l'inspection de la covariable et de la mise à jour du modèle en conséquence, l'estimation peut être plus performante (ligne pointillée rouge sur la figure A.5).

Les prédictions avec des inspections fréquentes ont montré une meilleure performance en précision grâce aux informations fournies par les inspections et à la mise à jour du modèle associée. Cependant, la fréquence des inspections entraîne un coût élevé proportionnel au nombre plus élevé d'inspections. Pour devenir réalisable sur un plan commercial, une inspection ne doit être effectuée que lorsque c'est utile. Nous avons donc proposé une inspection réalisée uniquement si les performances se dégradent. Les résultats confirment ce que nous attendions : en utilisant des informations pertinentes sur le SOH, le pronostic de la RUL est plus performant.

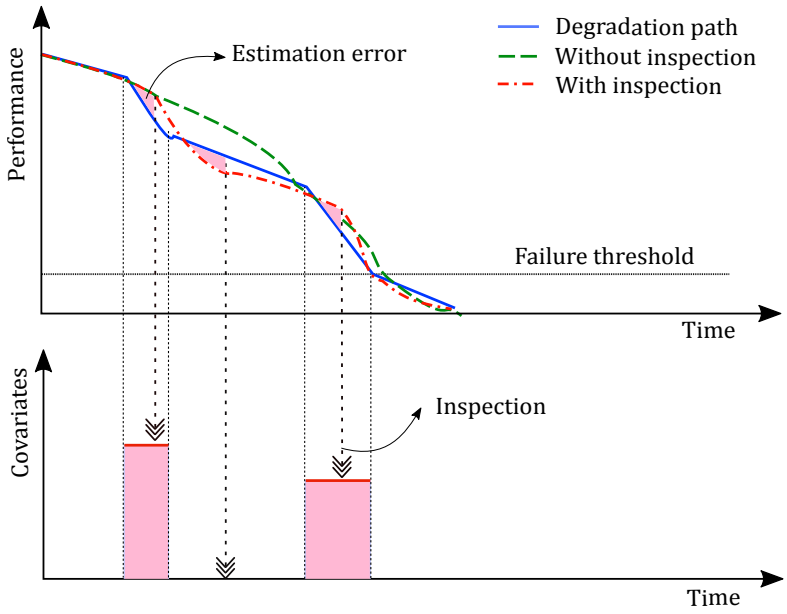

Figure A.5: Principe de l'estimation de la dégradation avec la procedure d'inspection.

Chapitre 6

La littérature fournit de nombreuse méthodes de pronostic basées sur une grande quantité de données historiques Run-to-Fail. Ces méthodes n'apparaissent que rarement dans les applications PEMFC en raison des coûts élevés des tests Run-to-Fail à qui sont rares. Cependant, à mesure que la croissance des recherches sur les pronostics pour PEMFC se poursuit, nous considérons que ces méthodes pourront être appliquées aux piles PEMFC. Nous proposons ici une approche dite « model-ensemble » qui utilise l'agrégation de plusieurs RUL issus de plusieurs modèles pour établir la prévision RUL.

Considérons alors un système en fonctionnement soumis à une dégradation. Cette dégradation peut être caractérisée par différentes mesures de dégradation à différents niveaux du système. Dans le cas de PEMFC, des mesures de deux signaux différents sur la pile sont disponibles :

1. Un signal externe tel que la tension de pile : il est facilement accessible, mesuré fréquemment, mais de "qualité médiocre", c'est-à-dire, avec un bruit de mesure significatif et comportant des informations d'origines diverses (dégradations reversibles/irréversibles);
2. Une caractérisation interne de la pile SOH: elle est mesurée uniquement à des pas de temps plus espacés en raison de sa complexité et de son coût, c'est-à-dire que la pile à combustible ne doit être en fonctionnement pour effectuer les mesures. Elle donne une information sur les dégradations irréversibles de la pile.

Nous avons développé une approche d'ensemble de modèles qui combine les prédictions RUL des deux sources différentes. Les prédictions RUL des deux modèles sont agrégées dynamique-

ment par une somme pondérée. Les poids de chaque modèle a été défini par les performances pronostiques évaluées sur un ensemble de données historiques.

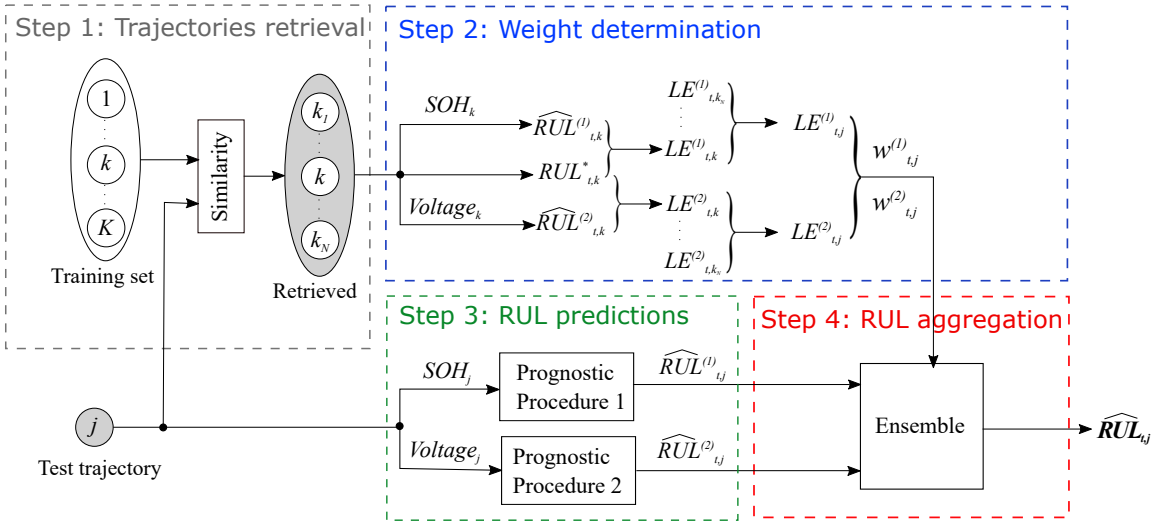

Figure A.6: Schéma d'approche pronostique proposée.

Nous avons développé une approche d'ensemble de modèles qui combine les prédictions RUL des deux sources différentes à différents niveaux. Les prédictions RUL des deux modèles sont agrégées dynamiquement en fonction de leurs poids locaux. Les poids des modèles ont été définis par les performances pronostiques évaluées sur un ensemble de données historiques. La Figure A.7 montre les prédictions RUL et l'agrégation pour l'une des trajectoires de test. Le pronostic basé sur l'ensemble des modèles tire parti des comportements complémentaires des deux extrants pronostiques des modèles individuels.

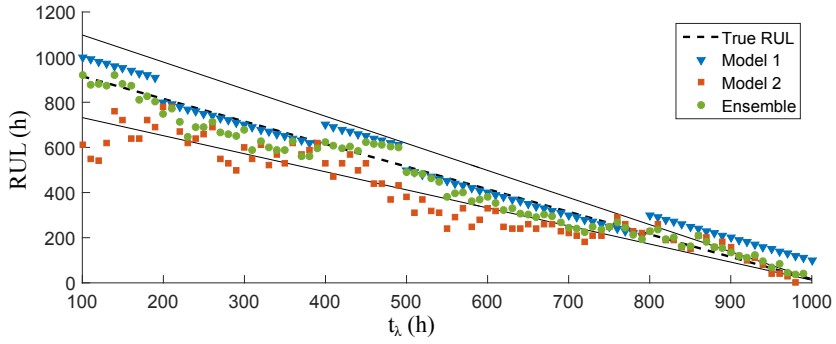

Figure A.7: Un exemple d'agrégation de prédictions RUL.

La Figure A.7 montre les prédictions des RUL et de son agrégation pour l'un des trajectoires de test. Le pronostic basé sur l'ensemble des modèles tire parti des comportements complémentaires des modèles. Les résultats ont montré que la précision de la prévision a été améliorée en surmontant les inconvénients des deux modèles et en tirant parti de leurs forces. Les performances montrent une supériorité de la méthode « modèle-ensemble » sur les modèles pris séparément.

Contributions principales

Les principales contributions de cette thèse peuvent être résumées comme suit :

1. Adaptation de l'état de l'art des modèles de détérioration stochastique et des méthodes d'estimation RUL associées à l'application PEMFC (Chapitre 3).
2. Extension au-delà de l'état de l'art pour prendre en compte de différentes manières les différentes informations de détérioration disponibles aux différents niveaux du système. Notre contribution est triple :
   - Développement d'une approche de pronostic RUL distinguant les dégradations irréversibles de celles réversibles en utilisant des indicateurs de dégradation multiples (Chapitre 4).
   - Proposition d'un schéma d'inspection des covariables de détérioration pour recueillir des informations supplémentaires sur la détérioration si nécessaire afin d'obtenir un compromis optimal entre performance et coût (dû aux inspections) pour l'estimation de la détérioration et la prédiction de la durée de vie résiduelle (RUL).
   - Développement d'une approche d'ensemble de modèles qui combine les prédictions RUL provenant de différentes sources à différents niveaux, pour améliorer la précision du pronostic. Les incertitudes des RUL de différentes sources sont également fusionnées par l'ensemble pour fournir des prédictions plus précises et plus complètes (Chapitre 6).

L'analyse de la littérature sur les pronostics PEMFC, et même sur les pronostics en général, montre qu'aucun travail (ou seulement quelques travaux en ce qui concerne les pronostics en général) a abordé la question de l'utilisation de la détérioration hétérogène pour effectuer une estimation RUL. Dans un système qui se détériore, il existe souvent des covariables de dégradation ou des indicateurs de détérioration qui ne peuvent pas être observés directement mais qui peuvent être intéressants et utiles à utiliser pour améliorer les performances pronostiques. Nous avons donc porté une attention particulière à l'utilisation possible de ces covariables de dégradation et nous avons concentré nos efforts sur la proposition de solutions pour effectuer des prédictions RUL en utilisant les informations du chapitre 4 à différents niveaux (pour résoudre le problème posé par l'existence de détérioration réversibles par rapport à une détérioration irréversible).

Liste des publications

Au cours de la thèse, plusieurs articles ont été publiés pour présenter ces contributions :

- D. Zhang, P. Baraldi, C. Cadet, N. Yousfi-Steiner, C. Bérenguer and E. Zio (2018) An ensemble of models for integrating dependent sources of information for the prognosis of the remaining useful life of Proton Exchange Membrane Fuel Cells. *Mechanical Systems and Signal Processing*, under review.
- D. Zhang, C. Cadet, N. Yousfi-Steiner and C. Bérenguer (2018) PEMFC RUL Prognostics Considering Degradation Recovery Phenomena. *Proceedings of the Institution of Mechanical Engineers, Part O: Journal of Risk and Reliability*, accepted
- D. Zhang, C. Cadet, N. Yousfi-Steiner, F. Druart and C. Bérenguer (2017) PHM-oriented Degradation Indicators for Batteries and Fuel Cells. *Fuel Cells*, 17(2), pp.268-276. DOI: 10.1002/fuce.201600075.
- D. Zhang, C. Cadet, N. Yousfi-Steiner and C. Bérenguer (2017) A Study of Online Inspection for Multi-level Prognostics. In: *IFAC-PapersOnLine*, 50(1), pp.13716-13721. DOI: 10.1016/j.ifacol.2017.08.2549.
- D. Zhang, P. Baraldi, C. Cadet, N. Yousfi-Steiner, C. Bérenguer and E. Zio (2017) A Study of Local Aggregation of An Ensemble of Models for RUL Prediction. In: *The 10th International Conference on Mathematical Methods in Reliability (MMR 2017)*, July 3-6, 2017, Grenoble, France.
- D. Zhang, C. Cadet, N. Yousfi-Steiner and C. Bérenguer (2016) Some Improvements of Particle Filtering Based Prognosis for PEM Fuel Cells. In: *IFAC-PapersOnLine*, volume 49. pp.162-167. DOI: 0.1016/j.ifacol.2016.11.028.
- D. Zhang, C. Cadet, N. Yousfi-Steiner and C. Bérenguer (2015) PHM-oriented degradation indicators for PEM fuel cells:What can be learnt from battery State of Charge estimation . In: *Proc. 6th International Conference on Fundamentals & Development of Fuel Cells*, Paper 190. Feb 2015, Toulouse, France.

GIPSA-LAB, 11 rue des Mathématiques, Grenoble Campus BP46
F-38402 SAINT MARTIN D'HERES CEDEX

Bibliography

[1] A. Barré, B. Deguilhem, S. Grolleau, M. Gérard, F. Suard, and D. Riu, "A review on lithium-ion battery ageing mechanisms and estimations for automotive applications", *J. Power Sources*, vol. 241, pp. 680–689, 2013 (cit. on p. 5).

[2] W. Waag, C. Fleischer, and D. U. Sauer, "Critical review of the methods for monitoring of lithium-ion batteries in electric and hybrid vehicles", *J. Power Sources*, vol. 258, pp. 321–339, 2014 (cit. on pp. 5, 19–21).

[3] D. Zhang, C. Cadet, N. Yousfi-Steiner, F. Druart, and C. Bérenguer, "PHM-oriented Degradation Indicators for Batteries and Fuel Cells", *Fuel Cells*, vol. 17, no. 2, pp. 268–276, 2017 (cit. on pp. 5, 90).

[4] B. Tylkowski, J. Walkowiak-Kulikowska, J. Wolska, and H. Koroniak, "Polymers application in proton exchange membranes for fuel cells (PEMFCs)", *Phys. Sci. Rev.*, vol. 2, no. 8, pp. 1–36, 2017 (cit. on p. 6).

[5] Department of Energy, *Comparison of fuel cell technologies*, 2017. [Online]. Available: https://energy.gov/eere/fuelcells/comparison-fuel-cell-technologies (cit. on p. 8).

[6] FuelCellToday, *Fuel cell applications*, 2017. [Online]. Available: http://www.fuelcelltoday.com/applications (cit. on p. 7).

[7] Netinform, *Hydrogen refuelling stations worldwide*, 2017. [Online]. Available: https://www.netinform.net/H2/H2Stations/ (cit. on p. 7).

[8] Université de Corse, *Plateforme myrte*, 2017. [Online]. Available: http://myrte.univ-corse.fr/La-plateforme_a4.html (cit. on p. 7).

[9] FuelCellsWorks, *Ene-farm program*, 2017. [Online]. Available: https://fuelcellsworks.com/archives/2015/09/23/ene-farm-installed-120000-residential-fuel-cell-units/ (cit. on p. 7).

[10] Hydrogen Mobility Europe, *H2ME Program*, 2017. [Online]. Available: http://h2me.eu/ (cit. on p. 7).

[11] Toyota, *Toyota FCEV Mirai*, 2017. [Online]. Available: https://www.toyota.fr/new-cars/new-mirai/meet-mirai#1 (cit. on p. 7).

[12] J. J. Hwang, "Transient power characteristic measurement of a proton exchange membrane fuel cell generator", *Int. J. Hydrogen Energy*, vol. 38, no. 9, pp. 3727–3740, 2013 (cit. on p. 9).

[13] R. Gouriveau, M. Hilairet, D. Hissel, S. Jemeï, M. Jouin, E. Lechartier, S. Morando, E. Pahon, M.-C. Péra, and N. Zerhouni, *IEEE PHM 2014 Data Challenge - Details for participants*, 2014. [Online]. Available: http://eng.fclab.fr/ieee-phm-2014-data-challenge/ (cit. on pp. 9, 10, 21–23, 31, 55, 62, 89).

[14] O. S. Burheim, H. Su, H. H. Hauge, S. Pasupathi, and B. G. Pollet, "Study of thermal conductivity of PEM fuel cell catalyst layers", *Int. J. Hydrogen Energy*, vol. 39, no. 17, pp. 9397–9408, 2014 (cit. on p. 10).

[15] Y Chen, O. Enearu, D Montalvao, and T Sutharssan, "A Review of Computational Fluid Dynamics Simulations on PEFC Performance", *J. Appl. Mech. Eng.*, vol. 05, no. 06, 2016 (cit. on p. 12).

[16] F. A. De Bruijn, V. A. T. Dam, and G. J. M. Janssen, "Review: Durability and degradation issues of PEM fuel cell components", *Fuel Cells*, vol. 8, no. 1, pp. 3–22, 2008 (cit. on p. 11).

[17] M. Jouin, R. Gouriveau, D. Hissel, and S. Member, "Joint Particle Filters Prognostics for Proton Exchange Membrane Fuel Cell Power Prediction at Constant Current Solicitation", *IEEE Trans. Reliab.*, vol. 65, no. 1, pp. 336–349, 2016 (cit. on pp. 11, 33).

[18] M. Fowler, R. F. Mann, J. C. Amphlett, B. A. Peppley, and P. R. Roberge, "Reliability issues and voltage degradation", in *Handbook of Fuel Cells*, John Wiley & Sons, Ltd, 2010 (cit. on p. 11).

[19] R. Petrone, Z. Zheng, D. Hissel, M. C. Péra, C. Pianese, M. Sorrentino, M. Becherif, and N. Yousfi-Steiner, "A review on model-based diagnosis methodologies for PEMFCs", *Int. J. Hydrogen Energy*, vol. 38, no. 17, pp. 7077–7091, 2013 (cit. on pp. 13, 24).

[20] L. Dubau, L. Castanheira, F. Maillard, M. Chatenet, O. Lottin, G. Maranzana, J. Dillet, A. Lamibrac, J. C. Perrin, E. Moukheiber, A. Elkaddouri, G. De Moor, C. Bas, L. Flandin, and N. Caqué, "A review of PEM fuel cell durability: Materials degradation, local heterogeneities of aging and possible mitigation strategies", *Wiley Interdisciplinary Reviews: Energy and Environment*, vol. 3, no. 6, pp. 540–560, 2014 (cit. on p. 13).

[21] J. Wu, X. Z. Yuan, H. Wang, M. Blanco, J. J. Martin, and J. Zhang, "Diagnostic tools in PEM fuel cell research: Part I Electrochemical techniques", *Int. J. Hydrogen Energy*, vol. 33, no. 6, pp. 1735–1746, 2008 (cit. on p. 13).

[22] T. Kim, H. Kim, J. Ha, K. Kim, J. Youn, J. Jung, and B. D. Youn, "A degenerated equivalent circuit model and hybrid prediction for state-of-health (SOH) of PEM fuel cell", in *2014 Int. Conf. Progn. Heal. Manag. PHM 2014*, 2014, pp. 1–7 (cit. on pp. 13, 16, 22–24, 32, 62, 96).

[23] G. M. Ehrlich, *Lithium-Ion Batteries*. McGraw-Hill Professional, 2002, pp. 35.1–35.94 (cit. on p. 14).

[24] N. Yousfi-Steiner, P. Moçotéguy, D. Candusso, D. Hissel, a. Hernandez, and a. Aslanides, "A review on PEM voltage degradation associated with water management: Impacts, influent factors and characterization", *J. Power Sources*, vol. 183, no. 1, pp. 260–274, 2008 (cit. on p. 15).

[25] X. Zhang, D. Yang, M. Luo, and Z. Dong, "Load profile based empirical model for the lifetime prediction of an automotive PEM fuel cell", *Int. J. Hydrogen Energy*, vol. 42, no. 16, pp. 11 868–11 878, 2017 (cit. on p. 16).

[26] S Tant, S Rosini, P.-X Thivel, F Druart, A Rakotondrainibe, T Geneston, and Y Bultel, "An algorithm for diagnosis of proton exchange membrane fuel cells by electrochemical impedance spectroscopy", *Electrochim. Acta*, vol. 135, pp. 368–379, 2014 (cit. on pp. 16, 24).

[27] A. Barai, G. H. Chouchelamane, Y. Guo, A. McGordon, and P. Jennings, "A study on the impact of lithium-ion cell relaxation on electrochemical impedance spectroscopy", *J. Power Sources*, vol. 280, pp. 74–80, 2015 (cit. on pp. 18, 19).

[28] S. Piller, M. Perrin, and A. Jossen, "Methods for state-of-charge determination and their applications", in *Journal of Power Sources*, vol. 96, 2001, pp. 113–120 (cit. on p. 20).

[29] S. M. Rezvanizaniani, Z. Liu, Y. Chen, and J. Lee, "Review and recent advances in battery health monitoring and prognostics technologies for electric vehicle (EV) safety and mobility", *J. Power Sources*, vol. 256, pp. 110–124, 2014 (cit. on p. 20).

[30] Y. H. Chiang, W. Y. Sean, and J. C. Ke, "Online estimation of internal resistance and open-circuit voltage of lithium-ion batteries in electric vehicles", *J. Power Sources*, vol. 196, no. 8, pp. 3921–3932, 2011 (cit. on p. 20).

[31] H. He, X. Zhang, R. Xiong, Y. Xu, and H. Guo, "Online model-based estimation of state-of-charge and open-circuit voltage of lithium-ion batteries in electric vehicles", *Energy*, vol. 39, no. 1, pp. 310–318, 2012 (cit. on p. 20).

[32] D. Wang, Q. Miao, and M. Pecht, "Prognostics of lithium-ion batteries based on relevance vectors and a conditional three-parameter capacity degradation model", *J. Power Sources*, vol. 239, pp. 253–264, 2013 (cit. on pp. 20, 30).

[33] H. Dong, X. Jin, Y. Lou, and C. Wang, "Lithium-ion battery state of health monitoring and remaining useful life prediction based on support vector regression-particle filter", *J. Power Sources*, vol. 271, pp. 114–123, 2014 (cit. on p. 20).

[34] J. Guo, Z. Li, and M. Pecht, "A Bayesian approach for Li-Ion battery capacity fade modeling and cycles to failure prognostics", *J. Power Sources*, vol. 281, pp. 173–184, 2015 (cit. on p. 21).

[35] M. Galeotti, L. Cinà, C. Giammanco, S. Cordiner, and A. Di Carlo, "Performance analysis and SOH (state of health) evaluation of lithium polymer batteries through electrochemical impedance spectroscopy", *Energy*, vol. 89, pp. 678–686, 2015 (cit. on pp. 21, 22).

[36] R. Onanena, L. Oukhellou, D. Candusso, F. Harel, D. Hissel, and P. Aknin, "Fuel cells static and dynamic characterizations as tools for the estimation of their ageing time", *Int. J. Hydrogen Energy*, vol. 36, no. 2, pp. 1730–1739, 2011 (cit. on pp. 23, 24).

[37] M. Jouin, R. Gouriveau, D. Hissel, M.-C. Péra, and N. Zerhouni, "Prognostics and Health Management of PEMFC - State of the art and remaining challenges", *Int. J. Hydrogen Energy*, vol. 38, no. 35, pp. 15 307–15 317, 2013 (cit. on pp. 24, 27, 33, 46, 56).

[38] S. Chevalier, B. Auvity, J. C. Olivier, C. Josset, D. Trichet, and M. Machmoum, "Detection of cells state-of-health in PEM fuel cell stack using EIS measurements coupled with multiphysics modeling", *Fuel Cells*, vol. 14, no. 3, pp. 416–429, 2014 (cit. on p. 24).

[39] E. Zio, "Prognostics and Health Management of Industrial Equipment", in *Diagnostics and Prognostics of Engineering Systems: Methods and Techniques*, S. Kadry, Ed., Kuwait: IGI Global, 2012, pp. 333–356 (cit. on p. 27).

[40] J Coble and J. Hines, "Applying the General Path Model to Estimation of Remaining Useful Life", *Int. J. Progn. Heal. Manag.*, vol. 2, no. 1, pp. 1–13, 2011 (cit. on p. 27).

[41] ISO 13372:2012, *Condition monitoring and diagnostics of machines – vocabulary*, 2012 (cit. on p. 27).

[42] A. Saxena, J. Celaya, B. Saha, S. Saha, and K. Goebel, "Metrics for Offline Evaluation of Prognostic Performance", *Int. J. Progn. Heal. Manag.*, vol. 1, no. 1, pp. 1–20, 2010 (cit. on pp. 28, 29, 49, 105).

[43] A. Saxena, J. Celaya, B. Saha, S. Saha, and K. Goebel, "Evaluating prognostics performance for algorithms incorporating uncertainty estimates", in *IEEE Aerosp. Conf. Proc.*, 2010, pp. 1–11 (cit. on pp. 29, 49, 67, 105).

[44] A. Saxena, J. Celaya, I. Roychoudhury, S. Saha, B. Saha, and K. Goebel, "Designing data-driven battery prognostic approaches for variable loading profiles: Some lessons learned", in *Eur. Conf. Progn. Heal. Manag. Soc*, 2012, pp. 1–11 (cit. on pp. 29, 30, 49, 105).

[45] Y. Hu, P. Baraldi, F. Di Maio, and E. Zio, "Online Performance Assessment Method for a Model-Based Prognostic Approach", *IEEE Trans. Reliab.*, vol. 65, no. 2, pp. 718–735, 2016 (cit. on pp. 29, 105).

[46] M. Rigamonti, P. Baraldi, E. Zio, I. Roychoudhury, K. Goebel, and S. Poll, "Echo State Network for the Remaining Useful Life Prediction of a Turbofan Engine", in *Eur. Conf. Progn. Heal. Manag. Soc. 2016*, 2016, pp. 1–15 (cit. on p. 29).

[47] S. Al-Dahidi, F. Di Maio, P. Baraldi, and E. Zio, "A locally adaptive ensemble approach for data-driven prognostics of heterogeneous fleets", *Proc. Inst. Mech. Eng. Part O J. Risk Reliab.*, vol. 231, no. 4, pp. 1–14, 2017 (cit. on pp. 29, 30, 105).

[48] M. Rigamonti, P. Baraldi, E. Zio, D. Astigarraga, and A. Galarza, "Particle Filter-Based Prognostics for an Electrolytic Capacitor Working in Variable Operating Conditions", *IEEE Trans. Power Electron.*, vol. 31, no. 2, pp. 1567–1575, 2016 (cit. on pp. 29, 105).

[49] P. Baraldi, M. Compare, S. Sauco, and E. Zio, "Ensemble neural network-based particle filtering for prognostics", *Mech. Syst. Signal Process.*, vol. 41, no. 1-2, pp. 288–300, 2013 (cit. on pp. 29, 53, 88, 105, 106).

[50] J. Z. Sikorska, M. Hodkiewicz, and L. Ma, "Prognostic modelling options for remaining useful life estimation by industry", *Mech. Syst. Sig. Process.*, vol. 25, no. 5, pp. 1803–1836, 2011 (cit. on p. 29).

[51] M. S. Kan, A. C. Tan, and J. Mathew, "A review on prognostic techniques for non-stationary and non-linear rotating systems", *Mech. Syst. Sig. Process.*, vol. 62, pp. 1–20, 2015 (cit. on p. 30).

[52] T. Sutharssan, D. Montalvao, Y. K. Chen, W.-C. Wang, C. Pisac, and H. Elemara, "A review on prognostics and health monitoring of proton exchange membrane fuel cell", *Renewable Sustainable Energy Rev.*, vol. 75, no. November, pp. 440–450, 2017 (cit. on pp. 30, 34).

[53] M. Tahan, E. Tsoutsanis, M. Muhammad, and Z. A. Abdul Karim, "Performance-based health monitoring, diagnostics and prognostics for condition-based maintenance of gas turbines: A review", *Appl. Energy*, vol. 198, pp. 122–144, 2017 (cit. on p. 30).

[54] K. Javed, R. Gouriveau, N. Zerhouni, and D. Hissel, "Prognostics of Proton Exchange Membrane Fuel Cells stack using an ensemble of constraints based connectionist networks", *J. Power Sources*, vol. 324, pp. 745–757, 2016 (cit. on p. 30).

[55] A. Nuhic, T. Terzimehic, T. Soczka-Guth, M. Buchholz, and K. Dietmayer, "Health diagnosis and remaining useful life prognostics of lithium-ion batteries using data-driven methods", *J. Power Sources*, 2013 (cit. on p. 30).

[56] P. Baraldi, F. Mangili, and E. Zio, "Investigation of uncertainty treatment capability of model-based and data-driven prognostic methods using simulated data", *Reliab. Eng. Syst. Saf.*, vol. 112, pp. 94–108, 2013 (cit. on p. 30).

[57] R. E. Silva, R. Gouriveau, S. Jemeï, D. Hissel, L. Boulon, K. Agbossou, and N. Yousfi Steiner, "Proton exchange membrane fuel cell degradation prediction based on Adaptive Neuro-Fuzzy Inference Systems", *Int. J. Hydrogen Energy*, vol. 39, no. 21, pp. 11 128–11 144, 2014 (cit. on p. 30).

[58] X. S. Si, W. Wang, C. H. Hu, and D. H. Zhou, "Remaining useful life estimation - A review on the statistical data driven approaches", *Eur. J. Oper. Res.*, vol. 213, no. 1, pp. 1–14, 2011 (cit. on pp. 30, 40, 41).

[59] K. L. Tsui, N. Chen, Q. Zhou, Y. Hai, and W. Wang, "Prognostics and health management: A review on data driven approaches", *Math. Probl. Eng.*, vol. 2015, pp. 1–17, 2015 (cit. on p. 30).

[60] Y. Xing, E. W. M. Ma, K. L. Tsui, and M. Pecht, "An ensemble model for predicting the remaining useful performance of lithium-ion batteries", *Microelectron. Reliab.*, vol. 53, no. 6, pp. 811–820, 2013 (cit. on pp. 30, 88).

[61] K. Le Son, M. Fouladirad, A. Barros, E. Levrat, and B. Iung, "Remaining useful life estimation based on stochastic deterioration models: A comparative study", *Reliab. Eng. Syst. Saf.*, vol. 112, pp. 165–175, 2013 (cit. on p. 30).

[62] M. Compare, L. Bellani, and E. Zio, "Reliability model of a component equipped with PHM capabilities", *Reliab. Eng. Syst. Saf.*, vol. 000, pp. 1–8, 2016 (cit. on p. 30).

[63] M. Jouin, R. Gouriveau, D. Hissel, M.-C. Péra, and N. Zerhouni, "Degradations analysis and aging modeling for health assessment and prognostics of PEMFC", *Reliab. Eng. Syst. Saf.*, vol. 148, pp. 78–95, 2016 (cit. on p. 30).

[64] D. Zhou, F. Gao, E. Breaz, A. Ravey, and A. Miraoui, "Degradation prediction of PEM fuel cell using a moving window based hybrid prognostic approach", *Energy*, vol. 138, pp. 1175–1186, 2017 (cit. on pp. 30, 34).

[65] L. Liao and F. Köttig, "Review of hybrid prognostics approaches for remaining useful life prediction of engineered systems, and an application to battery life prediction", *IEEE Trans. Rel.*, vol. 63, no. 1, pp. 191–207, 2014 (cit. on p. 30).

[66] ——, "A hybrid framework combining data-driven and model-based methods for system remaining useful life prediction", *Appl. Soft Comput.*, vol. 44, pp. 191–199, 2016 (cit. on p. 30).

[67] D. Hissel and M. C. Pera, "Diagnostic & health management of fuel cell systems: Issues and solutions", *Annu. Rev. Control*, vol. 42, pp. 201–211, 2016 (cit. on p. 31).

[68] Z. Li, S. Giurgea, R. Outbib, and D. Hissel, "Online diagnosis of PEMFC by combining support vector machine and fluidic model", *Fuel Cells*, vol. 14, no. 3, pp. 448–456, 2014 (cit. on p. 31).

[69] A. Bouaicha, H. Allagui, E.-H. Aglzim, A. Rouane, and A. Mami, "Validation of a methodology for determining the PEM fuel cell complex impedance modelling parameters", *Int. J. Hydrogen Energy*, vol. 42, no. 17, pp. 12 738–12 748, 2017 (cit. on p. 31).

[70] E. Dijoux, N. Y. Steiner, M. Benne, M.-C. Péra, and B. G. Pérez, "A review of fault tolerant control strategies applied to proton exchange membrane fuel cell systems", *J. Power Sources*, vol. 359, pp. 119–133, 2017 (cit. on p. 31).

[71] W. Daud, R. Rosli, E. Majlan, S. Hamid, R. Mohamed, and T. Husaini, "PEM fuel cell system control: A review", *Renew. Energy*, vol. 113, pp. 620–638, 2017 (cit. on p. 31).

[72] N. Herr, J. M. Nicod, C. Varnier, L. Jardin, A. Sorrentino, D. Hissel, and M.-C. Péra, "Decision process to manage useful life of multi-stacks fuel cell systems under service constraint", *Renew. Energy*, vol. 105, pp. 590–600, 2017 (cit. on p. 31).

[73] S. Zhang, X. Z. Yuan, R. Hiesgen, K. A. Friedrich, H. Wang, M. Schulze, A. Haug, and H. Li, "Effect of open circuit voltage on degradation of a short proton exchange membrane fuel cell stack with bilayer membrane configurations", in *J. Power Sources*, vol. 205, 2012, pp. 290–300 (cit. on p. 31).

[74] J. K. Kimotho, T. Meyer, and W. Sextro, "PEM fuel cell prognostics using particle filter with model parameter adaptation", in *2014 Int. Conf. Progn. Heal. Manag.*, 2014, pp. 1–6 (cit. on pp. 31–33, 46, 56).

[75] M. Jouin, R. Gouriveau, D. Hissel, M.-C. Péra, and N. Zerhouni, "Prognostics of PEM fuel cell in a particle filtering framework", *Int. J. Hydrogen Energy*, vol. 39, no. 1, pp. 481–494, 2014 (cit. on p. 33).

[76] M. Jouin, "Contribution au pronostic d'une pile à combustible de type PEMFC - approche par filtrage particulaire a combustible de", PhD thesis, Université de Franche-Comté, 2015 (cit. on p. 33).

[77] E. Lechartier, E. Laffly, M.-C. Péra, R. Gouriveau, D. Hissel, and N. Zerhouni, "Proton exchange membrane fuel cell behavioral model suitable for prognostics", *Int. J. Hydrogen Energy*, vol. 40, no. 26, pp. 8384–8397, 2015 (cit. on pp. 33, 90).

[78] E. Lechartier, "Contribution au pronostic de pile à combustible PEMFC basé sur modèle semi-analytique", PhD thesis, Université de Franche-Comté, 2016 (cit. on p. 33).

[79] M. Bressel, M. Hilairet, D. Hissel, and B. Ould Bouamama, "Remaining useful life prediction and uncertainty quantification of proton exchange membrane fuel cell under variable load", *IEEE Trans. Ind. Electron.*, vol. 63, no. 4, pp. 2569–2577, 2016 (cit. on pp. 34, 90, 92, 112).

[80] M. S. Jha, G. Dauphin-Tanguy, and B. Ould-Bouamama, "Particle filter based hybrid prognostics of proton exchange membranefuel cell in bond graph framework", *Mech. Syst. Signal Process.*, vol. 75, pp. 301–329, 2016 (cit. on pp. 34, 90, 112).

[81] E. Pahon, S. Morando, R. Petrone, M. C. P??ra, D. Hissel, N. Yousfi-Steiner, S. Jemei, R. Gouriveau, D. Chamagne, P. Moçotéguy, and N. Zerhouni, "Long-term tests duration reduction for PEMFC μ-CHP application", *Int. J. Hydrogen Energy*, vol. 42, no. 2, pp. 1527–1533, 2017 (cit. on p. 34).

[82] W. Meeker, Y. Hong, and L. Escobar, "Degradation Models and Analyses", *Encycl. Stat. Sci.*, pp. 1–23, 2011 (cit. on p. 40).

[83] C. J. Lu, W. Q. Meeker, and Q Meeker, "Measures to Estimate Using Degradation a Distribution", *Technometrics*, vol. 35, no. 2, pp. 161–174, 1993 (cit. on p. 40).

[84] N. Gorjian, L. Ma, M. Mittinty, P. Yarlagadda, and Y. Sun, "Reliability issues and voltage degradation", in *Engineering Asset Lifecycle Management*, Springer, London, 2010, pp. 369–384 (cit. on p. 40).

[85] J. M. van Noortwijk, "A survey of the application of gamma processes in maintenance", *Reliab. Eng. Syst. Saf.*, vol. 94, no. 1, pp. 2–21, 2009 (cit. on pp. 41, 96).

[86] N. Gebraeel, M. Lawley, R. Li, and J. Ryan, "Residual-life distributions from component degradation signals: A Bayesian approach", *IIE Trans.*, vol. 37, no. 6, pp. 543–557, 2005 (cit. on p. 41).

[87] N. Gebraeel and J. Pan, "Prognostic degradation models for computing and updating residual life distributions in a time-varying environment", *IEEE Trans. Reliab.*, vol. 57, no. 4, pp. 539–550, 2008 (cit. on p. 41).

[88] N. Gebraeel, A. Elwany, and J. Pan, "Residual life predictions in the absence of prior degradation knowledge", *IEEE Trans. Reliab.*, vol. 58, no. 1, pp. 106–117, 2009 (cit. on p. 41).

[89] S. C. Patwardhan, S. Narasimhan, P. Jagadeesan, B. Gopaluni, and S. L. Shah, "Nonlinear Bayesian state estimation: A review of recent developments", *Control Eng. Pract.*, vol. 20, no. 10, pp. 933–953, 2012 (cit. on p. 42).

[90] M. Jouin, R. Gouriveau, D. Hissel, M.-C. Péra, and N. Zerhouni, "Particle filter-based prognostics: Review, discussion and perspectives", *Mech. Syst. Signal Process.*, vol. 72-73, pp. 2–31, 2016 (cit. on pp. 42, 47).

[91] K. Rickard, "Particle filtering for positioning and tracking applications", PhD thesis, Linköping University, 2005 (cit. on p. 42).

[92] M. S. Arulampalam, S. Maskell, N. Gordon, and T. Clapp, "A tutorial on particle filters for online nonlinear/non-Gaussian Bayesian tracking", *IEEE Trans. Signal Process.*, vol. 50, no. 2, pp. 174–188, 2002 (cit. on pp. 43, 91).

[93] T. Li, M. Bolic, and P. M. Djuric, "Resampling methods for particle filtering: Classification, implementation, and strategies", *IEEE Signal Process. Mag.*, vol. 32, no. 3, pp. 70–86, 2015 (cit. on p. 43).

[94] M Dalal, J Ma, and D He, "Lithium-ion battery life prognostic health management system using particle filtering framework", *Proc. Inst. Mech. Eng. Part O J. Risk Reliab.*, vol. 225, no. 1, pp. 81–90, 2011 (cit. on p. 46).

[95] M. J. Daigle and K. Goebel, "Model-based prognostics with concurrent damage progression processes", *IEEE Trans. Syst. Man, Cybern. Part ASystems Humans*, vol. 43, no. 3, pp. 535–546, 2013 (cit. on pp. 46, 57).

[96] D. An, J. Choi, and N. Kim, "A tutorial for model-based prognostics algorithms based on matlab code", in *Annu. Conf. Progn. Heal. Manag. Soc. 2012*, 2012, pp. 1–9 (cit. on p. 46).

[97] D. Zhang, C. Cadet, C. Bérenguer, and N. Yousfi-Steiner, "Some Improvements of Particle Filtering Based Prognosis for PEM Fuel Cells", *IFAC-PapersOnLine*, vol. 49, no. 28, pp. 162–167, 2016 (cit. on p. 55).

[98] P. Baraldi, A. Cammi, F. Mangili, and E. Zio, "Local fusion of an ensemble of models for the reconstruction of faulty signals", *IEEE Trans. Nucl. Sci.*, vol. 57, no. 2 PART 2, pp. 793–806, 2010 (cit. on pp. 67, 88, 93, 94).

[99] D. Zhang, C. Cadet, N. Yousfi-Steiner, and C. Bérenguer, "A Study of Online Inspection for Multi-level Prognostics", *IFAC-PapersOnLine*, vol. 50, no. 1, pp. 13 716–13 721, 2017 (cit. on pp. 71, 74).

[100] D. An, J. H. Choi, and N. H. Kim, "Prognostics 101: A tutorial for particle filter-based prognostics algorithm using Matlab", *Reliab. Eng. Syst. Saf.*, vol. 115, pp. 161–169, 2013 (cit. on p. 77).

[101] D. Zhang, C. Cadet, N. Y. Steiner, P. Baraldi, C. Bérenguer, and Enrico Zio, "A Study of Local Aggregation of an Ensemble of Models for RUL Prediction", in *10th International Conference on Mathematical Methods in Reliability*, Grenoble, 2017, pp. 1–8 (cit. on p. 87).

[102] S. Al-Dahidi, F. Di Maio, P. Baraldi, and E. Zio, "Remaining useful life estimation in heterogeneous fleets working under variable operating conditions", *Reliab. Eng. Syst. Saf.*, vol. 156, pp. 109–124, 2016 (cit. on p. 88).

[103] J. Larminie and A. Dicks, "Fuel cell systems explained", in *Fuel Cell Syst. Explain.* 2nd ed., Chichester: John Wiley & Sons Ltd, 2003, pp. 45–66 (cit. on p. 90).

[104] G. Vachtsevanos, F. L. Lewis, M. Roemer, A. Hess, and B. Wu, *Intelligent Fault Diagnosis and Prognosis for Engineering Systems*. Hoboken: John Wiley & Sons, 2006, p. 456 (cit. on p. 91).

[105] P. P. Bonissone, F. Xue, and R. Subbu, "Fast meta-models for local fusion of multiple predictive models", *Appl. Soft Comput. J.*, vol. 11, pp. 1529–1539, 2011 (cit. on p. 92).

[106] M. Rigamonti, P. Baraldi, E. Zio, I. Roychoudhury, K. Goebel, and S. Poll, "Ensemble of optimized echo state networks for remaining useful life prediction", *Neurocomputing*, vol. 0, pp. 1–18, 2017 (cit. on pp. 92, 93).

[107] Robert T. Clemen and R. L. Winkler, "Aggregating Probability Distributions", in *Adv. Decis. Anal.* W. Edwards, J. Ralph F. Miles, and D. von Winterfeldt, Eds., 1st ed., New York: Cambridge University Press, 2007, ch. 9, pp. 172–194 (cit. on p. 94).

[108] M. D. Pandey, X. X. Yuan, and J. M. van Noortwijk, "The influence of temporal uncertainty of deterioration on life-cycle management of structures", *Struct. Infrastruct. Eng.*, vol. 5, no. September 2014, pp. 145–156, 2009 (cit. on p. 96).

[109] D. Gamerman and H. F. Lopes, *Markov Chain Monte Carlo - Stochastic Simulation for Bayesian Inference*. Chapman and Hall/CRC, 2006, p. 343 (cit. on p. 96).

[110] L. Devroye, "Complexity questions in non-uniform random variate generation", in *Non-Uni form Random Variate Gener.* New York: Springer Verlag, 1986, pp. 586–587 (cit. on pp. 99, 100).

[111] W. Kahle, S. Mercier, and C. Paroissin, "Gamma Processes", in *Degrad. Process. Reliab.* 1st ed., Wiley-ISTE, 2016, pp. 238–243 (cit. on p. 99).

[112] S. Mercier and H. H. Pham, "A preventive maintenance policy for a continuously monitored system with correlated wear indicators", *Eur. J. Oper. Res.*, vol. 222, no. 2, pp. 263–272, 2012 (cit. on p. 99).

[113] H. H. Pham and S Mercier, "An imperfect replacement policy for a periodically tested system with two dependent wear indicators", in *Safety, Reliability and Risk Analysis Beyond the Horizon*, R. D. J. M. Steenbergen, P. H.A.J. M. van Gelder, S. Miraglia, and A. C.W. M. Vrouwenvelder, Eds., CRC Press, 2013, pp. 1033–1041 (cit. on p. 99).